Titel der Arbeit:

Biophysical properties of AMPA receptor complexes

D i s s e r t a t i o n

zur Erlangung des akademischen Grades

Doctor of Philosophy (Ph.D.)

eingereicht an der

Lebenswissenschaftlichen Fakultät der Humboldt-Universität zu Berlin

von

Irene Riva

Präsidentin der Humboldt-Universität zu Berlin:

Prof. Dr.-Ing. Dr. Sabine Kunst

Dekan der Lebenswissenschaftlichen Fakultät der Humboldt-Universität zu Berlin:

Prof. Dr. Bernhard Grimm

Gutachter/innen:

1. Prof. Andrew Plested

2. Prof. Peter Hegemann

3. Dr. Tanja Maritzen

Tag der mündlichen Prüfung: 24/02/2020

ERKLÄRUNG

Hiermit erkläre ich, die Dissertation selbstständig und nur unter Verwendung der angegebenen Hilfen und Hilfsmittel angefertigt zu haben. Ich habe mich anderwärts nicht um einen Doktorgrad beworben und besitze keinen entsprechenden Doktorgrad. Ich erkläre, dass ich die Dissertation oder Teile davon nicht bereits bei einer anderen wissenschaftlichen Einrichtung eingereicht habe und dass sie dort weder angenommen noch abgelehnt wurde. Ich erkläre die Kenntnisnahme der dem Verfahren zugrunde liegenden Promotionsordnung der Lebenswissenschaftlichen Fakultät der Humboldt-Universität zu Berlin vom 5. März 2015. Weiterhin erkläre ich, dass keine Zusammenarbeit mit gewerblichen Promotionsbearbeiterinnen/Promotionsberatern stattgefunden hat und dass die Grundsätze der Humboldt-Universität zu Berlin zur Sicherung guter wissenschaftlicher Praxis eingehalten wurden.

DECLARATION

I hereby declare that I completed the doctoral thesis independently based on the stated resources and aids. I have not applied for a doctoral degree elsewhere and do not have a corresponding doctoral degree. I have not submitted the doctoral thesis, or parts of it, to another academic institution and the thesis has not been accepted or rejected. I declare that I have acknowledged the Doctoral Degree Regulations which underlie the procedure of the Faculty of Life Sciences of Humboldt-Universität zu Berlin, as amended on 5th March 2015. Furthermore, I declare that no collaboration with commercial doctoral degree supervisors took place, and that the principles of Humboldt-Universität zu Berlin for ensuring good academic practice were abided by.

SUMMARY

Excitatory neurotransmission throughout the vertebrate central nervous system (CNS) is largely mediated by the α-amino-3-hydroxy-5-methyl-4-isoxazolepropionic acid receptors (AMPARs). AMPA receptors are glutamate-gated ion channels located at the postsynaptic membrane, where they compose the hub of macromolecular complexes with a number of auxiliary proteins that concertedly regulate the receptor function. Stargazin (or γ2) is the prototypical AMPAR auxiliary subunit, belonging, together with the related γ3, γ4, γ5, γ7 and γ8 isoforms, to the family of the transmembrane AMPA receptor regulatory proteins (TARPs). TARPs show a bewildering array of effects on the trafficking, synaptic anchoring, gating kinetics and pharmacology of AMPARs. Despite the growing knowledge gathered about the structural features of the AMPAR-TARP complex, the molecular mechanisms underlying TARP modulation of AMPA receptors have not been fully revealed. Higher brain functions rely upon AMPAR activity and dysregulation of AMPA receptors has been associated to life-threatening CNS disorders. These observations provide motivation to unravel the molecular machinery behind AMPAR regulation and to identify AMPAR auxiliary proteins as potential pharmacological targets.

In the present study, AMPAR-TARP interactions were investigated using electrophysiology in human embryonic kidney (HEK) 293 cells. The role of TARP extracellular loops, Loop1 (L1) and Loop2 (L2), in the modulation of AMPAR gating was analysed. By modifying γ2 and γ8 L1 and L2, mutant TARPs that both lacked modulatory properties ("null" TARPs) and also those that had greatly enhanced modulation ("super" TARP) were obtained, without affecting formation of AMPAR-TARP complexes. A model for TARP modulation has been proposed, based on predicted state-dependent interactions of TARP L1 and L2 with the AMPAR ligand binding domain (LBD) and linkers between the LBD and the transmembrane domain (TMD). L1 of γ8 emerged as a very powerful positive modulator of AMPAR gating, most likely by virtue of its length that enables extensive interactions with multiple sites of the receptor LBD. Moreover, considering that native AMPARs in the brain mainly consist of heterotetrameric assemblies of four distinct subunits (GluA1-4), null and super TARP mutants were also tested on different AMPAR subunit compositions. Common as well as subunit-dependent mechanisms of AMPAR modulation by TARPs have been observed. In particular, in

complexes of heteromeric GluA1 and mRNA-edited GluA2 AMPARs with TARPs, dominance of the GluA2 subunit in channel gating was detected.

In summary, these experiments provided evidence that TARP L1 and L2 are not involved in association of AMPAR-TARP complexes and can entirely account for the modulation of AMPAR gating by TARPs. Ultimately, by overexpression in organotypic brain slices, null and super TARP mutants may serve as useful tools to further examine, for the first time, the effects of TARP modulation on the function of synaptic AMPA receptors.

ZUSAMMENFASSUNG

Im zentralen Nervensystem (ZNS) werden exzitatorische Signale zum großen Teil durch α-Amino-3-hydroxy-5-methyl-4-isoxazol-Propionsäure-Rezeptoren (AMPARs) vermittelt. AMPARs sind Glutamat-gesteuerte Kationenkanäle und befinden sich in der postsynaptischen Membran. Dort bilden sie Komplexe mit „Hilfsproteinen“ (engl. Auxiliary Proteins), um die Rezeptorfunktion zu steuern. Der typische Vertreter, Stargazin (oder γ2), gehört zusammen mit seinen Isoformen γ3, γ4, γ5, γ7 und γ8 zur Familie der transmembranen AMPAR-regulierenden Proteine (TARPs). TARPs regulieren den Transport, die postsynaptische Insertion, die Steuerung (engl. Gating), sowie die Pharmakologie von AMPARs. Trotz der stetigen Aufklärung struktureller Merkmale von AMPAR-TARP-Komplexen, sind die molekularen Mechanismen, welche der TARP-Modulierung von AMPARs unterliegen, noch weitgehend unerforscht. Die normale Funktion von AMPARs ist Voraussetzung für die uneingeschränkte Hirntätigkeit, wohingegen Fehlfunktionen mit lebensbedrohlichen Störungen des ZNS in Verbindung gebracht werden konnten. Diese Beobachtungen bieten Grundlage und Motivation für die Aufklärung der molekularen Regulierung von AMPARs und der Identifikation von TARPs als potentielle pharmakologische Targets.

In dieser Arbeit wurden Interaktionen von AMPAR-TARP-Komplexen mithilfe elektrophysiologischer Methoden an HEK293-Zellen (engl. human embryonic kidney) untersucht. Insbesondere wurden die extrazellulären TARP-Schleifen (engl. Loops), Loop1 (L1) und Loop2 (L2) und deren Auswirkungen auf AMPAR-Gating studiert. Durch Mutationen von γ2- und γ8- L1 und L2 konnten TARPs generiert werden, die entweder keine modulierenden Eigenschaften an AMPARs aufwiesen („null“-TARP) oder eine verstärkte Modulierung zeigten („super“-TARP), ohne dabei die AMPAR-TARP-Komplexbildung zu beeinträchtigen. Zur Beschreibung der zustandsabhängigen Interaktionen von TARP- L1 und L2 mit der AMPAR-Ligandenbindedomäne (LBD), sowie den Linkern zwischen LBD und Transmembrandomäne (TMD), wurde ein Modell erstellt. Bezüglich AMPAR-Gating erwies sich γ8-L1 als verstärkender Modulator, der vermutlich aufgrund seiner Länge zahlreiche Wechselwirkungen mit der LBD eingehen kann. Da native AMPARs im Hirn vorwiegend als Heterotetramere mit unterschiedlichen Kombinationen der Untereinheiten (GluA1-A4) vorkommen, wurden die null- und die super-TARP-Mutanten an AMPARs mit verschiedenen

Kompositionen der Untereinheiten getestet. Es konnten sowohl untereinheitsabhängige als auch allgemeine Mechanismen beschrieben werden, die aufgrund von TARP-Modulationen von AMPARs entstehen. Besonders in Komplexen von heteromerem GluA1 und mRNA-editiertem GluA2 AMPARs mit TARPs konnte ein dominantes Gating der GluA2-Untereinheit beobachtet werden.

Zusammenfassend konnte durch die Experimente gezeigt werden, dass L1 und L2 nicht bei der Bildung von AMPAR-TARP-Komplexen involviert sind, sondern vielmehr der Modulierung von AMPAR-Gating durch TARPs dienen. Durch Überexpression der null- und super-TARP-Mutanten in organotypischen Gehirnschnitten könnten diese zukünftig als nützliches Werkzeug dienen, um die Effekte von TARP-Modulationen erstmalig an synaptischen AMPARs zu studieren.

TABLE OF CONTENTS

LIST OF ABBREVIATIONS

3D	three-dimensional
Å	angstrom
ACSF	artificial cerebrospinal fluid
AMPAR	α-amino-3-hydroxy-5-methyl-4-isoxazolepropionic acid receptor
ATD	amino-terminal domain
C-	carboxyl-
C-tail	cytoplasmic tail
Ca^{2+}	calcium
CaMKII	calcium/calmodulin-dependent protein kinase II
CGN	cerebellar granule neuron
CKAMP44	cystine-knot AMPAR modulating protein
CNIH-2	cornichon homologs-2
CNIH-3	cornichon homologs-3
CNQX	6-cyano-7-nitroquinoxaline-2,3-dione
CNS	central nervous system
Cryo-EM	cryogenic electron microscopy
CTD	carboxyl-terminal domain
CTZ	cyclothiazide
Cα	alpha carbon
D1	lobe 1
D2	lobe 2
DDM	n-Dodecyl-β-D-Maltopyranoside
DG	dentate gyrus
DIC	differential interference contrast
DIV	days in vitro
DNQX	6,7-dinitroquinoxaline-2,3-dione
DsRed	discosoma red
EBSS	Earle's balanced salt solution
ECD	extracellular segment

EGFP	enhanced green fluorescent protein
EM	electron microscopy
EPSC	excitatory postsynaptic current
ER	endoplasmic reticulum
E_{rev}	reversal potential
FBS	fetal bovine serum
G	conductance
G-V	conductance-voltage
Glu	glutamate
GS	glycine-serine
GSG1L	germ cell-specific gene 1-like protein
GΩ	gigaohm
HEK	human embryonic kidney
Hz	Herz
I	current
I-V	current-voltage
iGluR	inotropic glutamate receptor
IRES	internal ribosome entry site
I_{ss}	steady-state current
K^+	potassium
KA	kainate
k_{deact}	deactivation rate
k_{des}	desensitisation rate
L1	Loop1
L2	Loop2
LBD	ligand binding domain
LTD	long-term depression
LTP	long-term potentiation
M1	membrane helix 1
M2	membrane helix 2
M3	membrane helix 3

M4	membrane helix 4
MAGUK	membrane-associated guanylate kinase
MD	molecular dynamics
MEM	minimum essential medium
mEPSC	miniature excitatory postsynaptic current
mGluR	metabotropic glutamate receptor
MW	molecular weight
MΩ	megaohm
N-	amino-
NBQX	2,3-dioxo-6-nitro-1,2,3,4-tetrahydrobenzo[f]quinoxaline-7-sulfonamide
NMDA	N-methyl-D-aspartate
NMDAR	NMDA receptor
NP	negative patch
P	postnatal day
pA	picoampere
PA	polyamine
pC	picocoulomb
PEG	polyethylene glycol
PEI	polyethylenimine
PEPA	4-[2-(phenylsulfonylamino)ethylthio]-2,6-difluorophenoxyacetamide
PKA	protein kinase A
PKC	protein kinase C
P_{open}	open channel probability
PP1	protein phosphatase 1
PP2B	protein phosphatase 2B
PSD	postsynaptic density
PSD-95	PSD protein-95
PTFE	polytetrafluoroethylene
PVDF	polyvinylidene fluoride
R	resistance
RI	rectification index

RMSD	root-mean-square deviation
RR	rectification ratio
S1	amino acid segment 1
S2	amino acid segment 2
SCC	Schaffer collateral/commissural
SCE	single-cell electroporation
SEM	standard error of the mean
SNP	single nucleotide polymorphism
TARP	transmembrane AMPA receptor regulatory protein
TCM	trichloromethiazide
t_{deact}	deactivation time
t_{des}	desensitisation time
TE	tris-EDTA
TM1	transmembrane helix 1
TM2	transmembrane helix 2
TM3	transmembrane helix 3
TM4	transmembrane helix 4
TMD	transmembrane domain
UPR	unfolded protein response
V	voltage
WT	wild-type

1. INTRODUCTION

1.1 AMPA receptors

1.1.1 Overview of AMPA receptor physiology

Within the mammalian central nervous system (CNS), the vast majority of fast excitatory synaptic transmission is mediated by the α-amino-3-hydroxy-5-methyl-4-isoxazolepropionic acid receptors (AMPARs). Together with the NMDA (*N*-methyl-D-aspartate)- and kainate-type receptors, AMPA-type receptors belong to the family of the ionotropic glutamate receptors (iGluRs), ligand-gated ion channels located at excitatory synapses where they are activated by the neurotransmitter glutamate. Following binding of presynaptically released glutamate these three classes of iGluRs are characterised by different gating kinetics. The AMPAR produces a rapidly rising conductance that also rapidly decays (1-2 ms), whereas the NMDA and kainate receptors show much slower gating kinetics. In particular, the NMDA receptor (NMDAR) activates in milliseconds and deactivates between tens and thousands of milliseconds (Traynelis et al., 2010). Moreover, AMPA and kainate receptors undergo a rapid and pronounced desensitisation that occurs within milliseconds after activation; NMDARs instead are subject to weak or no desensitisation, whose rate and degree depend on the NMDAR subtype (Traynelis et al., 2010). The diversity in the gating kinetics of the iGluRs precisely defines the time course of synaptic currents and their role in synaptic physiology.

AMPARs sit at the postsynaptic density (PSD) of glutamatergic synapses, where binding of glutamate to their extracellular ligand binding domain (LBD) allows the influx of cations such as Na^+ and Ca^{2+} through the channel pore, thus depolarising the postsynaptic membrane. AMPAR signaling is typically mediated by tetrameric AMPARs (Rosenmund et al., 1998) assembled from differing combinations of the four subunits GluA1 to GluA4. AMPAR subunit composition is developmentally regulated, region and cell type-specific and activity-dependent (Henley & Wilkinson, 2016). In the adult brain diheteromeric GluA1-GluA2 and GluA2-GluA3 receptors are the most common assemblies (Wenthold et al., 1996; Lu et al., 2009; Zhao et al., Science 2019), whereas GluA4 is highly expressed in the early postnatal period and then down-regulated. GluA4 remains enriched in the adult in certain cerebellar cell types (Petralia & Wenthold, 1992; Zhu et al., 2000). A critical determinant of the AMPAR

function is dictated by the presence or absence of the GluA2 subunit. The vast majority of GluA2 RNA is post-transcriptionally modified by editing at a codon residing in the pore channel region that is converted from glutamine to arginine (Q/R site). By virtue of Q/R site editing, the permeation properties of GluA2-containing AMPARs are altered: they have low calcium (Ca^{2+}) permeability, are insensitive to the voltage-dependent block by endogenous polyamines and have a low single-channel conductance (Sommer et al., 1991; Jonas & Burnashev, 1995; Swanson et al., 1997). On the contrary, GluA2-lacking AMPARs, or AMPARs containing the unedited GluA2(Q) form, have high permeability to Ca^{2+}, are blocked by endogenous polyamines and have higher single-channel conductance. During early postnatal development, expression of GluA2 is low compared to that of the other GluA subunits, but it increases rapidly from the first postnatal week (Pickard et al., 2000). This, coupled with the above-mentioned transient high expression of GluA4, renders many neonatal AMPARs Ca^{2+}-permeable, suggesting that such receptors may play a role in neonatal synaptic functions (Isaac et al., 2007).

Thus, the kinetics and amplitude of the excitatory synaptic responses are crucially determined by the biophysical properties of the receptor subunit composition as well as by the density of the receptor expression (Traynelis et al., 2010). Activity-dependent changes in the composition and density of synaptic AMPARs are tightly regulated by dynamic receptor trafficking (i.e. lateral diffusion and vesicular trafficking) and intrinsically underlie some mechanisms of synaptic plasticity (Malinow & Malenka, 2002; Choquet & Triller, 2003; Newpher & Ehlers, 2008). In fact, short periods of specific patterns of activity can trigger long-lasting changes in the function of excitatory synapses by modifying their efficacy to store information, either through a strengthening (long-term potentiation, LTP) or weakening (long-term depression, LTD) of the synaptic responses (Bliss & Lomo, 1973; Lynch et al., 1977). These mechanisms are widely believed to constitute the molecular basis of higher cognitive functions such as hippocampal-dependent memory formation and learning (Martin et al., 2000; Kessels & Malinow, 2009). Both LTP and LTD are thought to be expressed through the insertion or removal, respectively, of synaptic AMPARs (Malenka & Bear, 2004). Especially, certain stimuli can induce the initiation of the LTP and LTD by activation of postsynaptic NMDARs (NMDAR-dependent LTP/LTD) and specific intracellular signaling cascades involving either protein kinases or phosphatases (Malenka, 1994) which determine,

respectively, an increase or a decrease in the number of synaptic AMPARs (Lüscher & Malenka, 2012; Choquet, 2018). It was then proposed that expression of the LTP and LTD might be associated with bidirectional changes in phosphorylation of the C-terminus of the AMPAR subunits GluA1 and GluA2 (Lee et al., 2000; Chung at al., 2000). More recently this notion has been the subject of strong debate (Buonarati et al., 2019; see following section).
Centrally, AMPAR function at synapses is influenced by a number of auxiliary proteins that physically associate in a complex with the receptor and control the receptor activity at many different levels, considerably adding to the variation in AMPAR properties and hence to the diversity of information processing within the brain (Jackson & Nicoll, 2011).

1.1.2 AMPA receptor structure and role of the distinct domains

AMPA receptors are integral membrane proteins composed of the four GluA1-4 subunits that assemble to form a central ion channel pore. Each AMPAR subunit has a modular structure that includes four discrete domains (**Fig. 1 A**): the extracellular amino-terminal domain (ATD) that is involved in receptor subtype-specific assembly and synaptic anchoring (Leuschner & Hoch, 1999; Ayalon et al., 2005; Watson et al., 2017; Díaz-Alonso et al., 2017), the extracellular ligand-binding domain (LBD) that binds the agonist and drives the activation gating (Baranovic et al., 2016), the transmembrane domain (TMD) that forms the membrane-spanning ion channel (Wollmuth & Sobolevsky, 2004) and an intracellular carboxyl-terminal domain (CTD) that takes part in synaptic localisation, trafficking and receptor regulation (Song & Huganir, 2002).
The first detailed crystallographic structure of a full-length GluA2 receptor in a closed antagonist-bound state showed that the receptor harbours an overall axis of two-fold symmetry, with the extracellular domains organised as pairs of local dimers and the ion channel domain exhibiting a four-fold symmetry (Sobolevsky et al., 2009; **Fig. 1 B**). The symmetry mismatch between the extracellular (ATD and LBD) and ion channel (TMD) domains as well as a subunit crossover (or domain swapping) from the LBD to the ATD give rise in the homotetrameric GluA2 receptor to two conformationally distinct types of subunits: A/C and B/D. As a consequence of the swapping of domains, local ATD and LBD dimers are not formed by the same pairs of subunits, with the ATD dimers being formed by the A/B and C/D subunits and the LBD dimers by the A/D and B/C subunits. The ATD and LBD generate

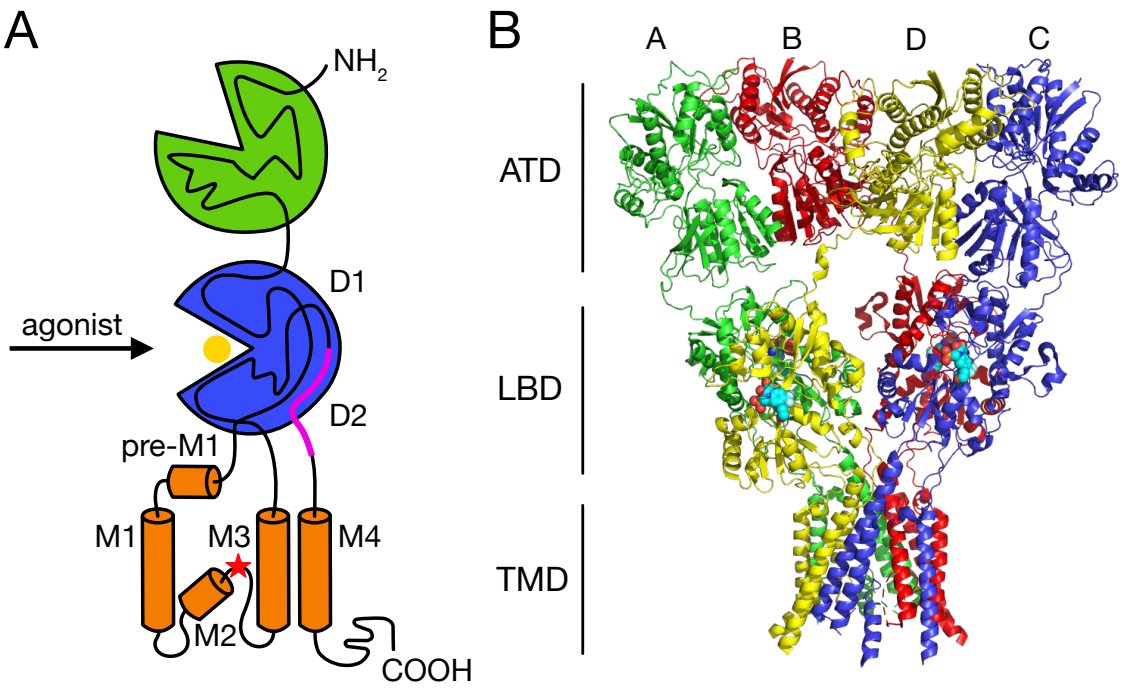

Figure 1. Modular and crystal structure of an AMPAR. (**A**) Schematic representation of the modular structure of a single AMPAR subunit comprising the extracellular ATD (*green*) and LBD (*blue*), the pore-forming TMD (*orange*) and the intracellular CTD. The polypeptide chain is traced through the distinct domains. Two amino acid segments (S1 and S2) compose the upper (D1) and lower (D2) lobes of the LBD. Glutamate (*yellow sphere*) binds between the two LBD lobes. The TMD contains three membrane-spanning helices (M1, M3 and M4), preceded by a short helix oriented nearly parallel to the membrane (pre-M1), and a central pore-like helix (M2). The Q/R editing site (*red star*) is positioned in the membrane re-entrant loop of the M2. The location of the flip/flop cassette is indicated by a magenta line. (**B**) Crystal structure of the full-length homotetrameric rat GluA2 receptor bound to the competitive antagonist ZK200775 (PDB code: 3KG2, 3.6 Å resolution; Sobolevsky et al., 2009). Each subunit is assigned a different colour. The extracellular ATD and LBD, organised as pairs of local dimers (A/B and C/D for the ATD, A/D and B/C for the LBD), show a two-fold symmetrical arrangement, while the TMD is characterised by a four-fold symmetry.

two types of subunit-subunit contacts: within each dimer (A-B or C-D for the ATD and A-D and B-C for the LBD) and between dimers (mediated by residues at the B-D dimer-dimer interface for the ATD and at the A-C dimer-dimer interface for the LBD). The subunit crossover between the ATD and LBD layers is primarily mediated by the ATD-S1 amino acid linkers that connect the ATD with the first of the two amino acid segments (S1 and S2) that define the LBD. Similarly, the symmetry mismatch between the extracellular and ion channel

domains is mediated by the linkers connecting the LBD and TMD layers (S1-M1, M3-S2 and S2-M4 linkers). In both cases, these linkers adopt two different conformations corresponding to the A/C and the B/D subunits. It was demonstrated that mutations of all three LBD-TMD linkers and their swap between different iGluR classes produce drastic effects on receptor gating, thus indicating that their structure as well as their length are important for proper coupling of neurotransmitter signal and channel opening (Schmid et al., 2007; Talukder et al., 2010).

Around the 4-fold rotational symmetry axis of the TMD, each subunit is composed by three transmembrane helices (M1, M3 and M4), a central pore-like helix (M2) and a polypeptide pore-lining loop. At the apex of the M1, a short helix (pre-M1) is oriented nearly parallel to the membrane, residing at the top of the ion channel domain and acting like a cuff around it. The M2 helix lies within the pore and at the apex of its reentrant loop it holds the Q/R editing site (residue 586). The M3 helices line the inside of the ion channel domain and in the antagonist-bound state they are crossing each other unambiguously closing the ion channel. The M4 helices instead are located on the exterior, mediating extensive subunit-subunit interactions with the TMD of an adjacent subunit. It has been shown that AMPAR subunits lacking the M4 segment do not express at the plasma membrane because the interaction of a specific face of the M4 with the pore domain of a neighbouring subunit is necessary for AMPAR tetramerisation (Salussolia et al., 2011; Salussolia et al., 2013). Unlike AMPARs, the M4 segment in NMDAR subunits does not substantially contribute to their biogenesis (Amin et al., 2017). However, mutations of the M4 dramatically affect NMDAR gating and different missense mutations have been associated with neurological disorders (Amin et al., 2018).

The LBD is highly conserved within the distinct glutamate receptor classes, conversely the CTD is the most variable domain both in the amino acid sequence and in length (Traynelis et al., 2010). It encodes short docking motifs for intracellular PDZ domain-containing proteins, such as the glutamate receptor-interacting proteins GRIP1 and GRIP2 and the protein interacting with C kinase or PICK1 (Dong et al., 1997; Dong et al., 1999; Xia et al., 1999). Furthermore, the CTD is thought to be important in the targeting and anchoring of AMPARs to specific synapses and therefore to be involved in mechanisms underlying synaptic plasticity (Buonarati et al., 2019). Nevertheless, since it has been excised in crystallographic structures to date, no structural details of this part of the receptor are available yet. Phosphorylation of

two sites, Ser831 and Ser845, in the CTD of the AMPAR subunit GluA1 by, respectively, the calcium/calmodulin-dependent protein kinase II (CaMKII) and the protein kinase A (PKA) has been shown to potentiate the receptor function (Roche et al., 1996; Barria et al., 1997; Derkach et al.,1999) and to be reversibly modified during induction of LTP and LTD in the CA1 region of the hippocampus (Lee et al., 2000; Man et al., 2007). In particular, it was proposed that phosphorylation of these sites mediates an accumulation of GluA1-containing AMPARs into the perisynaptic space, which is thought to be located somewhere on the dendritic spines between the postsynaptic sites and the dendritic shaft, making them readily available to move to the PSD and contribute to LTP expression (Esteban et al., 2003; Lee et al., 2003; Lu et al., 2003; Oh et al., 2006; Yang et al., 2008; Gao et al., 2006; He et al., 2009). Despite this long acknowledged role of GluA1 in synaptic plasticity, the level of phosphorylated GluA1 at Ser831 and Ser845 in the adult hippocampus was recently found to be almost negligible both upon basal transmission or LTP induction (Hosokawa et al., 2015). Moreover, the requirement not only of GluA1 CTD for LTP (Granger et al., 2013) but also of AMPARs in general for LTD has been ruled out (Granger & Nicoll, 2014). Likewise, the phosphorylation of one site in the CTD of the AMPAR subunit GluA2 (Ser880) by protein kinase C (PKC) has been correlated to hippocampal LTD expression (Chung et al., 2000; Kim et al., 2001), nonetheless LTD was demonstrated to be intact in GluA2 knockout mice (Meng et al., 2003). Questioning again the role of GluA1 and GluA2 in synaptic plasticity, a study from last year made use of CTD replacement mutant mice to reveal that the CTDs of GluA1 and GluA2 are effectively necessary and sufficient for NMDAR-dependent LTP and LTD, respectively (Zhou et al., 2018). Zhou et al. conveyed that a major reason for the controversy of the previous studies might be the investigation of nonphysiological conditions (for example, using global or conditional AMPAR subunit knockout mice) that could perturb baseline AMPAR properties or synaptic function, making the interpretation of the data inconclusive.

In addition to the extensively studied role of the AMPAR CTD in synaptic trafficking, recent reports provided evidence that the ATD is also a central player in this process (Watson et al., 2017; Díaz-Alonso et al., 2017). The extracellular AMPAR ATD, accounting for nearly half of the receptor polypeptide, projects midway into the synaptic cleft. Similarly to the CTD, its sequence is highly diverse between the four AMPAR subunits, hence offering great ability for

subunit-specific control. Although it has been proposed to be involved in the subunit assembly of receptors into functional tetramers (Leuschner & Hoch, 1999; Ayalon et al., 2005) and modulate receptor gating (Möykkynen et al., 2014; Cais et al., 2014), ATD truncated subunits can form robust glutamate-activated channels (Tomita et al., 2007). The work from Watson (2017) and Díaz-Alonso (2017) and respective coauthors showed that AMPAR anchoring during LTP requires the ATD of GluA1, probably through the interplay with proteins of the synaptic cleft such as N-cadherin (Saglietti et al., 2007), neuronal pentraxins (Sia et al., 2007; Pelkey et al., 2015) and neuropilin-2 (Wang et al., 2017). How exactly these interactions might take place though remains to be elucidated.

1.1.3 Mechanisms of AMPA receptor gating

Crystallographic and cryo-electron microscopic (cryo-EM) structures of isolated domains or of the full-length AMPAR, alone or in complex with auxiliary proteins, in the presence of different kinds of agonists, antagonists and allosteric modulators have facilitated the understanding of the mechanisms underlying receptor gating. As already mentioned, an AMPAR hallmark is the ultrafast (sub-millisecond) gating kinetics, which shapes the fast component of excitatory neuronal signaling. The gating cycle develops as follows. From a resting state during which the receptor ion channel is closed, agonist binding rapidly activates the receptor into a conductive state. Subsequently, if the neurotransmitter release is short enough (within 1 ms) and the neurotransmitter is immediately cleared from the synaptic cleft, the receptor promptly deactivates moving back to the resting state. Otherwise, in the continuous presence of the neurotransmitter it profoundly desensitises into a non-conductive agonist-bound state. From desensitisation to return back to the closed resting state, the receptor must undergo conformational rearrangements in a process termed ‘recovery from desensitisation’.

The AMPA receptor LBD shows a bilobed clamshell-like arrangement, in which the polypeptide segment S1 constitutes the upper lobe (D1) and the segment S2 the lower one (D2). In the LBD layer the dimers, arranged in a back to back manner, are mainly stabilised by the D1-D1 interface (Armstrong et al., 1998; Sun et al., 2002). Binding of full agonists, such as glutamate, quisqualate or AMPA, in a pocket located deep within the cleft between the two lobes D1 and D2 induces the closure of the clamshell and a movement of the D2 lobes

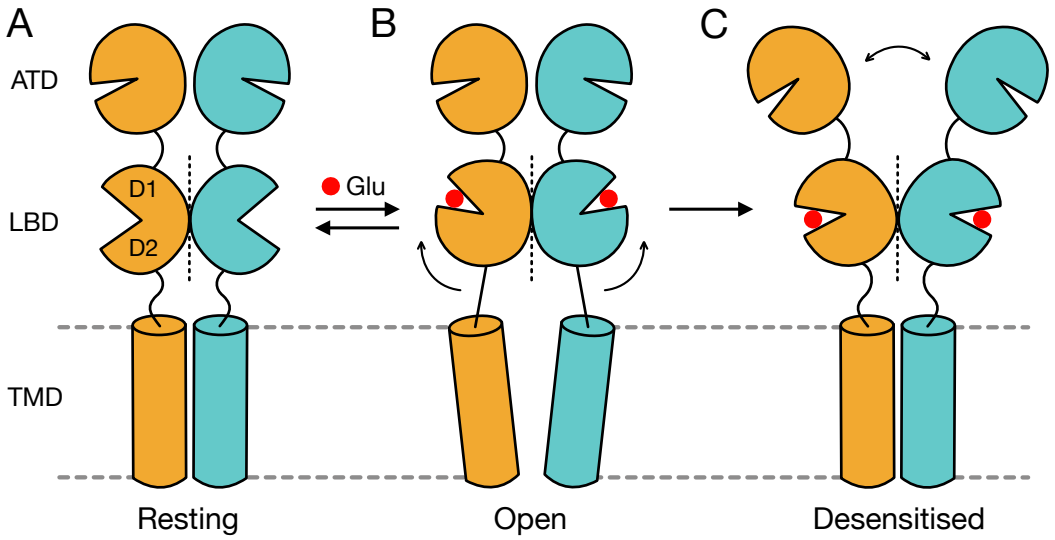

Figure 2. Structural transitions during AMPAR gating. Cartoon representing the movements that the distinct domains of the AMPAR (depicted here as a dimer) undergo to sustain the gating transitions from the (**A**) closed resting to the (**B**) open active state, and back, and from the active to the (**C**) agonist-bound desensitised state. Glutamate is shown as a red sphere.

that leads to separation of the linkers connecting the LBD with the TMD (**Fig. 2**). The degree of the cleft closure is dependent on the size of the ligand (Armstrong & Gouaux, 2000). This transition results in a reorientation of the transmembrane helices and opening of the ion channel. When successive LBDs are closed, the pore generates subconductance levels of increasing amplitude, up to a main conductance when the receptor is fully ligated (Rosenmund et al., 1998; Smith & Howe, 2000). Within the conformational changes triggering AMPAR activation a critical role is played by the M3 helix and the M3-S2 linker. In fact, upon agonist binding the movement of the M3-S2 linkers pulls apart the M3 helices at the bundle crossing fundamentally providing the energy required to open the ion channel (Sobolevsky et al., 2009). Given the 2-fold symmetry relating one LBD dimer to the other, the movements of the M3-S2 linkers are 2-fold symmetric, implying large conformational changes within dimers and smaller changes between dimers.

After activation, in the continuous presence of the agonist AMPARs rapidly undergo a profound desensitisation. Desensitisation can be triggered by just a single LBD closure and at similar rates independently of the number of receptor subunits bound to glutamate (Robert & Howe, 2003). Recently though, a very surprising finding reported that homomeric Q/R edited

GluA2 receptors still allow ions to flow when the receptors are desensitised, originating 'conducting desensitised' receptors that would account for the large steady-state current generated by GluA2(R) receptors both alone or in the presence of auxiliary proteins. This unusual phenomenon is attributable to the arginines at the Q/R site of the pore loop that would prevent desensitisation-mediated closure of GluA2(R) channels (Coombs et al., 2019). The conformational change onto which desensitisation is usually based is represented by the rupture of the LBD D1-D1 interface, followed by a rotation of the entire LBD to allow for the D2 domains and the LBD-TMD linkers to adopt a closed-state-like conformation (Sun et al., 2002). These rearrangements involve movements of the ATDs and ATD-LBD linkers. Under conditions that favour the stabilisation of a desensitised receptor conformation, structural studies of the homomeric GluA2 receptor have described that during desensitisation the LBD dimers accommodate strong rearrangements, losing their local 2-fold rotational symmetry towards a more 4-fold symmetrical architecture (Twomey et al., 2017). This was in agreement with previous findings about the kainate receptor subtype GluK2 that showed a pseudo-4-fold symmetric arrangement of the LBD upon desensitisation and suggested that a disruption of this 'desensitisation ring' might be the key mechanism for the restoration of the receptor resting state (Meyerson et al., 2016). Concerning the movements of the ATD layer sustaining the large LBD rearrangements during desensitisation, some three-dimensional (3D) classifications of GluA2 cryo-EM particles identified a separation, with a variable degree of displacement, of the ATD dimers, that was not observed for either the closed or active states nor for GluK2 receptors (Meyerson et al., 2014). Such separation was explained as the result of strain onto the ATD layer deriving from the symmetry switch of the LBD layer. However, this was not noticed according to other 3D classifications (Twomey et al., 2017) and there are still some discrepancies regarding the movements of the ATDs during AMPAR gating. Another interesting recent study demonstrated that alternative splicing of the LBD flip/flop cassette, a region of 38 amino acids located at the C-terminal end of the LBD and known to influence desensitisation (Sommer et al., 1990; Mosbacher et al., 1994; **Fig. 1 A**), controls distant motions of the ATD in the resting state (Dawe et al., 2019). Specifically, it was shown that the flop variant of GluA2 (GluA2flop) imparts greater mobility of the ATD at rest compared to the flip variant (GluA2flip). Moreover, contrary to GluA2flip, GluA2flop receptors were found to be insensitive to regulation by anions, binding to a newly identified

pocket near the base of the LBD D1-D1 dimer interface, and also by auxiliary proteins. Consistent with this result, alternative flip/flop splicing had previously been associated with differential sensitivity to allosteric modulators such as cyclothiazide (Partin et al., 1994; Partin et al., 1995). The authors conclude that this intrinsic diversity in the nanoscale mobility of the resting state would favour/disfavour interactions that stabilise/destabilise the receptor open state and, in other words, predetermine the receptor gating behaviour in the presence of neurotransmitters, allosteric modulators and auxiliary proteins.

It is relevant to mention here that auxiliary proteins of the AMPAR can deeply affect the receptor gating, both positively and negatively, but this will be extensively addressed in the following paragraphs.

1.2 AMPA receptor complex

1.2.1 AMPA receptor auxiliary proteins

In the postsynaptic membrane AMPARs are not alone, but rather the hub of dynamic supramolecular complexes with other intracellular and transmembrane proteins that concertedly regulate the receptor function. In order to unravel the molecular machinery behind this regulation, over the past 30 years tremendous progress has been made towards the identification of AMPAR interacting proteins. As aforementioned, different cytosolic proteins (such as GRIP1, GRIP2 and PICK1) have been discovered to interact with the cytoplasmic tail (C-tail) of the AMPAR and to play a role in the receptor membrane trafficking and synaptic anchoring and in intracellular signaling cascades (Jackson & Nicoll, 2011). The first transmembrane protein described to regulate the AMPAR was actually discovered through a seemingly unrelated investigation. In fact, in a mouse inbred line a spontaneous mutation was found to be associated with a neurological phenotype reminiscent of human absence epilepsy. This phenotype was particularly distinguished by a characteristic head-tossing behaviour, after which the mouse mutant was named *stargazer* (Noebels et al., 1990). The analysis of the *stargazer* mutation lead to the identification of a novel, brain-specific, tetraspanin membrane protein with structural homology to the gamma 1 (γ1) subunit of the skeletal muscle voltage-gated Ca^{2+} channel and therefore it was termed γ2, or stargazin (Letts et al., 1998). Stargazin though was displayed to only subtly modulate the functional properties of voltage-gated Ca^{2+}

channel in heterologous systems (Letts et al., 1998; Klugbauer et al., 2000; Kang et al., 2001; Rousset et al., 2001), but to be essential for the regulation of AMPARs in the cerebellum (Hashimoto et al., 1999; Chen et al., 2000). In cerebellar granule cells of the *stargazer* mouse, AMPAR-mediated synaptic as well as extrasynaptic currents were observed to be largely absent and to be both rescued by transfection with full-length recombinant stargazin. Hence, stargazin was proven to be required for surface expression and synaptic targeting of AMPARs in cerebellar granule cells.

Following the discovery of stargazin as the prototypical AMPAR auxiliary subunit, database mining revealed the existence of closely related γ subunits with widespread expression within the CNS (γ3, γ4, γ5, γ7, γ8) (Burgess et al., 1999; Klugbauer et al., 2000; Burgess et al., 2001) and together with stargazin they were collectively classified as "transmembrane AMPA receptor regulatory proteins" (TARPs). TARPs are present in the majority of AMPAR complexes in the brain (Fukata et al., 2005). However, in addition to TARPs, unrelated transmembrane proteins (such as SOL-1, CNIH-2 and 3, SynDIG1; CKAMP44, GSG1L) have been recently identified through genomic and proteomic analyses as other candidate AMPAR auxiliary subunits (Zheng et al., 2004; Schwenk et al., 2009; Kalashnikova et al., 2010; von Engelhardt et al., 2010; Shanks et al., 2012). These findings provided evidence for bewildering combinatorial possibilities of interaction of these auxiliary proteins with the AMPAR and between each other, moving the focus from the function of the receptor by itself to the joint action of a dynamic network of interacting proteins.

1.2.2 Transmembrane AMPA receptor regulatory proteins (TARPs)

TARPs are a family of four-pass transmembrane proteins composed of the γ subunits γ2 (or stargazin), γ3, γ4, γ5, γ7 and γ8. They are integral components of native AMPAR complexes (**Fig. 3**), with discrete patterns of expression throughout the brain, both in neurons and glial cells, depending on the neuronal cell-type and the course of development (Tomita et al., 2003). Stargazin shows highest levels of expression in the cerebellum, γ3 in the cerebral cortex, γ4 in the olfactory bulb and γ8 in the hippocampus. The highest levels of γ7 expression instead occur in cerebellar Purkinje cells (Kato et al., 2007), while γ5 is particularly enriched in hippocampal CA2 neurons and cerebrellar Bergmann glia (Kato et al., 2008). Moreover, it was shown that in the cerebral cortex of rat pups γ4 expression peaks at

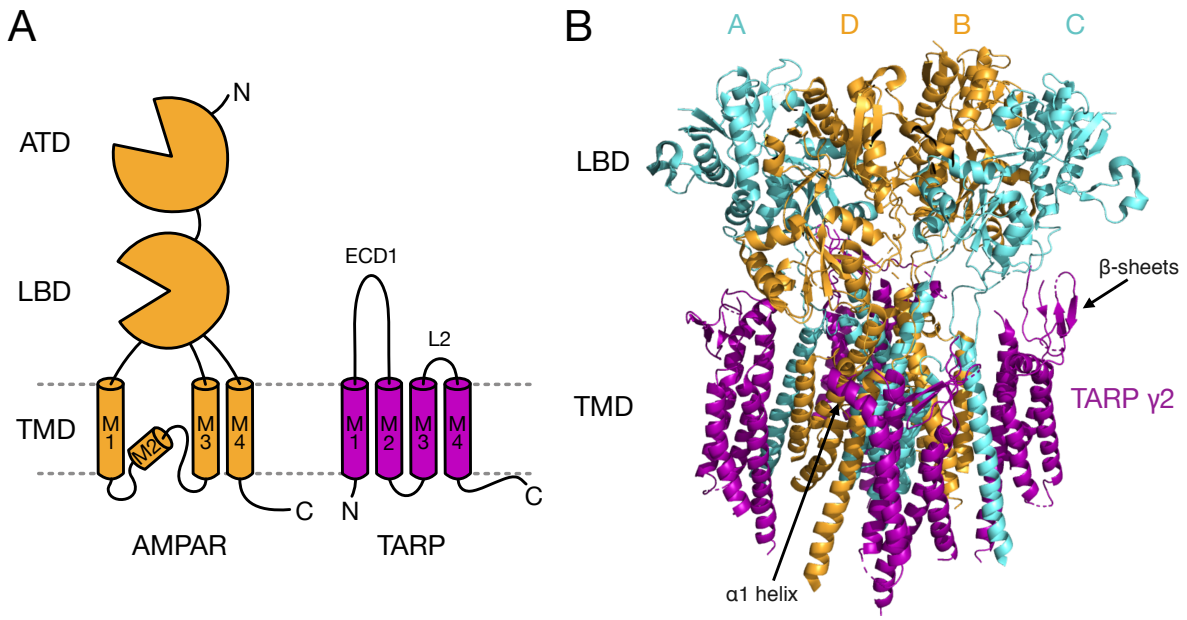

Figure 3. Complex of the AMPAR with TARPs. (**A**) Cartoon depicting the structure of a monomeric AMPAR (*orange*) and next to it that of a TARP auxiliary subunit (*purple*). The TARP structure is formed by four transmembrane domains, intracellular amino (N)- and carboxyl (C)-terminus and two extracellular segments, of which the first one (ECD1) is the larger and includes Loop1 (L1) and the β2-TM4 loop (not indicated) and the second one is composed by the short Loop2 (L2). (**B**) Cryo-EM structure of the homomeric rat GluA2 receptor saturated with TARP γ2 subunits (PDB code: 5KK2, 7.3 Å resolution; Zhao et al., 2016). Extensive contacts take place between the transmembrane domains of the receptor (represented in *cyan* for subunit pair A/C and in *orange* for subunit pair B/D) and of γ2 (*purple*). γ2 extracellular loops (L1, β2-TM4 and L2) are not resolved, but density emanating from the extracellular β-sheets flanking the loops has been modelled, as well as from the pre-TM2 α1 helix following the β2-TM4 loop. β-sheets and α1 helix appear to be positioned in proximity to the receptor LBD and LBD-TMD linkers, allowing the extracellular loops to regulate these gating critical regions.

postnatal day 6 (P6) and decreases through later development. In contrast, expression of stargazin, γ3 and γ8 appears later and progressively increases during animal maturation (Tomita et al., 2003).

Based on phylogenetic analyses of the primary sequence, the extended family of the γ subunits, comprising also the skeletal muscle γ1 and γ6 subunits (Burgess et al., 2001), can be divided into subgroups with higher homology: with stargazin, γ3, γ4 and γ8 forming one group, γ5 and γ7 forming another, and γ1 and γ6 being yet another. A second type of

classification divides the TARP family into two categories fundamentally differing in the functional properties exerted on the AMPAR: type I (or canonical) TARPs including stargazin, γ3, γ4 and γ8 and type II TARPs comprising γ5 and γ7. Type I TARPs were the first ones to be studied and, even if with some differences between distinct subunits, they show to qualitatively similarly regulate the AMPAR by enhancing its function (Cho et al., 2007; Milstein et al., 2007). γ5 and γ7 instead were initially thought to be unable to modulate the AMPAR function (Tomita et al., 2003; Tomita et al., 2004) and only later they were established as a separate class of TARPs with definite physiological features on specific AMPAR subtypes (Kato et al., 2007; Kato et al., 2008). The various modulatory effects of the different TARP subunits on the AMPAR will be thoroughly examined in the next section.

1.3 TARPs regulation of the AMPA receptor

1.3.1 TARPs mediate AMPA receptor trafficking and anchoring at the synaptic membrane

In both heterologous systems and neurons TARPs dramatically and selectively promote surface expression of mature AMPARs. It was revealed that in cerebellar granule cells of *stargazer* there was an approximate 75% decrease in the surface expression of the AMPAR subunit GluA2, whereas expression of the NMDAR subunit NR2A was not affected (Tomita et al., 2003). Remarkably, transfection of full-length stargazin as well as of the other type I TARPs γ3, γ4 and γ8 (but not of type II TARP γ5) in *stargazer* granule neurons could restore AMPAR surface expression and glutamate-evoked responses. This effect of TARPs on trafficking is specific to AMPARs and does not apply to structurally related receptors such as kainate-type channels (Chen et al., 2003). It was later proved that, similarly to type I TARPs, γ7 can promote AMPAR trafficking to the membrane surface and modestly enhance glutamate-evoked currents in transfected *stargazer* granule cells (Kato et al., 2007). Its effect though seems to be limited to channels containing the GluA1 or GluA2 subunits (Kato et al., 2008). Even more restrictively, γ5 was eventually discovered to be capable of modulating specific GluA2-containing AMPARs, with properties entirely dissimilar from those of canonical TARPs and without promoting receptor trafficking (Kato et al., 2008).

Concerning the molecular mechanisms underlying the deficit of AMPAR expression in *stargazer* cerebellar granule cells, it was found that a large proportion of GluA2 receptors did not receive mature endoplasmic reticulum (ER)-type glycosylation, a post-translational modification that allows exit of the receptors from the ER (Mah et al., 2005; Traynelis et al., 2010). This result suggested that stargazin plays a role in the early stages of the AMPAR biogenesis (Tomita et al., 2003). In support of this, it was also described that in TARP-deficient cells, such as heterologous cells or stargazer granule neurons, AMPAR expression induces the unfolded protein response (UPR), a homeostatic pathway activated by the accumulation of unfolded or misassembled proteins in the ER (Vandenberghe et al., 2005). In parallel, stargazin-mediated enhancement of AMPAR surface expression was verified not to be the result of the inhibition of constitutive receptor endocytosis (Vandenberghe et al., 2005). Experiments using γ2-γ5 chimeras and γ2 deletion mutants displayed that the C-tail of γ2, as opposed to γ5, is necessary for the surface expression and the potentiation of glutamate-evoked responses of GluA1 receptors in heterologous systems (Tomita et al., 2004; Tomita et al., 2005; Turetsky et al., 2005). It was subsequently demonstrated that the C-terminus of stargazin encodes a membrane sorting signal that mediates AMPAR trafficking from the ER to specific membrane compartments (Bedoukian et al., 2008). Moreover, TARPs seem to associate exclusively with tetrameric AMPARs, thus being incorporated in nascent AMPAR complexes at some point between tetramerisation and ER export (Vandenberghe et al., 2005; Shanks et al., 2010).

In neurons, not only are TARPs essential for the surface expression of AMPARs, but they also play a central role in anchoring and stabilising the receptors at synapses. In fact, TARPs regulate the lateral diffusion of AMPARs between extrasynaptic and synaptic sites, thank to the interaction of a PDZ binding motif on the TARP C-tail with PDZ domain-containing scaffolding proteins that are intrinsic components of the PSD (Chen et al., 2000; Bats et al., 2007; Sainlos et al., 2011). Such proteins include the PSD protein-95 (PSD-95) and the related members of the membrane-associated guanylate kinase (MAGUK) family (Schnell et al., 2002; Dakoji et al., 2003). The ability of TARPs to bind to PSD-95 is actually itself modulated by post-translational modifications of the TARP C-terminus. For instance, phosphorylation of a threonine (Thr321) located within stargazin PDZ binding motif was shown to be associated with opposing effects on AMPAR clustering during synaptic plasticity

depending on the kinase (PKA or the mitogen-activated protein kinase, MAPK) that phosphorylates it (Stein & Chetkovich, 2010). Furthermore, in its C-tail stargazin contains a series of nine serines, surrounded by a highly basic region, closely conserved in all four type I TARPs (Burgess et al., 2001; Klugbauer et al., 2000; Rousset et al., 2001) and constituting the phosphorylation substrate for CaMKII and PKC (Tomita et al., 2005; Tsui & Malenka, 2006). Interestingly, under basal conditions in cultured cortical neurons these serines are phosphorylated. Dephosphorylation of the C-terminal poly-serine region by the protein phosphatase 1 (PP1) and 2B (PP2B) seems to be involved in NMDAR-dependent LTD in the hippocampal CA1 region. On the other hand, expression of a phospho-null stargazin construct prevents LTP induction. With these findings, Tomita et al. (2005) identified a key role for TARPs phosphorylation in the bidirectional regulation of synaptic plasticity. To explain how TARP C-tail controls AMPAR synaptic delivery in a phosphorylation-dependent manner, it was proposed that phosphorylation of the nine serines might inhibit the interaction of the surrounding basic residues with the negatively charged membrane lipid bilayer. This dissociation, that is likely to be graded by the multiplicity of phosphorylation sites, would enhance graded binding of the TARP C-tail to PSD-95 and thus regulate targeting of AMPAR/ TARP complexes at synapses (Sumioka et al., 2010). Therefore, synaptic anchoring of AMPARs relies both upon the interaction of TARPs PDZ-binding motif with PSD-95 and also of the AMPAR CTD with intracellular PDZ domain-containing proteins, although the true influence of this second kind of interaction is less clear (Buonarati et al., 2019).

1.3.2 TARP modulation of the AMPA receptor gating

In addition to their role in trafficking, both type I and II TARPs modulate AMPAR gating and pharmacology to varying degrees in a subtype-specific manner (Jackson & Nicoll, 2011). Type I TARPs in general augment the functional properties of AMPARs. It is indeed well known from studies in heterologous expression systems that stargazin slows down the entry into desensitisation, enhances the steady-state current remaining upon desensitisation, slows down the rate of deactivation and accelerates the recovery from desensitisation of glutamate-elicited AMPAR currents (Yamazaki et al., 2004; Priel et al., 2005; Tomita et al., 2005; Turetsky et al., 2005). Coexpression of distinct type I TARPs results in differential effects on the gating kinetics of AMPARs and for example γ4 and γ8 have been shown to slow

deactivation to a greater extent than stargazin and γ3 (Kott et al., 2007; Körber et al., 2007; Milstein et al., 2007; Cho et al., 2007; Suzuki et al., 2008; Pierce & Niu, 2019). TARP subtype-dependent effects observed in heterologous systems were found to be largely mirrored in *stargazer* cerebellar granule neurons. Here, overexpression of specific TARP isoforms differentially modulates the amplitude, rise-time and decay of the AMPAR-mediated miniature excitatory postsynaptic currents (mEPSCs), with γ4 having the strongest effect in the slowing down of the mEPSCs decay (Milstein et al., 2007; Cho et al., 2007).

The effects of type II TARPs on AMPAR gating are complex and contradictory. Experiments in human embryonic kidney (HEK) 293 cells assessed that γ7 can enhance glutamate-evoked steady-state currents and modestly slow down the deactivation and desensitisation kinetics of GluA1 receptors. γ5 instead, originally showed unable to rescue AMPAR responses in *stargazer* granule cells (Tomita et al., 2003), displayed no significant effect (Kato et al., 2007). Other experiments in heterologous systems and neuron cultures indicated that, in contrast to the lack of effects on GluA1, γ5 induces an augment of the peak current of specific GluA2-containing AMPARs, without promoting receptor trafficking, coupled with a marked suppression of the steady-state current. γ7 instead would only enhance currents from channels containing the GluA1 or the GluA2 subunit (Kato et al., 2008). It was then found that γ5 increases single-channel conductance, comparably to the other TARP family members, but decreases the peak open probability (i.e. the probability that agonist-bound channels will open) of GluA1 and GluA4 receptors in tsA201 cells. Remarkably, the properties of recombinant AMPARs coexpressed with γ5 matched well those measured from outside-out patches of cerebellar Bergmann glial cells (Soto et al., 2009), neuronal cell type intensely expressing γ5 (Fukaya et al., 2005) and Ca^{2+}-permeable AMPARs formed of GluA1 and GluA4 subunits (Burnashev et al., 1992; Wisden & Seeburg, 1993; Iino et al., 2001). Additionally, γ5 was determined to preferentially modulate assemblies containing AMPARs with the longest C-tail (that are GluA1 and GluA4). Thus, γ5 was reestablished as an active member of the TARP family with unique properties in the selective regulation of long-form Ca^{2+}-permeable AMPARs in the Bergmann glia.

Another kinetic signature imparted to AMPAR gating by specific TARP isoforms is superactivation. In the continuous presence of glutamate (several seconds), desensitisation is followed by a slow increase in the steady-state current. γ4, γ7 and γ8 can boost

superactivation of GluA1 receptors, while stargazin was shown to be ineffective on GluA1 (Kato et al., 2010). Like γ8 though, γ2 is able to superactivate unedited GluA2(Q) receptors (Carbone & Plested, 2016). This phenomenon was initially interpreted as a reversal of desensitisation and hence termed 'resensitisation' (Kato et al., 2010). It was later observed that removal of desensitisation actually produces a more profound TARP-induced increase in AMPAR steady-state current, indicating that this effect is independent of desensitisation (Carbone & Plested, 2016). It was also proven to be independent of the peak current amplitude. On the other hand, the renamed 'superactivation' was found to be strongly correlated with the rate of recovery from the desensitised state, with stargazin massively increasing the steady-state current of mutant receptors with fast recovery and thus more available open state. This correlation lead to reinterpret superactivation as a positive feedback mechanism dependent on availability of receptors in the open state. The physiological significance of superactivation still has to be assessed, but it might be hypothesised as a postsynaptic process for facilitation of excitatory neurotransmission. Interestingly, AMPAR-mediated responses in hippocampal pyramidal neurons do not exhibit superactivation. However, γ8 overexpression in *stargazer* cerebellar granule neurons elicits superactivation and this is prevented by the cotransfection of the AMPAR auxiliary protein cornichon homolog-2 or CNIH-2 (Kato et al., 2010). The superactivating behaviour of native AMPARs is therefore likely to be governed by the synergetic effect of a number of interacting proteins that intercross to regulate the receptor.

At the level of unitary currents of single channels, AMPARs are known to visit multiple discrete conductance states (Rosenmund et al., 1998). It was demonstrated that stargazin increases the open channel probability (P_{open}) of GluA4 receptors by pushing the channel openings to large conductance states and that it prolongs the duration of bursts of channel openings (Tomita et al., 2005). Nonetheless, in line with previous findings (Soto et al., 2007), a recent report, in which GluA4 P_{open} was estimated based on channel-opening and -closing rates from whole-cell currents, showed that P_{open} is unchanged when stargazin, or γ4, is present (Pierce & Niu, 2019). Other single-channel data with the GluA1 subunit instead suggested that TARP γ4 produces a fundamental change in the receptor behaviour, by enhancing the amplitude of all conductance states including the largest one (Shelley et al., 2012). Nonstationary fluctuation analysis of currents evoked by ultrafast glutamate

application, a powerful method for estimating single-channel properties underlying macroscopic currents, revealed that type I TARPs differentially increase the mean channel conductance of recombinant GluA2-containing receptors, with γ8 enhancing it to the greatest extent (Jackson et al., 2011). In addition, it was proposed that TARP association generates an heterogenous population of receptors whose gating behaviour switches between a low-P_{open} and a high-P_{open} mode (modal gating), resulting in ensemble currents with variable decay kinetics that may contribute to shape the multi-component decay of AMPAR synaptic currents (Zhang et al., 2014).

1.3.3 TARPs regulate AMPA receptor pharmacology

TARPs also modify the pharmacological properties of AMPARs. First of all, stargazin and the other type I TARPs potentiate AMPAR affinity to glutamate (Yamazaki et al., 2004; Priel et al., 2005; Tomita et al., 2005), by a degree that is dependent on the specific TARP subtype (Kott et al., 2007; Tomita et al., 2007; Kott et al., 2009). Recombinant AMPARs show a typical sigmoid glutamate dose-response curve and it is the same case when measuring the steady-state instead of the peak current (Robert & Howe, 2003). Conversely, native and TARPed recombinant AMPARs exhibit a bell-shaped steady-state dose-response curve that indicates a decline of the current at high concentrations of glutamate (above 10-100 μM), a phenomenon referred to as 'autoinactivation' (Raman & Trussell, 1992; Morimoto-Tomita et al., 2009; Semenov et al., 2012). Autoinactivation has first been ascribed to a desensitisation-induced complete dissociation of TARPs from AMPARs (Morimoto-Tomita et al., 2009), then rather to subunit-dependent structural rearrangements leading to the functional uncoupling of the AMPAR-TARP complex (Semenov et al., 2012). This concentration-dependent TARP action has been suggested to serve to modulate synaptic short-term plasticity upon neuronal overactivation or elevated levels of glutamate (Morimoto-Tomita et al., 2009). Subsequently, an alternative mechanism has been proposed to account for autoinactivation without implying physical dissociation of the AMPAR-TARP complex (Coombs et al., 2017). In fact, it has been observed that at low glutamate concentrations stargazin exerts a dual effect on AMPAR gating, overall shifting the balance from desensitisation to activation. On one hand, it reduces the sensitivity to desensitisation, by markedly slowing the desensitisation rate (at concentrations below 100 μM). On the other hand, it enhances gating of partially occupied

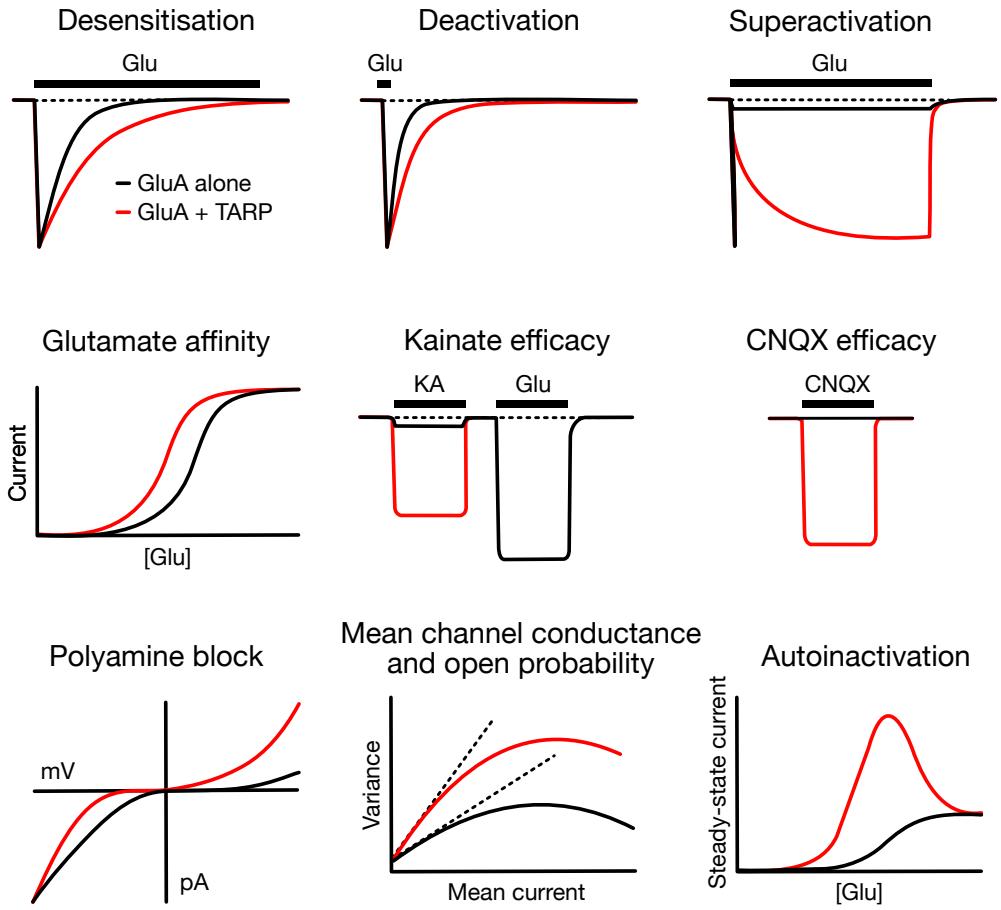

Figure 4. TARP modulation of AMPAR gating and pharmacology. Schematic summary of some of the various effects that TARP association (*red*) determines on the gating and pharmacology of AMPARs (alone, *black*). The following TARP-induced changes in AMPAR properties are illustrated from left to right, top to bottom: slowing in the desensitisation and deactivation kinetics, slow augment of the steady-state current upon long agonist exposure (superactivation), increase in affinity to the full agonist glutamate and in efficacy of the partial agonist kainate and the competitive antagonist CNQX, relief of the voltage-dependent block by intracellular polyamines, increase in the mean channel conductance and open probability and decline of the current at high glutamate concentrations (autoinactivation). Adapted from Jackson & Nicoll, 2011.

AMPARs, by increasing glutamate efficacy at low occupancy (i.e. fewer agonist events are necessary to gate the receptors). This behaviour has been related to a possible ability of TARPs of amplifying the synaptic signal transduction mediated by glutamate spillover, a phenomenon described by the diffusion of glutamate from the site of release to neighbouring synapses (Diamond, 2002).

Furthermore, TARPs robustly enhance AMPAR kainate efficacy. Kainate is a partial agonist of AMPARs, meaning that even at saturating concentrations it only induces submaximal channel activation in the form of small, non-desensitising currents (Patneau & Mayer, 1991). Structurally, partial agonism is due to an incomplete cleft closure of the LBD (Armstrong & Gouaux, 2000; Jin et al., 2003). The presence of TARPs turns kainate into an almost full agonist in both heterologous cells and neurons (Tomita et al., 2005; Turetsky et al., 2005) and the ratio of kainate-evoked to glutamate-evoked currents (I_{KA}/I_{Glu}) has been a long-established indicator of TARP association in AMPAR measurements (Shi et al., 2009). Type II TARP γ7 slightly increases AMPAR kainate efficacy, while γ5 is ineffective (Tomita et al., 2005; Kato et al., 2007).

The quinoxalinediones are a family of compounds –such as 6-cyano-7-nitroquinoxaline-2,3-dione (CNQX), 6,7-dinitroquinoxaline-2,3-dione (DNQX), 2,3-dioxo-6-nitro-1,2,3,4-tetrahydrobenzo[f]quinoxaline-7-sulfonamide (NBQX)– widely used as competitive AMPAR antagonists (Honoré et al., 1988; Sheardown et al., 1990). By definition, competitive antagonists bind to the AMPAR LBD in the same pocket as agonists, thereby occluding agonist binding, but without leading to opening of the ion channel. It was then observed that CNQX application in neurons induces depolarising currents (McBain et al., 1992; Maccaferri & Dingledine, 2002) that are blocked by the non-competitive AMPAR antagonist GYKI 53655 and potentiated by the allosteric AMPAR modulator trichloromethiazide (TCM), disclosing a new role for CNQX as an AMPAR agonist rather than antagonist (Menuz et al., 2007). DNQX was shown to behave similarly to CNQX, whereas NBQX purely acts as a competitive receptor antagonist. It was demonstrated that TARPs are responsible for converting CNQX competitive antagonism into a partial agonist activity, possibly by strengthening the coupling between the partial LBD closure induced by CNQX binding and channel opening (Menuz et al., 2007; Cokić et al., 2008; Kott et al., 2009). Subsequent work revealed instead that the degree of CNQX block is time-dependent and under non-equilibrium conditions (shortly after receptor activation, before CNQX and glutamate reach steady-state occupancy), which prevail at glutamatergic synapses, CNQX operates as a non-competitive antagonist and blocks AMPAR-TARP complexes with high affinity (MacLean & Bowie, 2011). Additionally, these authors suggested that the reduction of CNQX block by TARPs

could be independent of CNQX binding properties and almost entirely attributable to a TARP-mediated increase in agonist potency both under non-equilibrium or equilibrium-conditions.

Stargazin association also changes the pharmacology of allosteric AMPAR potentiators such as cyclothiazide (CTZ), which selectively boosts responses of GluA flip variants (Partin et al., 1994), and 4-[2-(phenylsulfonylamino)ethylthio]-2,6-difluorophenoxyacetamide (PEPA), acting preferentially on GluA flop variants (Sekiguchi et al., 1997) and makes both spliced forms sensitive to both classes of potentiators (Tomita et al., 2006). In contrast, stargazin increases the affinity for the non-competitive AMPAR antagonist GYKI 53655 (Cokić et al., 2008).

As already mentioned, among the other effects TARPs can modify AMPAR mean channel conductance, which implies an alteration of the receptor pore properties. An extremely relevant feature conferred by TARP association to AMPAR permeability is that it partially relieves the voltage-dependent block by endogenous intracellular polyamines (like spermine and spermidine) to which GluA2-lacking Ca^{2+}-permeable AMPARs are subject (Soto et al., 2007; Jackson & Nicoll, 2011). As a consequence of polyamine block, current-voltage (I-V) relationships of Ca^{2+}-permeable AMPARs show strong inward rectification, with maximal current decline between 0 and +40 mV (Kamboj et al., 1995; Koh et al., 1995; Bowie & Mayer, 1995). The degree of TARP-induced polyamine block relief is expressed by a 'rectification index' calculated as the ratio of the peak current at given positive to negative voltages. Analogously to the I_{KA}/I_{Glu} ratio, the rectification index can be used as a tool to evaluate proper assembly of AMPAR-TARP complexes (Carbone & Plested, 2016). However, relief from rectification can also represent a metric for GluA2 content and this might disguise TARP-dependent effects on the I-V shape especially of synaptic receptors (Milstein & Nicoll, 2008). TARP reduction of polyamine block was initially explained as a diminished affinity of the AMPAR pore for cytoplasmic polyamines (Soto et al., 2007). It was later demonstrated that stargazin increases the permeability of large cations but not the pore size of Ca^{2+}-permeable AMPARs, suggesting that relief of polyamine block by TARPs does not reflect altered pore diameter (Soto et al., 2014). Moreover, within the same study, the membrane proximal region of stargazin C-tail was found to be crucial for full TARP attenuation of polyamine block. Previously, three positive residues in this region of the C-tail of Neto1 and Neto2, auxiliary subunits of the kainate receptor, had been identified to be required for

attenuation of kainate receptors polyamine block (Fisher & Mott, 2012). Despite their importance in shaping synaptic transmission, the mechanisms by which TARPs regulate AMPAR channel properties remain poorly understood. One hypothesis is that TARP association influences the local charge environment in proximity of the region with the Q/R site, imparting substantial changes to the pore architecture that affect ion flux and polyamine block (Soto et al., 2014).

1.4 AMPA receptor-TARP interaction

1.4.1 Structures of the AMPA receptor-TARP complex

Great effort has been made in the last years to elucidate the structure of the AMPAR complex with auxiliary subunits. Despite initial negative-stain electron microscopy (EM) studies showing that stargazin contributes to the TMD of native AMPAR complexes (Nakagawa et al., 2005), detailed structural information about the AMPAR-TARP interactions, including TARP stoichiometry (Shi et al., 2009; Kim et al., 2010; Hastie et al., 2013), remained for long time elusive. Thank to strong recent advancements in the cryo-EM technique, the architecture of the AMPAR-TARP complex has finally started to be disclosed.

Resting state

The first two published AMPAR-TARP cryo-EM structures illustrated the complex of the homomeric GluA2 AMPAR with TARP γ2 (or stargazin) in an antagonist-bound state, in one case with zero, one or two stargazin-bound (Twomey et al., 2016) and in the other with four TARP subunits fully saturating the receptor (Zhao et al., 2016; **Fig. 3 B**). This divergent complex occupancy was due to the use of different protein purification detergents, n-Dodecyl-β-D-Maltopyranoside (DDM) and digitonin, the second of which better retained the complex integrity allowing TARP subunits to remain associated to the receptor during the purification procedure. In both cases, the structure of stargazin includes a TMD with four transmembrane helices (TM1 to TM4) and on the top of it an extracellular domain (ECD). Stargazin ECD is composed of two segments: the first segment connects TM1 and TM2 and comprises four beta-sheets (β1-β4) and two loops (β1-β2, or Loop1, and β4-TM2), the second one spans between TM3 and TM4 and is formed by a β-sheet (β5) and a loop (TM3-β5, or Loop2). The

main GluA2-stargazin interactions are mediated by interfaces between the transmembrane helices and in particular TM3 and TM4 of stargazin with M1 and M2 of one GluA2 subunit and with M4 of the adjacent subunit (Twomey et al., 2016; Zhao et al., 2016). This is suggesting a possible structural mechanism by which TARPs can modulate the properties of the ion channel (Milstein & Nicoll, 2008). Stargazin ECD and the receptor LBD-TMD linkers were not completely resolved in these structures, but the β4-TM2 loop and Loop2 were identified to be positioned in close proximity to the LBD and LBD-TMD linkers (especially the S1-M1 linker) of the GluA2 subunits B and D. Interestingly, the lower lobes of the B/D LBDs have been proposed to play a greater role in ion channel gating (Chen et al., 2014). An interaction of electrostatic nature was predicted to involve an electronegative acidic patch in the β4-TM2 loop of stargazin and a positively charged 'KGK motif' on the lower surface of GluA2 LBD facing stargazin (Twomey et al., 2016; Zhao et al., 2016). Functional mutagenesis experiments formerly showed that this KGK motif, highly conserved among AMPARs, is determinant of stargazin modulation of GluA2 deactivation and desensitisation (Dawe et al., 2016). The acidic patch did not appear to make direct contact with the receptor LBD, but it was speculated that lowering of the LBD layer upon activation could determine such interaction (Chen et al., 2014; Dürr et al., 2014; Zhao et al., 2016).

Active and desensitised state

Since up to date there are no structures of the AMPAR with an open ion channel, it was thought that TARP coexpression, enhancing the receptor function, might have helped capturing the open state of the receptor and gaining insights into the molecular mechanisms behind partial and full agonism. Cryo-EM structures of the GluA2-γ2 complex were thus obtained in the presence of the partial agonist kainate or the full agonist quisqualate (Jin et al., 2002) together with the positive allosteric modulator (R,R)-2b (Kaae et al., 2007; Chen et al., 2017). The structural rearrangements of the receptor LBD observed upon full and partial agonist-driven activation were in accordance with previous studies on isolated LBDs or intact receptors (Armstrong & Gouaux, 2000; Dürr et al., 2014; Chen et al., 2014), showing: extensive D1-D1 interactions, clamshell closure (by an higher degree in the presence of the full agonist) and an expansion of the D2 layer (also progressive from partial to full agonist). These movements translate into a pulling force on the M3-S2 linkers (that is greater for the B/

D subunits) leading to opening of the ion channel. However, despite the presence of TARPs, a full agonist and an allosteric modulator, from measurements of alpha carbon (Cα) atoms of opposing pore residues and molecular dynamics (MD) simulations, the ion channel resulted only partially open. Interactions between the KGK motif in the GluA2 LBD and the acidic loop of γ2 were visualised, but only for subunits B/D. The S2-M4 linkers of subunits A/C were instead found to be near the β-sheets of γ2 ECD (Chen et al., 2017). In addition, for a better understanding of the mechanisms dictating TARP modulation of AMPAR desensitisation, the GluA2-γ2 complex was incubated with quisqualate alone, which favours AMPAR desensitised state (Jin et al., 2002; Zhang et al., 2006; Twomey et al., 2017). TARPs seem to prevent large-scale LBD rearrangements upon desensitisation, with the LBD layer harbouring a 2-fold rather than 4-fold symmetry (Chen et al., 2017). This discovery was in contrast to what found with isolated iGluRs (Dürr et al., 2014; Meyerson et al., 2014; Meyerson et al., 2016), as well as with the AMPAR complex with the auxiliary subunit GSG1L (germline-specific gene 1-like) like quisqualate promoting receptor desensitisation (Twomey et al., 2017).

Another cryo-EM study made use of TARP γ2, a positive allosteric modulator (cyclothiazide, CTZ) and a full agonist (glutamate) to try to obtain the active state of the GluA2(Q) AMPAR (Twomey et al., 2017). Measurements of the pore radius and distances between Cα atoms indicated that the pore was wide open for ion conductance and this was further supported by the observation of ion conducting events through MD simulations. It was noticed that channel opening was accompanied by the outward flipping, away from the central pore axis, of Gln586 at the tip of the M2 (Q/R site). In the closed state, this residue occludes the channel, therefore serving as a lower gate below the upper gate at the bundle crossing of the M3 helices. The prominent placement of Gln586 in the ion channel pore would explain the markedly reduced conductance of AMPARs containing the R-edited GluA2 subunit, probably due to the insertion of a bulky, charged residue into the permeation pathway. Remarkably, in this active state reconstruction γ2 β4-TM2 loop, which was found to interact with the KGK motif in the GluA2 LBD of the quisqualate/ and kainate/(R,R)-2b structures (Chen et al., 2017), appears to be disordered even though juxtaposed to the receptor LBD basic patch. Thus, rather than a direct interaction in the activated state, an important role in the structural

transitions necessary for receptor activation was suggested for this TARP extracellular element (Twomey et al., 2017).

Heteromeric and native complexes

A meaningful contribution to the elucidation of the architecture of the AMPAR complex has been made by two very recently published cryo-EM structures of the heteromeric GluA1/A2 AMPAR associated with TARP γ8 (Herguedas et al., 2019), that is the most abundant AMPAR complex in the hippocampus (Tomita et al., 2003; Schwenk et al., 2014), and of native AMPARs isolated from rat brain (Zhao et al., 2019). Herguedas and coworkers revealed the subunit arrangement of the GluA1/A2_γ8 complex in the resting state (i.e. bound to the competitive antagonist NBQX). This architecture consisted of GluA2 preferentially occupying the gating-dominant pore-distal B/D positions and, by using γ8 in a tandem configuration with GluA2, two TARP-bound, which was reported to be the favoured γ8 stoichiometry (Hastie et al., 2013). γ8 structure showed close structural similarities to the current γ2 structures and, as it is the case for γ2, the three extracellular loops originating from the β-sheets (β1-β2 or Loop1, β4-TM2 and TM3-β5 or Loop2) are incomplete because of their inherent flexibility. Nevertheless, the β4-TM2 loop appeared to be positioned beneath the LBD and contacts of Loop2 with the residue Lys511 in GluA2 S1-M1 linker were detected. Furthermore, density could be seen emanating from Loop1 β1-β2 strands toward the upper lobe of GluA2 LBD, suggesting that γ8 Loop1 is able to reach up to this part of the receptor LBD. This hypothesis was functionally tested by introducing an N-glycan modification at the predicted interaction site in GluA2 LBD and γ8 modulation of GluA1/A2 desensitisation was indeed disrupted.

More or less simultaneously, through cryo-EM analysis of native AMPARs, Zhao et al. demonstrated that GluA1/A2 and GluA2/A3 heteromers are predominant AMPAR populations and that receptor subunit composition is not stochastic, confirming that GluA2 preferentially occupies the B/D positions. Western blot analysis of the brain extracts indicated the presence of γ2 and also of lower quantities of γ8, CNIH-2 and CNIH-3. Density at the positions flanking the receptor subunits B/D (B'/D') was tentatively assigned to γ2, leading to the assumption that γ2 is more inclined to reside at the B'/D' positions to modulate the receptor gating-dominant B/D subunits. On the other hand, less resolved density features at

the A'/C' positions might account for a more permissive occupancy of these sites by a broader spectrum of auxiliary subunits participating in additional functional activities.

1.4.2 Molecular basis for TARP modulation of AMPA receptor gating

Regardless of the growing knowledge that is being gathered about the structural aspects of the AMPAR complex with TARPs, there is still a lot to understand concerning the molecular interactions mediating TARP modulation of AMPAR function and in particular gating. Both extracellular and intracellular domains of the prototypical TARP stargazin have been shown to interact with AMPARs. Stargazin C-tail has been demonstrated to be necessary for AMPAR trafficking to the cell membrane (Tomita et al., 2004; Tomita et al., 2005; Turetsky et al., 2005; Bedoukian et al., 2008), synaptic targeting of AMPAR complexes (Tomita et al., 2005; Sumioka et al., 2010) and, through its membrane proximal region, also attenuation of Ca^{2+}-permeable AMPARs polyamine block (Soto et al., 2014). The TMD of stargazin, which, as noted from the cryo-EM data, encircles the membrane-spanning ion channel, has been attributed to the regulation of the ion channel properties (Zhao et al., 2016) such as the relief of intracellular polyamine block and the increase in the mean channel conductance and open probability (Tomita et al., 2005; Milstein & Nicoll, 2008; Jackson et al., 2011). Despite the ascription of some TARP functional effects to specific domains of the auxiliary proteins, the role of their extracellular loops has not been completely puzzled out yet. Unfortunately, no full disclosure has come from up to date structures of the AMPAR-TARP complex in different states, since features of these extracellular elements are poorly resolved due to their highly dynamic nature. Notably though, based on the density emanating from the β-sheets from which the TARP extracellular loops originate and structural reconstruction, the distinct cryo-EM analyses agreeingly predicted the following types of interactions: the β4-TM2 acidic loop in the TARP first extracellular segment to electrostatically interact with the basic KGK motif in the AMPAR LBD (Twomey et al., 2016; Zhao et al., 2016; Chen et al., 2017; Twomey et al., 2017; Herguedas et al., 2019), Loop2 in the TARP second extracellular segment to be in close proximity to the receptor LBD-TMD S1-M1 (Twomey et al., 2016; Zhao et al., 2016;) and S2-M4 (Chen et al., 2017) linkers and Loop1, included together with the β4-TM2 loop in the TARP first extracellular segment, to be able to span a long distance, especially for γ8, reaching up to receptor LBD layer (Herguedas et al., 2019). Interestingly, there exists some

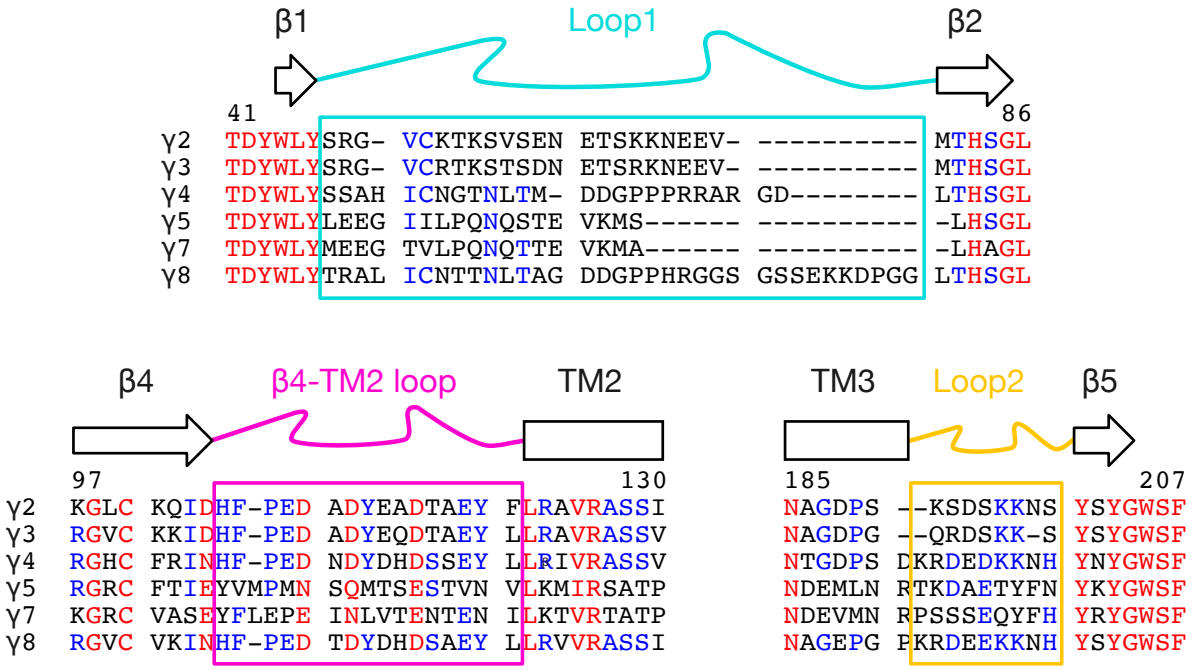

Figure 5. Sequence alignment of TARP extracellular loops. Sequence alignment of Loop1 (*cyan*), β4-TM2 loop (*magenta*) and Loop2 (*yellow*) among all TARP subtypes, showing differences in length and composition of these extracellular regions. On the top, secondary structure elements are illustrated as arrows for β-sheets, rectangles for transmembrane domain helices and lines for unstructured loops. High and low consensus residues are represented, respectively, in red and blue, whereas non-conserved residues are represented in black.

diversity in the length, composition and sequence homology of the three extracellular loops across the different TARP isoforms. The electronegative patch in the β4-TM2 loop is highly conserved between type I TARPs (γ2, γ3, γ4 and γ8) and in contrast it is not present in type II TARPs (γ5 and γ7). Similarly Loop2, which is the shortest of the three extracellular loops and whose sequence is composed by alternating charge residues, is more homologous among type I TARPs. Loop1 instead is the most extended extracellular loop and its length varies from TARP to TARP, with γ8 carrying the largest one (approximately 30 residues), followed by γ4, then γ2 and γ3 equally (approximately 20 residues) and γ5 and γ7 possessing the shortest version (approximately 12 residues) (Twomey et al., 2016). Bearing in mind the differential properties of the two TARP subgroups type I and II, but also within each TARP subgroup, it is reasonable to hypothesise a correlation between the structure of the extracellular loops and the functional effects of each TARP isoform. Studies in heterologous systems that made use of

chimeric mutants of γ2 and γ5, initially considered as a numb TARP, in which the first extracellular segment was swapped between the two auxiliary subunits, showed that this region is involved in modulation of AMPAR desensitisation and deactivation as well as kainate efficacy (Tomita et al., 2005; Turetsky et al., 2005). Further evidence was brought by another chimera study demonstrating that replacement of the first extracellular segment of γ2 with the longer one of γ4 affects AMPAR entry into desensitisation, being γ4 a stronger desensitisation blocker than γ2 (Cho et al., 2007).

It was determined that TARPs interact with the AMPAR LBD and that the receptor ATD is not required for the increase of glutamate-evoked currents and kainate efficacy in oocytes (Tomita et al., 2007). Using peptide spot arrays, a later work tested the regions of interaction between TARP γ2 and the AMPAR subunit GluA2 (Cais et al., 2014). Contact points of γ2 were identified on critical regulatory sites of GluA2 LBD, such as the upper and lower "lip" of the LBD clamshell, the LBD-TMD linker region and the alternatively spliced flip/flop cassette. Curiously though, γ2 interaction sites mapped also to the ATD of GluA2. Given that the gating properties of ATD-lacking AMPARs retained modulation by γ2, but mutations in the ATD-LBD linker region (devoid of γ2 binding on the peptide array) altered it, the authors conveyed that TARP association might trigger a reorientation of the ATD layer that is facilitated by the ATD-LBD linkers. Furthermore, from the peptide array extensive contacts were apparent on the first and second extracellular segments of both γ2 and γ8 analogously for GluA2 ATD and LBD. In the multiple cryo-EM structures of the AMPAR-TARP complex, the receptor ATD layer has often been masked due to its conformational heterogeneity, in order to improve the TARP resolution. When it has been kept for the refinement, no contact with the TARP emerged neither in the resting, nor in the active or desensitised state. Another line of evidence of TARP interaction with the AMPAR LBD has been provided by the identification of the aforementioned KGK motif, well conserved across AMPARs, in the LBD D2 lobe, the mutation of which resulted in an attenuation of GluA2 modulation by γ2 (Dawe et al., 2016).

1.5 TARPs in mutant mice and in human central nervous system disorders

1.5.1 TARPs in mutant mice

Throughout the brain, expression of the distinct type I and II TARPs is widespread, cell type-dependent, but at the same time largely overlapping. In order to learn about the complex subtype-specificity and apparent functional redundancy of TARP expression, the genetic deletion of selected TARP isoforms in mouse models has contributed a great deal.

Stargazer mice, lacking the stargazin (or γ2) protein, display a distinctive human absence epilepsy-like phenotype (Noebels et al., 1990), which at the cellular level is associated to different substrates depending on the specific brain region and neuronal type. In *stargazer* cerebellar granule neurons (CGNs), a severe loss of AMPAR-mediated synaptic and extrasynaptic currents is observed, hence indicating that stargazin is essential here for AMPAR function (Hashimoto et al., 1999; Chen et al., 2000). Purkinje cells (PCs) are another cerebellar cell type that represents the primary output of the cerebellar cortex and are innervated by inputs from both CGNs (via parallel fibres) and brainstem neurons (via climbing fibres). PCs from *stargazer* mice exhibit a very pronounced reduction in both parallel and climbing fibre-evoked synaptic transmission (Menuz & Nicoll, 2008). The reduction in PC climbing fibre responses gets worse in a conditional knockout (KO) mouse in which stargazin is deleted together with γ7, type II TARP highly enriched in this cell type, and it is accompanied by a more severe ataxia than the one of *stargazer* mice (Yamazaki et al., 2010). It thus appears that γ7 is implicated in mediating some synaptic targeting in the absence of stargazin. The relative contribution of stargazin and γ7 to cerebellar synaptic transmission and also to motor behaviour was later examined (Yamazaki et al., 2015). It was found that the loss of γ7 alone has little effect on PC climbing fibre responses, whereas the additional loss of γ7 on the background of a PC-specific deletion of stargazin results in a severe impairment of the motor behaviour, most consistent with cerebellar abnormalities and which is only moderate when removing stargazin alone. Therefore, γ7 seems capable of supporting a component of excitatory transmission in PCs, sufficient to maintain normal motor behaviour in the absence of stargazin. Additionally, cerebellar stellate cells (SCs), small molecular layer interneurons receiving parallel fibre inputs and mediating feedforward inhibition onto PCs, from *stargazer* mice show a profound deficit in synaptic but not

extrasynaptic AMPARs (Jackson & Nicoll, 2011). In contrast, AMPAR-mediated synaptic transmission in cerebellar Golgi cells (GoCs), neuronal population residing in the granule cell layer, is unaffected in *stargazer* mice and likewise in mice lacking the γ3 subunit, robustly expressed uniquely in this cerebellar cell type. Nonetheless, GoCs from γ2/γ3 double KO mice exhibit severe defects in AMPAR-mediated synaptic transmission and these animals display a worse ataxic phenotype than that of *stargazer* mice (Menuz et al., 2008). In another brain region, the thalamus, it was demonstrated that glutamatergic synapses onto inhibitory thalamic nucleus reticularis (nRT) neurons, but not onto excitatory thalamocortical relay neurons (TRNs), were disrupted in *stargazer* mice, suggesting that disinhibition in the thalamus may contribute to the *stargazer* typical seizure activity (Menuz & Nicoll, 2008).

In hippocampal CA1 pyramidal neurons the absence of stargazin alone (Hashimoto et al., 1999), as well as in combination with γ3 KO (Menuz et al., 2008), does not determine any significant impairment in AMPAR-mediated synaptic transmission. CA1 pyramidal neurons are known to express multiple TARP family members, including stargazin, γ3, γ4 and γ8, of which γ8 is the most abundant subtype. γ8 KO in this hippocampal cell type causes a modest decline in synaptic AMPARs but a great reduction in the extrasynaptic pool and an impairment in LTP but not in LTD (Rouach et al., 2005). To identify the molecular mechanisms underlying the variable density of synaptic AMPARs, that is determinant of synaptic strength, different types of Schaffer collateral/commissural (SCC) synapses in the CA1 area of the hippocampus were investigated and classified on the basis of the AMPAR density. By genetic deletion of TARP γ2 or γ8 and quantitative immunogold EM, it was revealed that AMPAR density across SCC synapses correlates with that of γ2, that potently increases AMPAR number turning low-density synapses into high-density ones. In comparison, γ8 was discovered to be essential for the low-density or basal expression of AMPARs at specific (nonperforated) synapses on CA1 pyramidal cells (Yamasaki et al., 2016). However, in γ2/γ8 double KO CA1 pyramidal neurons AMPAR-mediated synaptic transmission is diminished but not entirely abolished (Rouach et al., 2005). γ3/γ4/γ8 triple KO mice instead display defects similar to those due to the loss of γ8 by itself, while γ2/γ3/γ4 and γ2/γ3/γ8 triple KOs generate a nonviable offspring (Menuz et al., 2009).

Stargazin is the only TARP whose deletion produces a behavioural phenotype, as mice lacking γ3 (Menuz et al., 2008), γ4 (Letts et al., 2005) or γ8 (Rouach et al., 2005*;* Gleason et

al., 2015) appear behaviourally indistinguishable from littermates. Although γ4 was reported to be the only TARP expressed in the brain of neonatal rats (Tomita et al., 2003), its deletion does not preclude normal development of the animals (Letts et al., 2005). In fact, the insertion of a targeted mutation in the *Cacng4* gene leading to the absence of the γ4 protein in the homozygous mutant resulted in apparently normal mutant mice with no ataxic gait or absence seizures. Introducing though the *Cacng4* mutation onto a *stargazer* background increased the seizure activity of *stargazer* mice, thus suggesting a possible seizure suppressing role for γ4, that is only revealed when stargazin expression is compromised, and an overlapping function of the two TARP subunits *in vivo* (Letts et al., 2005).

TARP redundancy likely explains the absence of phenotypes in most single TARP KO mice, since, with the exception of the special role of stargazin in the cerebellum, it allows a single TARP subtype to be sufficient to preserve the AMPAR function in the different brain regions, types of cells and synapses.

1.5.2 TARPs in human central nervous system disorders

Representing glutamate the main excitatory neurotransmitter in the CNS, several neuronal functions, such as synaptic transmission and plasticity, rely upon glutamatergic synapses. Thus, it is not surprising that glutamatergic dysregulation is implicated in the pathogenesis of numerous psychiatric, neurodevelopmental and neurodegenerative disorders, including schizophrenia, intellectual disability and epilepsy (Miladinovic et al., 2015; Salpietro et al., 2019). These disorders are characterised by an impairment in the function of the iGluRs (AMPA, NMDA and kainate receptors) and the G-protein coupled metabotropic glutamate receptors (mGluRs), but also in the general postsynaptic organisation (involving for example mutations of the major scaffolding proteins). Emerging evidence suggests that TARPs may as well play a role in the aetiology of some of these disorders.

Homozygosity mapping, a powerful method of localising genes for autosomal recessive disorders, in consanguineous families with high frequency of epilepsy, schizophrenia and hearing loss identified, among others, stargazin gene (*Cacng2*) as a strong candidate. No exonic mutation was found in *Cacng2*, yet mutations in intronic regulatory regions might be present (Knight et al., 2008). Another study based on linkage analyses of families with a proband affected by childhood absence epilepsy, a form of idiopathic generalised epilepsy

characterised by absence seizures and spike-wave discharges, recognised γ3 gene (*Cacng3*) as a susceptibility locus. However, sequencing of the coding regions did not spot any plausible causal sequence variant (Everett et al., 2007). In addition, quantification of the expression levels of stargazin in post-mortem brain samples revealed an overexpression of stargazin in patients with schizophrenia (Beneyto & Meador-Woodruff, 2006) and bipolar disorder (Silberberg et al., 2008). Tests for genetic association demonstrated that single nucleotide polymorphisms (SNPs) of stargazin may play a role in the responsiveness to lithium (Silberberg et al., 2008; Miranda et al., 2019), treatment of choice for bipolar disorder, reported to be effective in 60-80% of cases. Interestingly, lithium response appears to be familial, consistently with a genetic base of this trait (Grof et al., 2002). Stargazin SNPs have also been associated with a subgroup of schizophrenia that occurs without deficits in sustained attention and executive function (Liu et al., 2008).

The data collected from genetic and histological studies of human patients are still not conclusive, but conceivably point toward a link between TARPs and the pathophysiology of several neurological and psychiatric disorders, suggesting that AMPAR auxiliary proteins may serve as novel pharmacological targets. Moreover, the subtype-specific distribution of TARPs in the different brain tissues could be a useful therapeutical tool to selectively target specific AMPAR populations and neuronal circuitries. For instance, the only AMPAR antagonist that has been approved to control epileptic seizures (perampanel; Hibi et al., 2012) efficaciously blocks hippocampal AMPARs but also cerebellar ones, reason why it induces dizziness and falling in patients (Zwart et al., 2014). In the attempt to avoid these motor side effects, a new drug (LY3130481) has been discovered to selectively antagonise AMPAR complexes containing TARP γ8, particularly enriched in forebrain and hippocampus, but not γ2, highly expressed in the cerebellum. In rodents, LY3130481 showed to effectively prevent multiple seizure types without motor impairment (Kato et al., 2016). This remarkable finding indicated that by targeting specific auxiliary proteins of the AMPAR it is indeed possible to identify new drugs that selectively modulate brain areas involved in disease while minimising side effects.

1.6 Transmembrane AMPA receptor auxiliary subunits beyond TARPs

As previously introduced, even though most neuronal AMPARs appear to be associated with TARPs, other types of transmembrane proteins have been found to decorate the AMPAR complex with similar (and sometimes opposing) regulatory properties to those of TARPs. A brief description of some of these AMPAR auxiliary subunits beyond TARPs follows.

1.6.1 Cornichon homologs-2 and -3 (CNIH-2 and -3)

Through a proteomic analysis, two members of the cornichon family, CNIH-2 and -3, were identified to coassemble with the majority of AMPARs in the brain (Schwenk et al., 2009). CNIH-2 and -3 posses three transmembrane domains, instead of the four of TARPs, but even if structurally not alike, CNIHs and TARPs share some functional properties (Jackson & Nicoll, 2011). In fact, similarly to TARPs, in heterologous cells CNIH-2 and -3 were shown to promote surface expression and markedly slow the deactivation and desensitisation kinetics of AMPARs (Schwenk et al., 2009). Other similarities include that CNIH-2 increases AMPAR mean channel conductance and both CNIH-2 and -3 decrease spermine affinity of GluA2-lacking AMPARs. Though, in contrast to TARPs, CNIH-2 seems to have only a modest effect on kainate efficacy (Shi et al., 2010). Besides this, CNIH-2 was displayed to counteract superactivation (or resensitisation) of AMPAR complexes mediated by TARP γ8 (Kato et al., 2010). Controversially, in the work from Shi et al. (2010) CNIH-2 and -3 were not detected on the surface of neurons and failed to modulate the decay of AMPAR-mediated synaptic currents as well as glutamate-evoked currents from nucleated patches. On the other hand, Kato et al. (2010) demonstrated that CNIH-2 synergises with γ8 to slow AMPAR synaptic currents decay in transfected *stargazer* cerebellar granule neurons. Therefore, far from the well described TARP properties, the exact role of CNIH proteins in the regulation of the AMPAR function still remains to be convincingly interpreted.

1.6.2 Cystine-knot AMPAR modulating protein of 44 kDa (CKAMP44)

The Cystine-knot AMPAR modulating protein of 44 kDa (CKAMP44) was discovered through a proteomic approach combining immunoprecipitation and mass spectrometry (von Engelhardt et al., 2010) and proven to be a component of native AMPAR complexes

(Schwenk et al., 2012). CKAMP44 has a single membrane spanning domain (Greger et al., 2017). Its expression is brain-specific and widespread at modest levels throughout the brain, with peaks in dentate gyrus granule cells (von Engelhardt et al., 2010). In these cells, CKAMP44 KO increases the paired-pulse ratio of AMPAR currents, suggesting that this protein might be involved in the attenuation of short-term plasticity at synapses in the dentate gyrus. In oocytes, it was instead shown that CKAMP44, contrary to TARPs and CNIH-2 and -3, strongly reduces AMPAR agonist-evoked currents, with no change in the total or surface AMPAR protein levels, and that the current inhibition is dependent on the concentration of the injected CKAMP44-RNA. This effect might be explained by a significantly slower recovery from desensitisation that was recorded in nucleated patches from CKAMP44-overexpressing CA1 pyramidal cells. Subsequently, three novel proteins (namely CKAMP39, CKAMP52 and CKAMP59) with high homology to CKAMP44 have been identified in the mouse genome and found to be expressed in the mouse brain and interact with AMPARs in HEK 293 cells (Farrow et al., 2015). CKAMP39 resembles CKAMP44 in slowing down AMPAR recovery from desensitisation, leading to the assumption that it might also play a role in the modulation of short-term plasticity as observed for CKAMP44 in the dentate gyrus. CKAMP59, initially thought to have no effect on channel kinetics (Farrow et al., 2015), was later demonstrated to similarly slow down AMPAR recovery from desensitisation (Schmitz et al., 2017). Short-term plasticity in CA1 pyramidal neurons was not affected by the deletion of CKAMP59, but LTP was reduced and associative learning of CKAMP59 KO mice was strongly impaired. It therefore appears that CKAMP family members may diversely contribute to different forms of synaptic plasticity in specific areas of the brain.

1.6.3 Germ cell-specific gene 1-like (GSG1L) protein

The germ cell-specific gene 1-like (GSG1L) protein was also found to be present in AMPAR complexes from mammalian brain (Schwenk et al., 2012; Shanks et al., 2012). It is a tetraspanin membrane protein with a structure reminiscent of TARPs, composed of a cytoplasmic N-terminus, four transmembrane segments, two extracellular loops and a cytoplasmic C-terminus (Shanks et al., 2012; Twomey et al., 2017). The extracellular and cytoplasmic domains though are not conserved with TARPs and the first extracellular loop (Loop1) is much longer. In heterologous cells, it was shown that GSG1L, analogously to

TARPs and CNIHs, increases AMPAR surface expression and, in parallel with CKAMP44, dramatically slows recovery from desensitisation, despite only moderately slowing desensitisation (Schwenk et al., 2012; Shanks et al., 2012; Twomey et al., 2017). Taking advantage of this effect of GSG1L, its coexpression was used to investigate the structural bases of AMPAR desensitisation in a cryo-EM study of the GluA2-GSG1L complex (Twomey et al., 2017). In hippocampal CA1 pyramidal neurons GSG1L was observed to behave as a negative modulator of AMPAR-mediated synaptic transmission (Gu et al., 2016). Specifically, this negative regulation seems to depend on the juxtamembrane region of GSG1L C-tail and on the extracellular Loop1. Furthermore, it was reported that in heterologous systems GSG1L has a dominant effect in AMPAR gating over CNIH-2, but not TARPs, by suppressing CNIH-2-induced slowing of deactivation and desensitisation while being ineffective in altering γ2 modulation (Schwenk et al., 2012; Gu et al., 2016). Finally, GSG1L KO rats exhibit deficits in LTP and in behavioural tests for object recognition (Gu et al., 2016). With the discovery of GSG1L, the existence of a new class of AMPAR auxiliary subunits has been established, with unique functional properties that diverge from the canonical ones of TARPs.

1.7 Aim of the project

With this project, we aimed at a better understanding of the molecular mechanisms through which AMPA receptors are modulated by their auxiliary subunits TARPs. By physically assembling in a complex with the AMPAR, TARPs are capable of influencing the receptor function on multiple levels: from trafficking, to synaptic anchoring, to permeability and gating. This study has primarily concentrated on the effects on gating. Each TARP subtype shows specific modulatory properties, that we hypothesised being related to the structural heterogeneity of TARP extracellular elements Loop1 (L1) and Loop2 (L2). In order to address this point, L1 and L2 of the TARP isoforms γ2 and γ8 were mutated. Thus, the functional effects of the resulting mutants on the gating of homomeric mRNA-unedited GluA2(Q) AMPARs were analysed using electrophysiology in HEK 293 cells. Based on a structural model of GluA2 in complex with γ2 and γ8, mutations were introduced also in sites of the receptor predicted to interact with TARP L2, so that site-specificity could be assessed. Subsequently, we intended to examine whether the mechanisms of TARP modulation might

be common to the distinct types of AMPAR subunits (GluA1-4) or perhaps take place in a subunit-dependent manner. With this purpose, γ2 and γ8 L1 and L2 mutants were tested on different receptor subunit compositions and in particular on homomeric and heteromeric forms of GluA1 and mRNA-edited GluA2(R) AMPARs. Finally, in the last part of this work, TARP mutants of interest were overexpressed in organotypic brain slices through single-cell electroporation, to further investigate TARP modulation in the physiological context of synaptic transmission.

2. MATERIALS AND METHODS

2.1 HEK 293 cell culture

2.1.1 HEK 293 cell solutions

Complete Minimum Essential Medium (MEM)

MEM Eagle containing Earle's balanced salt solution (EBSS), stable glutamine and 2.2 g/L $NaHCO_3$ was supplemented with 10% fetal bovine serum (FBS) and 1% of a penicillin-streptomycin solution (10,000 U/mL penicillin, 10 mg/mL streptomycin). All components were purchased from PAN-Biotech (Aidenbach, Germany). The complete medium was stored at 4 °C.

Kynurenic Acid solution

The kynurenic acid solution contained (in mM): 50 kynurenic acid sodium salt (MW 211.15; Hello Bio, Bristol, UK) and 100 $MgCl_2$ ($MgCl_2$ x $6H_2O$, MW 203.30). The components were dissolved in MilliQ H_2O. The solution was titrated to pH 7.2 and sterile-filtered using a 0.22 µm Polyvinylidene Fluoride (PVDF) filter (STARLAB, Hamburg, Germany). Aliquots were stored at −20 °C.

NBQX solution

The NBQX (2,3-Dioxo-6-nitro-1,2,3,4-tetrahydrobenzo[*f*]quinoxaline-7-sulfonamide) solution was prepared by dissolving NBQX disodium salt (MW 380.24; Abcam, Cambridge, UK) in MilliQ H_2O to 2 mM concentration. The solution was titrated to pH 7.3 and sterile-filtered using a 0.22 µm PVDF filter. Aliquots were stored at −20 °C.

2.1.2 Cell cultivation

Human embryonic kidney (HEK) 293 cells were used for overexpression of AMPARs and their auxiliary proteins TARPs for electrophysiological recordings. The cells were purchased from the Leibniz Institute DSMZ-German Collection of Microorganisms and Cell Cultures (Braunschweig, Germany). HEK 293 cell cultures were maintained in complete MEM at 37 °C and 5% CO_2 and split twice a week as follows. Before starting, sterile DPBS (PAN-

Biotech) and MEM were warmed at 37 °C and a 0.05% trypsin-0.02% EDTA solution (Biochrom, Berlin, Germany) was incubated at room temperature. The confluent cells were first washed with pre-warmed DPBS, then added with 600 µL of trypsin solution for 1-2 min at room temperature. The detached cells were collected with 5 mL of fresh, pre-warmed MEM, transferred into a 15 mL Falcon tube (Sarstedt, Nümbrecht, Germany) and centrifuged at 200 x g for 5 min. The cell pellet was resuspended in fresh, pre-warmed medium and the cells were plated in a new flask (Sarstedt) containing fresh, pre-warmed MEM with a dilution of 1:10, in order to obtain a confluence of 70-80% for the next splitting in 4-5 days.

2.1.3 Coverslips preparation

For electrophysiological experiments HEK 293 cells were plated onto 10 mm diameter glass coverslips (A. Hartenstein, Würzburg, Germany). Before usage, new coverslips were immersed in 70% ethanol inside 50 mL Falcon tubes (Sarstedt) and sonicated for 15 min. Subsequently, the coverslips were stored in 99% ethanol at room temperature. Before cell plating, the coverslips were flame-sterilised and positioned into sterile 35 mm diameter culture dishes (Thermo Fisher Scientific, Waltham, MA, USA). Each coverslip was then coated with a drop of 0.01% poly-L-lysine (Sigma-Aldrich, Merck, Darmstadt, Germany), to facilitate adhesion of the cells to the surface of the coverslip. After about 5 min incubation, the poly-L-lysine drops were removed and the coverslips were washed twice with DPBS and let dry under the hood for approximately 10-15 min. During the splitting procedure, the cells were plated on the coverslips in the culture dishes with a dilution of 1:20, to achieve a confluence of 80-90% on the day of transfection.

2.1.4 DNA transfection

In order to obtain a transient overexpression of the constructs of interest, HEK 293 cells in the culture dishes were transfected using the transfection reagent polyethylenimine (PEI) (Polysciences Europe, Hirschberg an der Bergstraße, Germany) in combination with Opti-MEM reduced serum medium (GIBCO by Life Technologies, Thermo Fisher Scientific) 24 hours after cell splitting. Sterile 1.5 mL Eppendorf tubes (Sarstedt) with 200 µL Opti-MEM and 6 µL PEI (1:3 DNA:PEI ratio) were prepared for each cell dish and briefly mixed. A total of about 2 µg DNA (1 µg/µL concentration) was added to each tube and the tubes were briefly

mixed a second time. Wild-type or mutant GluA receptors and TARPs were cotransfected with a ratio of 1:2 for GluA:γ2 and 1:5 for GluA:γ8, always up to 2 μg total DNA. When a triple cotransfection of two different GluA subunits plus a TARP species was done, the ratio used was 1:1:2 for GluA1:GluA2:γ2 and 1:1:5 for GluA1:GluA2:γ8. The DNA transfection mixtures were incubated for 20 min at room temperature, then added drop-wise to each cell dish. The cells with the DNA transfection mixtures were then put in the dedicated incubator (37 °C, 5% CO_2) for 5 h-5 h 30 min when transfected with GluA constructs alone or for 4 h-4 h 30 min when cotransfected with TARP constructs. After the incubation period, the transfection medium was removed, the cells were washed twice with DPBS and then added with 2 mL of fresh MEM/dish. Both DPBS and MEM were previously warmed at 37 °C. Ultimately, the medium in each dish was supplemented with kynurenic acid to a final concentration of 1 mM, to avoid glutamate-mediated excitotoxicity due to overexpression of glutamate receptors (Prescott et al., 2006). If TARPs were also transfected, the medium was instead supplemented with 40 μM NBQX, a stronger AMPA receptor antagonist (Sheardown et al., 1990).

2.2 Molecular biology

2.2.1 Expression vectors

The pRK5 expression vector encoding the flip splice variant of the rat GluA2 subunit unedited at the Q/R site was used for expression of homomeric GluA2(Q) receptors. An Internal Ribosome Entry Site (IRES) between the GluA2(Q) gene and the gene for the protein EGFP (Enhanced Green Fluorescent Protein) permitted the coexpression of the receptor with a fluorescent reporter (A2iQG IRES-EGFP pRK5). A similar vector was used for expression of the rat GluA1 subunit (A1iQG IRES-EGFP pRK5), whereas for the mRNA-edited GluA2(R) subunit, also from rat, we used a non-fluorescent plasmid (A2iRG pRK5). Both GluA1 and GluA2(R) were also flip variants. Rat TARP γ8 was also encoded by the pRK5 expression vector, while mouse TARP γ2 by the pRK8 and both of them together with the non-cytotoxic version of the DsRed (Discosoma Red) fluorescent protein (DsRed-Max, Addgene plasmid 21718; γ8 IRES-DsRed-Max pRK5, γ2 IRES-DsRed-Max pRK8).

2.2.2 Cloning of TARP mutant constructs

Two sets of TARP γ2 and γ8 mutants in the extracellular loops (Loop1 or L1 and Loop2 or L2) were generated through overlap PCR of the wild-type γ2 IRES-DsRed-Max pRK8 and γ8 IRES-DsRed-Max pRK5 expression vectors (**Fig. 6**). γ2/γ8 chimeras were obtained by exchanging a part of the first extracellular segment between the two auxiliary subunit isoforms. Precisely, for γ2 the amino acid sequence involved was S36-M58 and for γ8 T47-L81. These residues were instead excised and replaced with a short glycine-serine (GS) linker in the mutants with L1 deleted (γ2 ΔL1: S37-G38-S39; γ8 ΔL1: G51-S52). In γ8, a few more amino acids at the beginning (T47-L50) and at the end (P78-L81) of L1 had to be maintained in order to allow a functional expression of the protein. Given the sequence of electrically charged residues in L2 of both γ2 and γ8 we reasoned that a deletion of this region would have inevitably affected the structure of the proteins. For this reason, we instead neutralised the amino acid stretch of γ2 and γ8 L2 by substitution with another GS-linker (γ2 L2_GS:

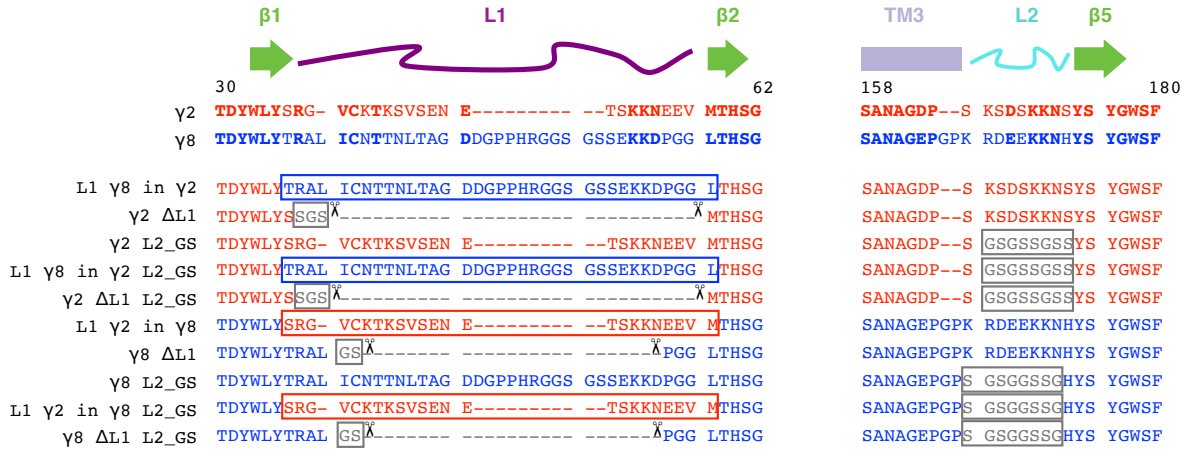

Figure 6. Mutations of TARP γ2 and γ8 extracellular loops. Sequence alignment of γ2 and γ8 wild-type and mutant constructs. Conserved residues in the wild-type sequences are marked in bold. The sequence of the extracellular regions L1 (*purple*) and L2 (*cyan*) of γ2 (*red*) and γ8 (*blue*) is aligned with the secondary structural elements on the top. Green arrows correspond to the beta sheets (β-sheets) flanking L1 (β1 and β2) and L2 (β5), while in violet a piece of transmembrane domain 3 (TM3) is represented. The part of L1 that was swapped in γ2 and γ8 chimeras is framed in blue and red respectively. Deletion of L1 is indicated by scissors and the insertions of glycine-serine (GS) linkers in correspondence of L1 and to neutralise L2 are illustrated by grey boxes. Amino acid numbering refers to the start of the γ2 polypeptide chain. From Riva et al., 2017.

G166-S173; γ8 L2_GS: S190-G197). All the mutations were confirmed by double-stranded DNA sequencing.

2.2.3 Cloning of AMPA receptor mutant constructs

GluA2 AMPA receptor mutants were also obtained via overlap PCR (**Fig. 7**). We mutated three electrically charged residues, one at the time or three in a raw, in the receptor linkers connecting the LBD to the TMD and in particular the LBD segment S1 to the TMD M1 (S1-M1 linker) and the LBD segment S2 to the TMD M4 (S2-M4 linker). In the S1-M1 linker Gln508, Lys509 and Ser510 (508QKS510) were neutralised by substitution with Gly-Ala-Gly (508GAG510), while in the S2-M4 linker Lys781, Glu782 and Lys783 (781KEK783) were neutralised by substitution with Gly-Ser-Gly (781GSG783). The numbering of the positions referred to the mature GluA2 polypeptide chain lacking 21 amino acids of the signal peptide sequence. All the mutations were confirmed by double-stranded DNA sequencing.

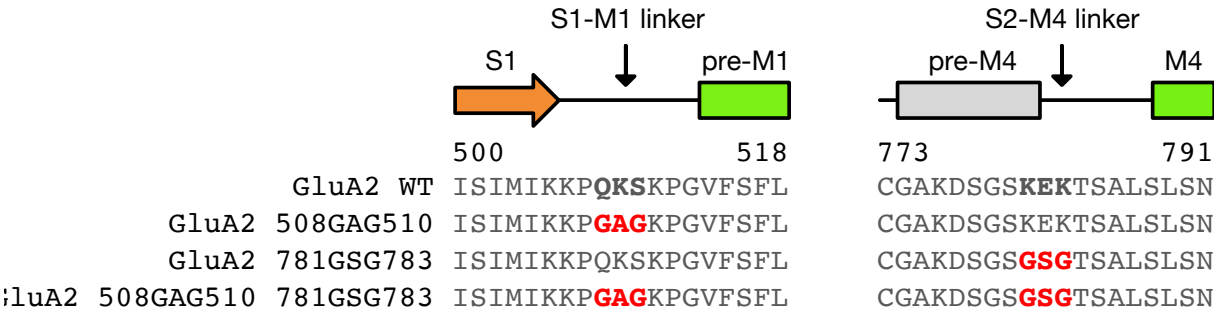

Figure 7. Mutations of GluA2 LBD-TMD linkers. Sequence alignment of wild-type and mutant GluA2 receptors in the LBD-TMD S1-M1 and S2-M4 linker regions. Gln508, Lys509, Ser510 (508QKS510, *bold*) and Lys781, Glu782, Lys783 (781KEK783, *bold*) were mutated in the S1-M1 and in the S2-M4 linker, respectively. 508QKS510 was neutralised by substitution with Gly-Ala-Gly (508GAG510, *red*), while 781KEK783 with Gly-Ser-Gly (781GSG783, *red*). Secondary structural elements are represented on the top as arrow (β-sheet), rectangles (alfa helices or α-helices) and lines (loops) and coloured according to LBD (*orange*) and TMD (*green*) domains and linker regions (*grey* and *black*). Numbering refers to the mature polypeptide chain of the rat GluA2 flip variant.

2.3 HEK 293 cell electrophysiology

2.3.1 Experimental setup

HEK 293 cell electrophysiological recordings were performed at a dedicated experimental setup. The setup core consisted of an inverted microscope (Zeiss, Oberkochen, Germany) mounted on a compressed air isolation table (TMC, Peabody, MA, USA), onto which a Faraday cage was installed to reduce external electric noise. A coverslip with cells was placed into a 35 mm glass Petri dish embedded in a plastic chamber that was positioned at the centre of the microscope stage. An AgCl pellet electrode (Warner Instruments, Hamden, CT, USA) was introduced in the bath as a ground. The microscope was equipped with a 10X and a 40X (Zeiss) objective and connected to a camera (Watec, Pine Bush, NY, USA) for image acquisition. EGFP and DsRed transfected cells were visualised thank to a fluorescent lamp light source (Excelitas Technologies, Waltham, MA, USA) and a sliding box incorporating the different excitation filters (AHF analysentechnik, Tübingen, Germany) located under the microscope objective. Inside the Faraday cage, a gravity driven perfusion system of valve-controlled containers (BD Plastipak, Wokingham, UK) and tubings (BOLA, Bohlender, Grünsfeld, Germany) was used to apply solutions to the cells. Cells were constantly perfused with extracellular solution and the outflow was collected from the bath through a low-noise pump. A costum-made four-barrel perfusion tool was also connected to the gravity driven perfusion system. This tool conducted the flow of the extracellular solutions with and without glutamate, to which the cell membrane outside-out patches on the tip of the recording pipette were exposed. To ensure the fast exchange of the patches between these two solutions, the motion of the perfusion tool was guided by a piezo-electric transducer (Physik Instrumente - PI, Karlsruhe, Germany) controlled by a piezo amplifier (PI). Patch pipettes were mounted onto an ISO-S-1.5G microelectrode holder (G23 Instruments, London, UK) attached to an headstage (Axon Instruments, Molecular Devices, San Jose, CA, USA) also contained inside the Faraday cage. The microelectrode inserted into the holder and onto which the patch pipette was put consisted of a silver wire (WPI, World Precision Instruments, Sarasota, FL, USA) coated with a drop of AgCl and regularly chlorided by dipping it into a sodium hypochlorite solution. The movement of the headstage was directed by the motorised PatchStar micromanipulator (Scientifica, Uckfield, UK). During the experimental procedure

the pipette resistance was monitored on a two channel oscilloscope (Tektronix, Beaverton, OR, USA). Through the micropipette electrode on the headstage, currents from outside-out patches were recorded in voltage clamp by an Axopatch 200B patch-clamp amplifier (Axon Instruments) using the AxoGraph software. Piezo amplifier, oscilloscope and patch-clamp amplifier were located together in a rack on a side of the microscope table. Piezo and patch-clamp amplifiers were connected to a digitiser (InstruTECH, HEKA Instruments, Holliston, MA, USA) and controlled with a computer through the AxoGraph software. The piezo command voltage was filtered at 285 Hz to reduce oscillation of the piezo transducer.

2.3.2 Solutions for electrophysiological recordings

Extracellular "Ringer" solution

The 1X extracellular or "Ringer" solution contained (in mM): 150 NaCl (MW 58.44), 0.1 $MgCl_2$ ($MgCl_2$ x $6H_2O$, MW 203.30), 0.1 $CaCl_2$ ($CaCl_2$ x $2H_2O$, MW 147.01) and 5 HEPES (MW 238.30). The components were dissolved in MilliQ H_2O. The solution was titrated to pH 7.3 with 1 M NaOH, filtered using a 0.2 μm nylon filter (Merck Millipore, MilliporeSigma, Burlington, MA, USA) and stored at 4 °C for no longer than 5-7 days.

Glutamate solution

The glutamate stock solution contained (in M): 2 L-glutamate (MW 147.13), 0.5 sucrose (MW 342.30) and 1.5 NaOH (MW 40). The components were dissolved in MilliQ H_2O. The solution was titrated to pH 7.3 with 1 M NaOH and filtered using a 0.22 μm PVDF filter (STARLAB). Stock aliquots were arranged in 1.5 mL Eppendorf tubes and stored at −20 °C. A 10 mM glutamate working solution was prepared freshly on the day of the experiment by dilution of the 2 M stock in the extracellular solution, then filtered with a 0.22 μm PVDF filter.

Intracellular solution

The intracellular solution contained (in mM): 115 NaCl (MW 58.44), 10 NaF (MW 41.99), 5 Na_4BAPTA (MW 564), 0.5 $CaCl_2$ ($CaCl_2$ x $2H_2O$, MW 147.01), 1 $MgCl_2$ ($MgCl_2$ x $6H_2O$, MW 203.30), 5 HEPES (MW 238.30) and 10 Na_2ATP (MW 551). The components were dissolved in MilliQ H_2O. The solution was titrated to pH 7.3 with 1 M NaOH and filtered

using a 0.22 µm PVDF filter. Aliquots were prepared in 1.5 mL Eppendorf tubes and stored at −20 °C. On the day of the experiment an intracellular solution aliquot was thawed.

Intracellular solution with spermine

The polyamine intracellular solution contained (in mM): 125 NaCl (MW 58.44), 10 NaF (MW 41.99), 5 Na_4BAPTA (MW 564), 0.5 $CaCl_2$ ($CaCl_2$ x $2H_2O$, MW 147.01), 0.05 spermine (MW 211.35) and 5 HEPES (MW 238.30). The components were dissolved in MilliQ H_2O. The solution was titrated to pH 7.2 with 1 M NaOH and filtered using a 0.22 µm PVDF filter. Aliquots were prepared in 1.5 mL Eppendorf tubes and stored at −20 °C. On the day of the experiment a polyamine intracellular solution aliquot was thawed.

2.3.3 Preparation of perfusion tools

To create the body of the perfusion tool, a 2 mm square four-barrel glass tubing (VitroCom, Mountain Lakes, NJ, USA) was cut in 10 cm pieces using a diamond pen. With a micropipette puller (P-1000, Sutter Instrument, Novato, CA, USA) the cut glasses were then pulled in order to obtain a thinning in the middle, ideally without breaking. Again using a diamond pen, each pulled glass was cut in the middle of the thinning and two pieces with a very thin tip (approximately 100-200 µm wide) were produced. If during the pulling the glass broke in the middle of the thinning, the cut was then refined always with the use of the diamond pen. Then, the glass tip was bent up to a 30-45 degree angle by applying heat from a metallic filament. The tip itself (approximately 0.6 cm) was cut off at the shaft to minimise dead volume in the perfusion tool, dipped into a drop of 48% hydrofluoric acid (Sigma-Aldrich) and incubated for 15-20 min to etch the glass walls. The etching time is critical for the preparation of a good perfusion tool: a too long etching time can erase the inner glass walls of the tip, whereas a too short etching time can result in a slow solution exchange at the moment of recording. After the hydrofluoric acid incubation period, the tip was abundantly washed with MilliQ H_2O, dried with compressed air and checked under the microscope. 0.320 mm diameter brown quartz capillaries with filament (Agilent Technologies, Santa Clara, CA, USA) were cut into 10-12 cm pieces and cleaned from impurities through sonication in 70% ethanol for 15 min. After sonication, the capillaries were washed with MilliQ H_2O and dried with compressed air. A drop of two-component glue (Araldite, Huntsman Advanced Materials,

Salt Lake City, UT, USA) was distributed at one edge of the capillaries, to allow the following connection with the tubings of the perfusion system at the patch-clamp setup. Four capillaries, one for each barrel, were inserted at the bottom of the piece of the perfusion tool that was not etched. At the front, the capillaries were made protrude a few mm and aligned, then the tip of the perfusion tool was mounted. Finally the two pieces were glued together using the two-component glue. Some glue was also applied at the bottom of the perfusion tool to secure the capillaries protruding at the back. The assembled perfusion tool was left to dry overnight at 42 °C and could be tested on the next day. Stored perfusion tools were kept in the same incubator at 42 °C and were repeatedly used for several experiments until getting irretrievably blocked by dust or broken glass particles or crashed by clumsy human hands.

2.3.4 Preparation of patch pipettes

1.5 mm outside diameter (OD) borosilicate thin wall capillaries with filament (Warner Instruments) were pulled with the micropipette puller (Sutter Instrument) and heat-polished to obtain a final resistance of approximately 5 MΩ.

2.3.5 Fast-perfusion outside-out patch-clamp recordings

For the characterisation of the kinetic properties of wild-type and mutant AMPAR-TARP complexes, macroscopic currents mediated by the complexes were recorded through electrophysiological patch-clamp experiments in the outside-out configuration (**Fig. 8**). Thank to the camera connected to the microscope, cells could be easily visualised on a screen and transfected cells with a decent level of expression could be identified based on the fluorescence signal. Once a transfected cell was selected, a pulled and polished micropipette was backfilled with intracellular solution using a 1 mL syringe (BD Plastipak) and a glass needle (WPI). The pipette was then mounted onto the microelectrode holder at the front of the headstage. Before introducing the pipette into the extracellular solution, positive pressure inside the pipette was applied by blowing into a silicon tubing (Deutsch & Neumann, Berlin, Germany) connected to the microelectrode holder. When the pipette tip was immersed in the bath, the pipette resistance was immediately checked on the oscilloscope (R ~ 5 MΩ). Using the micromanipulator in a fast mode the patch pipette was brought in close proximity above the cell. From this position, the micromanipulator was switched to a slow mode and as the

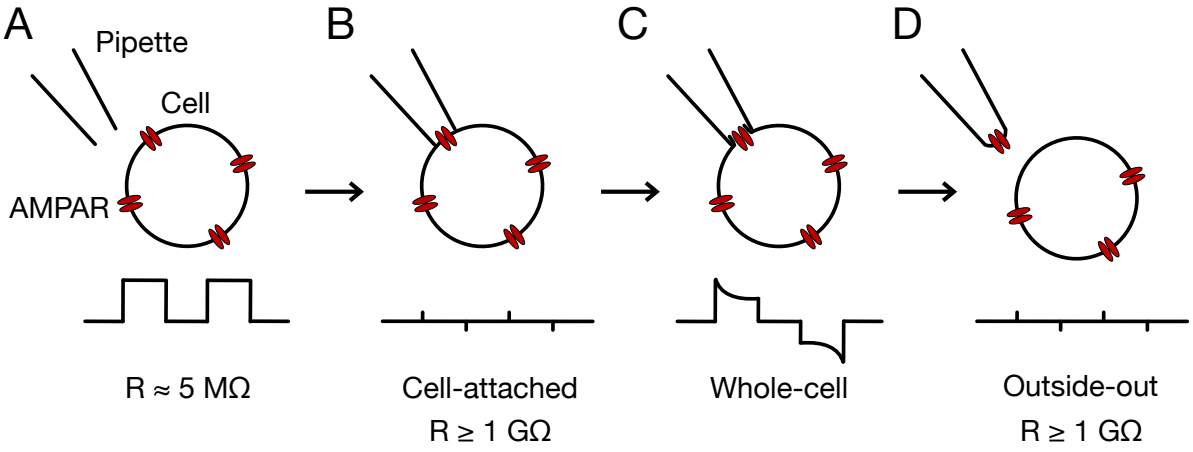

Figure 8. Outside-out patch-clamp technique. Schematic representation of the steps to obtain an outside-out patch for HEK 293 cells recordings. The patch pipette, an AMPAR-transfected cell and the pipette resistance as seen on the oscilloscope are depicted for each step. (**A**) The patch pipette is immersed in the bath solution ready to approach the cell. At this stage the pipette resistance following a test pulse is usually about 5 MΩ. (**B**) An increase in the pipette resistance indicates that the patch pipette is in contact with the cell membrane, leading to the formation of a gigaseal (R ≥ 1 GΩ) and to a cell-attached configuration. (**C**) Application of a gentle negative pressure results in the rupture of the plasma membrane reaching a whole-cell configuration. (**D**) By delicately pulling the patch pipette away from the cell, the plasma membrane reseals onto itself and an outside-out patch, with the AMPAR extracellular domains exposed to the bath solution, is finally pursued.

pipette got closer to the cell membrane an increase in the pipette resistance was carefully monitored on the oscilloscope. Releasing the positive pressure helped to increase the resistance and the formation of a gigaseal (R ≥ 1 GΩ) between the pipette tip and the cell membrane (cell-attached configuration). The plasma membrane was then broken by application of a gentle negative pressure to the pipette (whole-cell configuration). By slowly moving the pipette upward, a piece of membrane was pulled away from the cell and, when successful, the membrane closed onto itself producing an outside-out patch where the outer layer of the membrane was still on the outside. The patch on the tip of the pipette was positioned at the interface between the extracellular solutions with and without glutamate flowing through the barrels of the perfusion tool. Typical 10-90% solution exchange times were faster than 300 μs, as measured from junction potentials at the open tip of the patch

pipette. To measure AMPAR-mediated currents, patches were voltage-clamped at a holding potential of −60 mV. When TARPs were coexpressed, recordings were instead performed at +50 mV and the patch pipette was filled with polyamine (PA, i.e. spermine) intracellular solution. Since at +50 mV unTARPed AMPARs are mostly blocked by intracellular PAs, currents mediated by AMPAR-TARP complexes, and not by a complexed/non-complexed mixture, could be isolated. Currents were usually low-pass filtered at 5 kHz with the Axopatch amplifier.

2.4 Data analysis

2.4.1 Analysis of HEK 293 cell electrophysiology

The analysis of the electrophysiological recordings was done using the Axograph software. At least five outside-out patches from minimum three different transfections were recorded for each experimental condition. In case recordings were particularly challenging, that is, worse than 1 patch in 20 giving an acceptable recording, at least three patches were collected. Where less than three patches were gathered it indicates that recordings still need to be completed. Usually glutamate jumps were repeated for 20-30 episodes and then an average trace was produced for the analysis. Data were only excluded if the patches were excessively unstable, showed severe current rundown or the solution exchange was slower than 500 µs. Results were expressed as mean ± standard error of the mean (SEM) and statistical significance was assessed with a two-tailed Student's *t*-test.

Desensitisation and deactivation

To measure AMPAR desensitisation, 10 mM glutamate was applied to the outside-out patches for 500 ms. The rate of desensitisation (k_{des}) and the steady-state current (I_{ss}) were obtained by fitting the traces with a two-exponential (when necessary three-exponential) function from the activation peak to the current decay, including an added constant accounting for the steady-state current. The desensitisation time (t_{des}) was expressed as a weighted mean of two (or three) components (**Equation 1**), while I_{ss} was calculated as a percentage of the peak current (**Equation 3**). The deactivation time (t_{deact}) was determined by fitting the traces with a tri-exponential function from the activation peak to the current decay, without the steady-state

current constant, following a 1 ms pulse of 10 mM glutamate. t_{deact} was expressed as a weighted mean of three components (**Equation 4**). Time constants (ms) were then converted into rate constants (s^{-1}; k_{des} and k_{deact}) by dividing 1000 by the time constants (**Equation 2 and 5**).

Equation 1:

$$t_{des} = \frac{Amplitude_1 \times tconstant_1 + Amplitude_2 \times tconstant_2}{Amplitude_1 + Amplitude_2} \times 1000\ (ms)$$

Equation 2:

$$k_{des} = \frac{1000}{t_{des}}\ (s^{-1})$$

Equation 3:

$$I_{ss} = \frac{Added\ constant}{Peak\ current}\ \%$$

Equation 4:

$$t_{deact} = \frac{Amplitude_1 \times tconstant_1 + \ldots + Amplitude_3 \times tconstant_3}{Amplitude_1 + \ldots + Amplitude_3}\ (ms)$$

Equation 5:

$$k_{deact} = \frac{1000}{t_{deact}}\ (s^{-1})$$

Current-voltage relationship

Current-voltage (I-V) curves were obtained by measuring the peak current amplitude in response to different voltage steps (from −100 to +120 mV) and normalising each amplitude to the value at −80 mV. To prove the effect of TARP association on inwardly rectifying AMPARs in the presence of intracellular PAs, the rectification index was calculated as a ratio between the peak current at +60 mV and the peak current at −60 mV (RI (+60/−60); **Equation 6**). Conductance-voltage (G-V) curves were also derived from the I-V recordings,

by dividing the peak amplitudes by the corresponding voltage subtracted of the reversal potential (E_{rev}; **Equation 7**) and normalising to the value at −80 mV.

Equation 6:

$$RI\ (+60/-60) = -\frac{Peak\ current_{+60mV}}{Peak\ current_{-60mV}}$$

Equation 7:

$$G = \frac{Peak\ current}{V - E_{rev}}$$

Superactivation

Superactivation of AMPAR-TARP complexes was measured through 7 s application of 10 mM glutamate and determined as the excess of steady-state current following the trough of desensitisation, normalised to the peak current (**Equation 8**). In the equation, *Amplitude* 1 defines the steady-state current excess. Superactivation could also be detected by exposure of the outside-out patches to trains of short (1 ms) glutamate pulses at different frequencies (10, 20 and 50 Hz). The peak current increase over time was visualised by normalising each peak response to the first peak of the train (I_p/I_{p1}). The charge transfer increase was calculated by dividing the integral of the whole train by the first peak amplitude.

Equation 8:

$$Superact = -\frac{Amplitude\ 1}{Peak\ current}\ \%$$

2.4.2 Calculation of abundance of tripartite AMPA receptor-TARP complexes

In the triple transfection of two AMPAR types, such as GluA1 and GluA2(R), together with a TARP subunit, it is not possible to isolate tripartite AMPAR-TARP complexes. In fact, 1 mono-complex (GluA1), 3 binary complexes (GluA1/A2(R), GluA1/TARP and GluA2(R)/TARP) and the intended triple complex (GluA1/A2(R)/TARP) can all traffic to the plasma membrane. The mono-complex formed by homomeric GluA2(R) receptors alone is quite stably retained in the ER and therefore very unlikely to express at the cell surface. To account

for the side products of the triple transfection, a statistical model was created, first in Excel and subsequently in Python (see **Appendix**), to predict the abundance of tripartite GluA1/A2(R)/TARP complexes. This model was realised with the kind help of Prof. Andrew Plested, the supervisor and first reviewer of the present dissertation. Different abundances were presumed for each of the GluA1, GluA1/A2(R) and GluA1/TARP species. For GluA2(R)/TARP instead a range of abundances was tested, based on the assumption that this condition might prevail in the tripartite complexes either due to asymmetries in trafficking or to a real gating-dominant effect. Experimentally measured properties of rectification index, steady-state current and desensitisation rate of the mono- and binary complexes were used to estimate the properties of the tripartite complex. For each of these properties then, the weighted sum calculated for the guessed abundances was compared with the measured properties of the responses in the triple transfection condition. By normalising errors, the contours were combined to produce a single, unambiguous estimate of the triple complex abundance and properties for the super TARP mutant, while for wild-type γ2 in the tripartite complexes, a less definitive answer was obtained.

2.5 Organotypic mouse brain cultures

2.5.1 Organotypic slice solutions

Dissection medium for organotypic slices

The dissection medium for organotypic mouse brain slices contained (in mM): 0.5 $CaCl_2$ ($CaCl_2$ x $2H_2O$, MW 147.01), 2.5 KCl (MW 74.55), 0.66 KH_2PO_4 (MW 136.09), 2 $MgCl_2$ ($MgCl_2$ x $6H_2O$, MW 203.30), 0.28 $MgSO_4$ ($MgSO_4$ x $7H_2O$, MW 246.47), 50 NaCl (MW 58.44), 0.85 Na_2HPO_4 (Na_2HPO_4 x $12H_2O$, MW 358.14), 25 D-glucose (MW 180.16), 2.7 $NaHCO_3$ (MW 84.01), 175 sucrose (MW 342.30) and 2 HEPES (MW 238.30). The components were dissolved in MilliQ H_2O. The solution was titrated to pH 7.3 and added with a 0.5% phenol red solution (Sigma-Aldrich) to a final concentration of 10 µg/mL. Osmolarity was checked to be ~ 330 mOsm. The solution was sterile-filtered using a bottle-top vacuum filter system with a 0.2 µm nylon membrane (Corning, Sigma-Aldrich) and stored at 4 °C.

Mouse slice culture medium

Minimum Essential Medium (MEM) without glutamine (Thermo Fisher Scientific) was added with: 15% heat-inactivated horse serum (GIBCO, Thermo Fisher Scientific), 1X B27 supplement from a 50X stock solution (GIBCO), 25 mM HEPES (MW 238.30) from a 1 M stock solution at pH 7.3, 3 mM L-glutamine from a 200 mM stock solution (Sigma-Aldrich), 2.8 mM $CaCl_2$ ($CaCl_2$ x $2H_2O$, MW 147.01) from a 1 M stock solution, 1.8 mM $MgSO_4$ ($MgSO_4$ x $7H_2O$, MW 246.47) from a 1 M stock solution, 0.25 mM ascorbic acid (MW 176.12; Sigma-Aldrich) from a 50 mM stock solution and 6.5 g/L D-glucose (MW 180.16). The solution was sterile-filtered using a bottle-top vacuum filter system with a 0.2 µm nylon membrane and stored at 4 °C.

K^+-based intracellular solution

The potassium (K^+)-based intracellular solution contained (in mM): 135 CH_3KO_3S (MW 134.19), 4 NaCl (MW 58.44), 2 $MgCl_2$ ($MgCl_2$ x $6H_2O$, MW 203.30), 10 HEPES (MW 238.30), 2 ATP disodium salt (MW 551.14), 0.3 GTP sodium salt (MW 523.18), 0.06 EGTA (MW 380.35) and 0.01 $CaCl_2$ ($CaCl_2$ x $2H_2O$, MW 147.01). The components were dissolved in MilliQ H_2O. The solution was titrated to pH 7.2-7.3 with KOH and osmolarity was checked to be ~ 300 mOsm. The solution was sterile-filtered using a 0.22 µm PVDF filter. Aliquots were prepared in 1.5 mL Eppendorf tubes and stored at −20 °C. On the day of the experiment a K^+-based intracellular solution aliquot was thawed.

HEPES-based artificial cerebrospinal fluid (ACSF)

The HEPES-based ACSF solution contained (in mM): 145 NaCl (MW 58.44), 2.5 KCl (MW 74.55), 10 HEPES (MW 238.30), 1 $MgCl_2$ ($MgCl_2$ x $6H_2O$, MW 203.30), 2 $CaCl_2$ ($CaCl_2$ x $2H_2O$, MW 147.01) and 10 D-glucose (MW 180.16). The components were dissolved in MilliQ H_2O. The solution was titrated to pH 7.3 with 10 M NaOH and osmolarity was checked to be ~ 310 mOsm. The solution was sterile-filtered using a bottle-top vacuum filter system with a 0.2 µm nylon membrane and stored at 4 °C.

2.5.2 Preparation for mouse brain slice dissection

Organotypic slice cultures were prepared from the hippocampi of wild-type C57BL/6 mouse pups (postnatal day 6 or P6 to P9). Inside a laminar flow cabinet, 1 mL of sterile mouse slice culture medium was put into the wells of a 6 well plate (Sarstedt), calculating 2 wells per animal. With sterile forceps, a PTFE (polytetrafluoroethylene) cell culture insert with 0.4 µm pore size (Millipore, Merck) was placed into each well of the plate with culture medium. Four quarters of a previously cut 13 mm diameter PTFE membrane with 0.45 µm pore size (Millipore) were positioned onto each cell culture insert, avoiding contact between each other or with the edge of the insert. The 6 well plate was then incubated for about 1 h at 34 °C and 5% CO_2 in the slice incubator. Meanwhile, a razor blade was washed with 70% ethanol to remove traces of glue and inside the cabinet immersed into a 60 mm sterile Petri dish (VWR, Avantor, Radnor, PA, USA) filled with sterile dissection medium. The cabinet bench and the stereoscopic microscope (Zeiss) and the McIlwain Tissue Chopper (Campden Instruments, Loughborough, UK) inside the cabinet were cleaned with ethanol. The dissection tools were also cleaned with ethanol and positioned inside the cabinet. UV light was applied to the cabinet for 10-15 min. Before starting the dissection, three 35 mm sterile Petri dishes were filled with 5 mL each of dissection medium and one of them was added with a cut piece of a 0.2 µm nylon membrane (Millipore). The Petri dishes with the dissection medium were kept in the fridge until the start of the dissection. The razor blade, still wet with dissection medium, was installed onto the McIlwain Tissue Chopper and a P1000 pipette tip was cut at its extremity and connected to a rubber pipette dropper.

2.5.3 Mouse brain slice dissection

The head of the mouse was cut outside the laminar flow cabinet, sprayed with ethanol and transferred inside the cabinet into the first Petri dish filled with cold dissection medium. With one hand, tweezers were placed in a clamped position to hold the head still and with small scissors in the other hand the skin of the head was cut from the neck to the base of the muzzle and then removed with tweezers. Always clamping the head, using Vannas scissors an incision was made in the middle of the skull from the neck to the forehead and from the forehead to the sides. With curved Iris forceps, the two open skull shreds were ripped to make access to the brain. The Iris forceps were made slide under the brain from the cerebellum to

the eyeballs side; the brain was extracted from the skull and put into the second Petri dish with cold dissection medium and the piece of nylon membrane. The brain was placed onto the membrane to help the further dissection steps and clamped positioning the tweezers in correspondence of the cerebellum. Under the stereomicroscope, with a Wecker spatula the two brain hemispheres were separated at the top but left attached at the bottom. One of the hemispheres was delicately flipped over on a side on the membrane and always with the use of the spatula the first hippocampus was isolated. The same was repeated for the other hemisphere and the second hippocampus. The two isolated hippocampi were collected from the dissection medium in the Petri dish using the pipette dropper with the cut P1000 pipette tip and transferred onto a plastic plate located on the stage of the McIlwain Tissue Chopper. The thickness of the slices was set to 350 μm. Approximately 10 slices were produced from each hippocampus. By sprinkling the plate with dissection medium using the cut pipette tip and the pipette dropper, the slices were made slide from the plate into the third Petri dish with dissection medium. The slices were separated from each other by gentle resuspension with the P1000 tip and the pipette dropper. Under the microscope, eight slices were selected from the total and, again using the cut pipette tip and the pipette dropper, plated one by one on the cut PTFE membrane quarters on the cell culture inserts (4 cut membranes for one insert, two inserts per animal). The surplus of dissection medium was removed from the slices with a P200 pipette. Finally, the 6 well plate containing the hippocampal slices was incubated in the slice incubator.

2.5.4 Organotypic slice cultivation

Organotypic hippocampal slice cultures were maintained in a dedicated incubator set to 34 °C and 5% CO_2. The slices were fed twice a week (on Monday and Friday) by replacing most of the old culture medium with new pre-warmed culture medium. From the first change, the culture medium was supplemented with 10 μg/mL gentamicin (GIBCO) from a 50 mg/mL stock solution in MilliQ H_2O. The cultures were kept for a period of about 3 weeks.

2.6 Single-Cell Electroporation (SCE) in organotypic slices

2.6.1 Solutions for SCE

K^+-based intracellular solution

Same as for organotypic slice cultures (see paragraph 2.5.1).

HEPES-based artificial cerebrospinal fluid (ACSF)

Same as for organotypic slice cultures (see paragraph 2.5.1).

Polyethylene glycol (PEG)-$MgCl_2$ solution

30% PEG 8000 (Sigma-Aldrich) was dissolved in a 30 mM $MgCl_2$ ($MgCl_2$ x $6H_2O$, MW 203.30) solution in MilliQ H_2O by stirring at room temperature for about 30 min. Any PEG that did not dissolve could be dissolved by incubation at 37 °C with periodic mixing. The solution was then sterile-filtered using a 0.22 μm PVDF filter and stored at room temperature.

2.6.2 DNA preparation for SCE

Plasmid DNA was precipitated with PEG for purification before being injected in neurons during SCE. 0.3 μg/μL DNA aliquots were prepared in Eppendorf tubes by dilution of 1 μg/μL DNA working aliquots with endotoxin-free Tris-EDTA (TE) buffer from a DNA extraction kit (Macherey-Nagel, Düren, Germany). 50% volume of PEG-$MgCl_2$ solution was added to the Eppendorf tubes and the tubes were mixed by flicking several times. The tubes were then centrifuged for 15 min at 15,000 x g and room temperature to let the DNAs precipitate in pellets. The supernatant was discarded from each tube and the DNA pellets were washed with 70% ethanol by centrifuging for 5 min at 15,000 x g and room temperature. The supernatant was discarded again and the DNA pellets were let dry inside a laminar flow cabinet. After checking that the ethanol had completely evaporated, the DNA pellets were redissolved in the same initial volume of TE buffer by heating at 65 °C and repeatedly flicking the tubes. Finally, the DNAs were quantified using a NanoDrop spectrophotometer (Thermo Fisher Scientific). 0.3 μg/μL PEG-precipitated DNA aliquots were kept at 4 °C and used multiple times up to 2 weeks from the preparation.

2.6.3 Setup preparation for SCE

Organotypic hippocampal slices were transfected with TARP DNA constructs using Single-Cell Electroporation or SCE at 5-10 days in vitro (DIV). SCE is a method to inject DNA into single cells using a voltage stimulus delivered to the cell membrane through a patch pipette. It has the advantage of targeting individual cells for specific modifications. On the day of the electroporation, a freshly thawed K^+-based intracellular solution aliquot and the 0.3 µg/µL PEG-precipitated DNA aliquots were centrifuged for 15 min at 15,000 x g and 4° C. The DNAs were then diluted with intracellular solution to a final concentration of 10-30 ng/µL, taking the volumes for the dilution from the top of the respective aliquots. Generally, 100-200 µL of intracellular solution was a sufficient volume for an SCE experiment. The DNA-containing intracellular solutions were centrifuged a second time for 15 min at 15,000 x g and 4° C and kept on ice during the whole SCE procedure. Since the DsRed fluorescence signal expressed with the TARP constructs was not always easily detectable after SCE, an EGFP plasmid (pEGFP-N1) was sometimes cotransfected to help the visualisation of TARP transfections. In this case, EGFP and TARP DNAs were diluted into the same intracellular solution to a final concentration of 30 and 10 ng/µL respectively (40 ng/µL total DNA concentration). While preparing the DNA dilutions, approximately 30 mL of HEPES-based ACSF were incubated for about 1 h at 34° C in the slice incubator. SCE took place at an electrophysiology patch-clamp setup only devoted to organotypic slice experiments. All the surfaces of the setup that might have been a source of contamination for the slices (i.e. recording chamber, 60X water immersion objective, ground pellet electrode, slice anchor and tweezers) were cleaned with 70% ethanol and let dry. To increase electroporation efficiency, the silver wire electrode contained inside the patch pipette was regularly chlorided before each session. The silver wire was first rubbed with sandpaper, then dipped into bleach (Merck) for about 30 min and afterwards rinsed with MilliQ H_2O.

2.6.4 SCE procedure

1.5-2 mL of pre-warmed ACSF were put into the recording chamber. If the ethanol used to clean before had not completely dried, the chamber was first rinsed with ACSF. No perfusion was applied to the extracellular solution. A quarter of PTFE membrane with an organotypic hippocampal slice was collected from a 6 well plate in the incubator and with tweezers placed

into the chamber bath. A slice anchor was used to secure the slice in position. 1.5 mm OD borosilicate standard wall capillaries with filament (WPI) were pulled to a final resistance of 8-10 MΩ and backfilled with approximately 10 µL of DNA-containing intracellular solution. The pulled pipette was mounted onto the microelectrode holder and, through a silicon tubing connected to the holder, positive pressure was put inside the pipette. An upright microscope (Scientifica, Zeiss and Rapp OptoElectronic, Wedel, Germany) was connected to a camera (Jenoptik, Jena, Germany) and the image was displayed on a computer screen. The slice was observed with a 4X objective (Olympus, Shinjuku, Tokyo, Japan) and the hippocampal area CA1 was selected. With a 60X water immersion objective (Olympus), layers of CA1 pyramidal neurons were visualised. Neurons to be electroporated were chosen not immediately at the surface of the slice, but one or two cell layers underneath. With a PatchStar micromanipulator (Scientifica), the patch pipette was moved close to the slice surface and before entering the tissue, the pressure inside the pipette was slightly increased. Once inside the slice, cells of interest were approached under visual guidance. When approaching a cell with the pipette, on the appearance of a small dimple on the plasma membrane, pressure was released to allow the formation of a loose seal and the voltage stimulus was applied as follows: 50 pulses at 100 Hz frequency, with −12 V amplitude and 0.5 ms width. The voltage stimulus was delivered through an Axoporator 800A Electroporation System (Axon Instruments, Molecular Devices). After electroporating the first cell, the pipette was retracted, light positive pressure was reapplied and the next cell was approached. If cell approach was performed correctly (i.e. not too invasively), after delivering the stimulus the aspect of the cell appeared unchanged. Otherwise, the cell melted down and subsequently died, as noted by the plasma membrane being pulled away from the cell together with the pipette. About 10 cells per slice were electroporated using the same patch pipette, unless the pipette got clogged and needed to be changed. Each slice was maintained in the chamber for no longer than 30 min and then returned to the incubator in the culture medium supplemented with the antibiotic to prevent contamination. 24 hours later, SCE was checked by looking for TARP-DsRed or EGFP expressing cells. Sometimes to make sure that all the connections and the settings were correct, 20 µM Alexa 568 die (Thermo Fisher Scientific) was dissolved in the intracellular solution and with a source of blue light during the delivery of the SCE protocol it could be

seen diffusing in the neuron almost instantaneously. In order to achieve a good electroporation yield it is fundamental to have healthy organotypic slices.

3. RESULTS

3.1 Model of the AMPA receptor complex with TARPs

3.1.1 Comparison of a GluA2-γ8 model with the GluA1/A2_γ8 complex structure

In order to provide a structural basis for the electrophysiological functional experiments, a model of the AMPAR subunit GluA2 in complex with TARP γ2 and γ8 was created (Riva et al., 2017). The model was built by first modelling γ2 and γ8 on the crystal structure of the related protein claudin15 (PDB code: 4P79) and then superposing them onto the γ2 chains in one of the published cryo-EM structures of the GluA2-γ2 complex (PDB code: 5KK2; Zhao et al., 2016). TARP extracellular Loop1 (L1) and Loop2 (L2) have not been well-resolved in structures to date, most likely due to the highly dynamic nature of these elements (Twomey et al., 2016; Zhao et al., 2016; Twomey et al., 2017; Chen et al., 2017; Twomey et al., 2017; Herguedas et al., 2019; Zhao et al., 2019). Nevertheless our model also necessarily included L1 (in order to understand its possible structure) and showed that as a function of its length, especially for γ8, it can reach up to the receptor LBD adopting different conformations, consistent with it being a flexible element. The shorter L2 instead was predicted by the model to engage four times in the same way the linkers connecting the receptor LBD and TMD and in particular the S1-M1 and the S2-M4 linkers. Therefore, a range of TARP extracellular loop interaction sites with the AMPAR LBD and LBD-TMD linkers seemed physically plausible, whereas the receptor ATD was ruled out because L1 and L2 appeared too short to be capable of making contact with it. Recently, a new cryo-EM structure has been published elucidating the architecture of the heteromeric GluA1/A2 AMPAR in complex with γ8 (Herguedas et al., 2019). More specifically, in order to respect what is thought to be γ8 preferential stoichiometry, Herguedas et al. originated a two-TARP complex by coexpressing GluA1 with GluA2 in tandem with γ8 (GluA1/A2_γ8) and then trapped it in the resting state using the AMPAR antagonist NBQX. The overall resolution of the full-length GluA1/A2_γ8 complex was 6.3 Å (PDB code: 6QKZ), but after masking the ATD layer a model of the LBD/TMD/ TARP sector with a 4.4 Å resolution was produced (PDB code: 6QKC). At this resolution, as it is the case for the other current γ2 structures, L1 and L2 are incomplete because of their inherent flexibility. However, on a closer look at the GluA1/A2_γ8 structure, γ8 L1 is

expected to reach the upper (D1) lobe of the receptor LBD, similarly to what formerly predicted by our GluA2-TARP model. Moreover, again in coherence with our model, L2 seems to make contact with the LBD-TMD linkers and especially with the residue Lys511 in GluA2 S1-M1 linker. When superposing our GluA2-γ8 model with the GluA1/A2_γ8 complex, the two structures appear quite alike except for a small shift in the general positioning (**Fig. 9 A**). The superposition of the respective γ8 subunits alone revealed a good alignment of the transmembrane domains and of the β-sheets from which the extracellular loops emanate, resulting in a root-mean-square deviation (RMSD) of 1.5 Å with 105 Cα atoms aligned (**Fig. 9 B**). The alignment of a single receptor subunit together with one γ8 subunit from our GluA2-TARP model and from the GluA1/A2_γ8 structure also generated a quite low RMSD (1.7 Å, with 478 Cα atoms aligned), confirming a very close resemblance of the two structural models (**Fig. 9 C**). Comparing though L2 interacting regions, according to our model the residue Lys511 in GluA2 S1-M1 linker is located too deep to be effectively able to touch γ8 L2 and the residues directly above, Gln508, Lys509 and Ser510, were instead identified as more likely interacting sites.

3.2 TARP γ2 and γ8 extracellular loop mutants

3.2.1 Membrane expression of TARP mutants

To test the AMPAR-TARP interaction sites predicted by our structural model and investigate the role of TARP extracellular loops in controlling AMPAR gating, two series of chimeric and deletion mutants of γ2 and γ8 in L1 and L2 were made. Mutating the extracellular loops of these auxiliary subunits did not prevent their expression at the plasma membrane of HEK 293 cells, as assessed in the first place by a decent level of fluorescence of TARP-DsRed transfected cells. Only the γ8 construct with L1 entirely deleted did not show expression, but after reintroducing a few more amino acids in γ8 L1 (see **Materials and methods**) a functional mutant protein was produced (γ8 ΔL1).

3.2.2 Association with GluA2(Q) AMPA receptors

For the purpose of studying the modulatory properties of TARP mutants on AMPAR gating, primarily proper assembly of AMPAR-TARP complexes has to be validated. Recording of

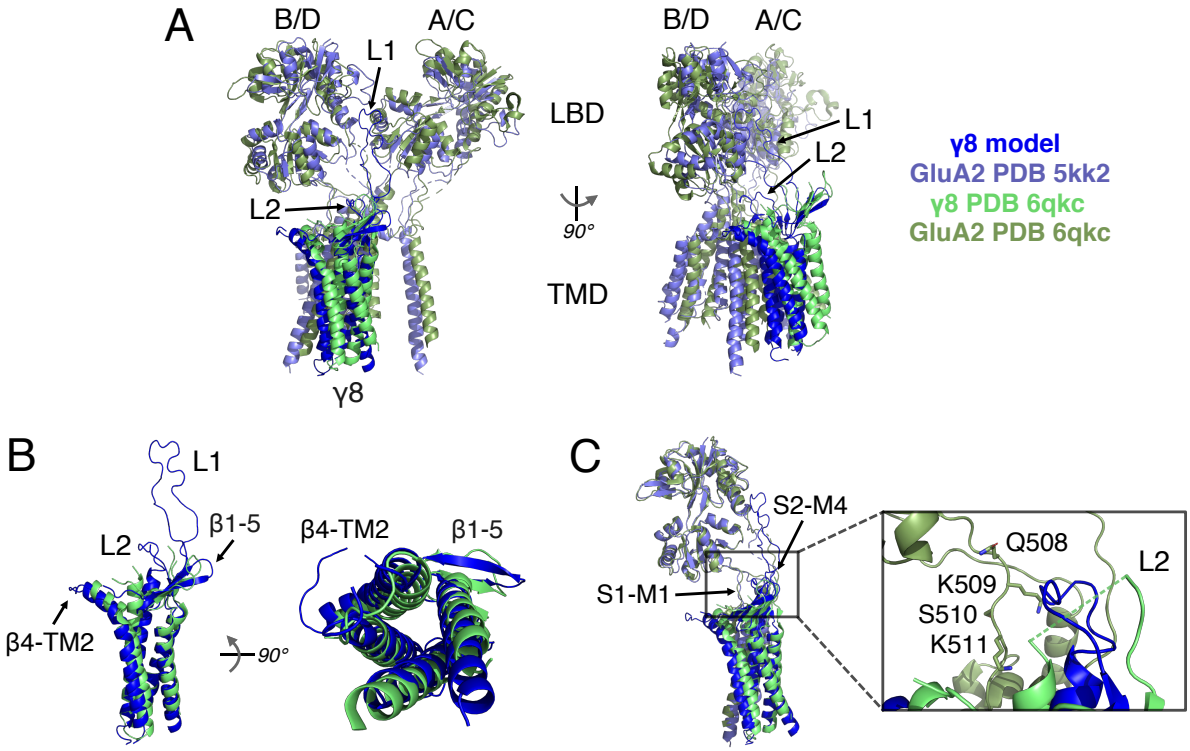

Figure 9. γ8 interactions in a GluA2 complex model and in the GluA1/A2_γ8 cryo-EM structure. (**A**) Front (*left*) and side (*right*) view of the superposition of a structural model of the homomeric GluA2 AMPAR in complex with TARP γ8 (*indigo* for GluA2 and *bright blue* for γ8; Riva et al., 2017) with the cryo-EM structure of the heteromeric GluA1/A2_γ8 complex without the receptor ATD (*dark green* for GluA1/A2 and *bright green* for γ8; PDB code: 6QKC; Herguedas et al., 2019). For simplicity, the receptor is shown as a dimer of equivalent A/C and B/D subunits, with one γ8 subunit associated in the B'/D' position. In the 6QKC structure (*green*), γ8 extracellular loops are not completely resolved. γ8 L1 and L2 were modelled in the GluA2-γ8 model (*blue*) and they are marked here based on it. (**B**) To the left, front view of the alignment of the γ8 subunits from the GluA2-γ8 model (*bright blue*) and the GluA1/A2_γ8 structure (*bright green*) (RMSD = 1.5 Å, with 105 Cα atoms aligned), illustrating the predicted positions of the extracellular loops L1, L2 and β4-TM2 and of the β-sheets β1-β5. To the left, bottom view displaying the alignment of the transmembrane domains and the β-sheets of the two γ8 subunits. (**C**) Alignment between single B/D receptor subunits associated with one γ8 subunit (RMSD = 1.7 Å, with 478 Cα atoms aligned) with a close-up on the receptor S1-M1 and S2-M4 linker region (from the 6QKC structure, *dark green*). The residues Gln508, Lys509 and Ser510 in the S1-M1 linker were identified in the GluA2-γ8 model as γ8 L2 (*bright blue*) likely interacting sites, while according to the GluA1/A2_γ8 structure L2 (*bright green dotted line*) would make contact with Lys511.

polyamine (PA) block sensitive mRNA-unedited GluA2(Q) homomeric receptors at +50 mV in the presence of 50 μM intracellular spermine permitted the isolation of currents mediated by GluA2(Q)-TARP complexes. In fact, at +50 mV non-complexed GluA2(Q) receptors are almost completely blocked by intracellular PAs. Normalised conductance-voltage (GV) curves of GluA2(Q) receptors in complex with wild-type γ2 or γ8 showed relief of PA block in respect to GluA2(Q) receptors without TARPs (**Fig. 10 A**). Notably, the GV relationships of GluA2(Q) complexes with γ2 and γ8 L1 and L2 mutants overlapped with those of GluA2(Q) complexes with the respective wild-type TARP (**Fig. 10 B-E**). Therefore, no impairment in AMPAR-TARP association due to the mutation of TARP extracellular loops was assumed. This could also be demonstrated by the rectification indices, calculated as the ratio between the peak current at +60 and at −60 mV (*RI* (+60/−60)). The rectification index is thus lower for PA-blocked unTARPed receptors, compared to receptors relieved by the presence of TARPs. Indeed the rectification indices of wild-type and mutant γ2 and γ8 complexes were all significantly higher than the rectification index of GluA2(Q) receptors alone and consistently comparable within the two populations of mutant TARPs (*RI* (+60/−60) = 0.07 ± 0.01 and *n* = 11 for GluA2(Q) alone, 0.24 ± 0.02 and *n* = 18 for GluA2(Q) + γ2, 0.25 ± 0.04 and *n* = 5 for GluA2(Q) + γ2 ΔL1, 0.23 ± 0.03 and *n* = 11 for GluA2(Q) + γ2 L2_GS, 0.24 ± 0.02 and *n* = 16 for GluA2(Q) + L1 γ8 in γ2, 0.18 ± 0.03 and *n* = 7 for GluA2(Q) + L1 γ8 in γ2 L2_GS, 0.15 ± 0.02 and *n* = 6 for GluA2(Q) + γ8, 0.15 ± 0.04 and *n* = 9 for GluA2(Q) + γ8 ΔL1, 0.15 ± 0.04 and *n* = 4 for GluA2(Q) + γ8 L2_GS, 0.20 ± 0.02 and *n* = 19 for GluA2(Q) + L1 γ2 in γ8, 0.20 ± 0.05 and *n* = 6 for GluA2(Q) + L1 γ2 in γ8 L2_GS; **Fig. 10 F**).

3.3 Measuring modulation of GluA2(Q) gating by γ2 and γ8 extracellular loops

3.3.1 Desensitisation properties of TARP Loop1 mutants

Once established the unaltered association of the TARP mutants with GluA2(Q) receptors, the effects of the extracellular loop mutations on GluA2(Q) gating were analysed. To start, the role of the first extracellular loop L1 on desensitisation of GluA2(Q) complexes was investigated by swapping it between γ2 and γ8 or deleting it from both. Although γ2 and γ8 in

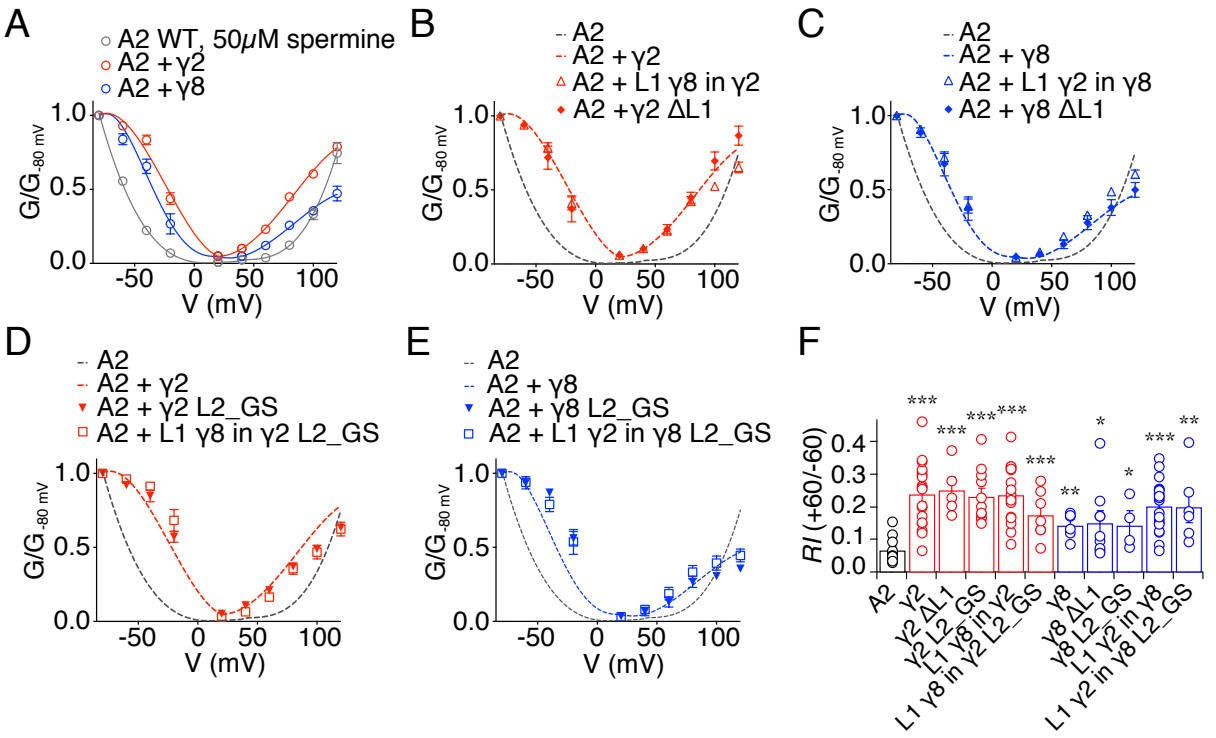

Figure 10. TARP γ2 and γ8 relief of PA block is not affected by extracellular loop mutations. (**A**) G-V relationships were normalised to the value at −80 mV and plotted for mRNA-unedited GluA2(Q) homomeric receptors without TARPs (A2; *grey*), with γ2 (*red*) and with γ8 (*blue*). The G-Vs show relief of PA block in the presence of TARPs, with γ2 relieving it more than γ8. (**B**) PA block relief by γ2 L1 mutants (*symbols*) is indistinguishable from that by wild-type (wt) γ2 (*red dotted line*). A2 alone is shown in grey for comparison. (**C**) G-V curves of γ8 L1 mutants (*symbols*) overlap with that of wt γ8 (*blue dotted line*) and they all differ from that of A2 without γ8 (*grey dotted line*). (**D**) Neutralising L2 in γ2 and (**E**) in γ8, alone (*full triangles*) or in combination with the swap of L1 (*empty squares*), does not alter γ2 and γ8 relief of PA block. (**F**) Bar graph summarising the rectification indices of A2 alone (*black*), coexpressed with γ2 wt or L1/L2 mutants (*red*), coexpressed with γ8 wt or L1/L2 mutants (*blue*). *p < 0.05, **p < 0.01 and ***p < 0.001 against A2. Currents were recorded at +50 mV in the presence of 50 μM spermine in the pipette solution. From Riva et al., 2017.

response to 10 mM glutamate apparently modulated GluA2(Q) desensitisation to the same level (I_{ss} = 23 ± 2%, n = 24 and 27 ± 4%, n = 9 for γ2 and γ8 respectively; **Fig. 11 A and D**), γ8 slowed down the entry into desensitisation more than γ2 (k_{des} = 61 ± 3 s^{-1}, n = 24 for γ2 and 40 ± 3, n = 9 for γ8; **Fig. 11 A and C**). The swap of L1 had a strong impact on γ2 (L1 γ8 in γ2), in which the introduction of the long L1 of γ8 doubled the steady-state current (52 ± 5%, n = 30; **Fig. 11 A and D**) and slowed down the entry into desensitisation to the same rate

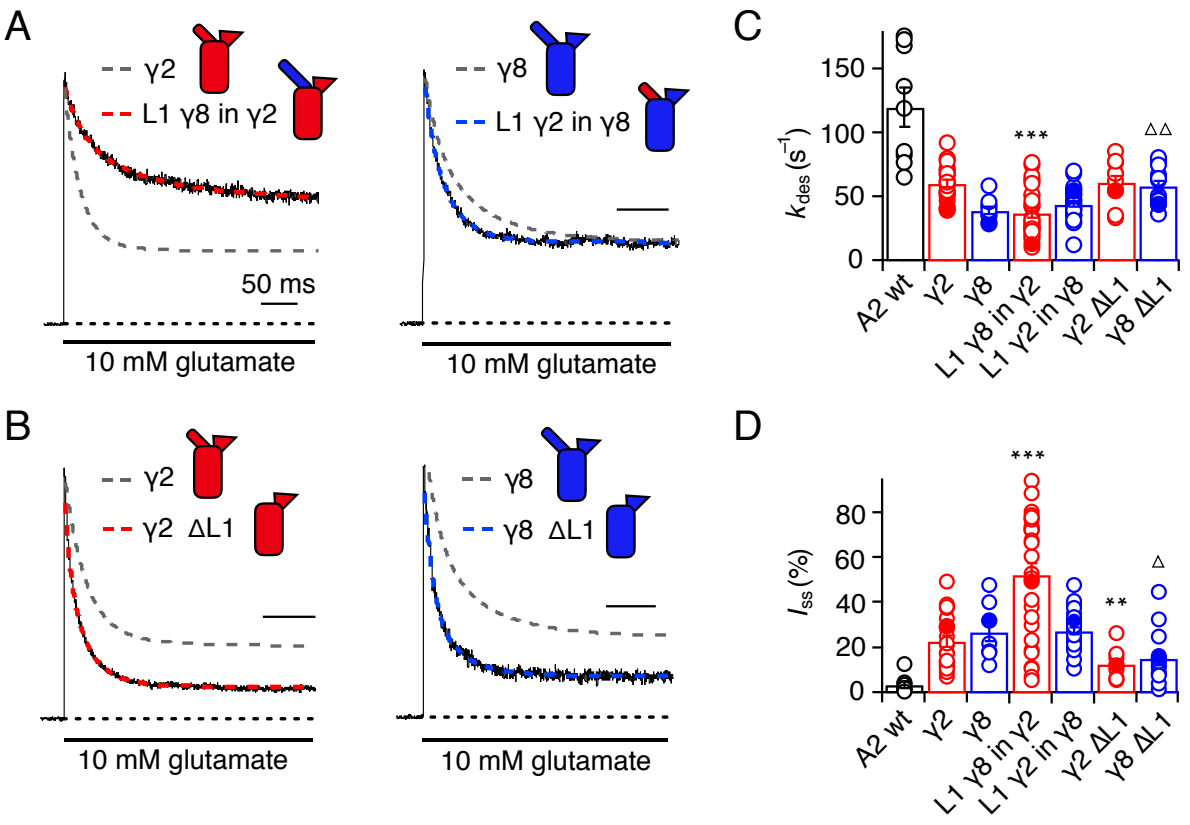

Figure 11. Effect of γ2 and γ8 L1 mutations on GluA2(Q) desensitisation. (**A**) Representative traces showing desensitisation of GluA2(Q) coexpressed with L1 chimeras of γ2 and γ8 (*red* and *blue*, respectively) in response to 500 ms application of 10 mM glutamate. The parent TARP is overlapped for comparison (*grey dotted line*). (**B**) Effect of L1 deletion on A2-γ2 (*red*) and A2-γ8 (*blue*) complexes desensitisation. (**C**) Bar graphs recapitulating desensitisation rate (k_{des}) and (**D**) steady-state current (I_{ss}) of γ2 and γ8 L1 mutants. Filled symbols correspond to the traces represented in (**A**) and (**B**). **p < 0.01 and ***p < 0.001 against γ2; Δp < 0.05 and ΔΔp < 0.01 against γ8. Currents were recorded at +50 mV in the presence of 50 µM spermine in the pipette solution. From Riva et al., 2017.

as for wild-type γ8 (37 ± 3 s^{-1}, *n* = 30; **Fig. 11 A and C**). In contrast, the chimera of γ8 with L1 of γ2 (L1 γ2 in γ8) maintained the original desensitisation behaviour of the parent TARP (k_{des} = 44 ± 2 s^{-1} and I_{ss} = 27 ± 2%, *n* = 28; **Fig. 11 A, C and D**). The deletion of L1 from γ2 (γ2 ΔL1) and γ8 (γ8 ΔL1) approximately halved the steady-state current of both (13 ± 2%, *n* = 11 for γ2 ΔL1 and 15 ± 3%, *n* = 15 for γ8 ΔL1; **Fig. 11 B and D**) and for γ8 it also slightly speeded up the entry into desensitisation of the complexes (58 ± 4 s^{-1}, *n* = 15; **Fig. 11 B and C**). These initial results proved that L1 plays a role in TARP modulation of AMPAR gating.

However, given that after these modifications some modulation could still be measured, they also suggested that some other elements must work together with L1.

3.3.2 Desensitisation properties of TARP Loop2 mutants

To test whether the second extracellular loop L2 was also taking part in modulation of AMPAR desensitisation by TARPs, 8 amino acids composing an electrically charged sequence in the loop were neutralised by substitution with a glycine-serine (GS) linker. The neutralisation of L2 had a very striking effect on γ2 (γ2 L2_GS), decreasing the steady-state current almost to the level of GluA2(Q) receptors without TARPs (6 ± 1%, n = 15 for γ2 L2_GS and 4 ± 1%, n = 9 for GluA2(Q) alone; **Fig. 12 A and D**). The entry into desensitisation though did not differ from that of wild-type γ2 (64 ± 4 s^{-1}, n = 15; **Fig. 12 A and C**). In γ8 instead the neutralisation of L2 (γ8 L2_GS) did not produce a change in γ8 modulation of GluA2(Q) gating (I_{ss} = 38 ± 4%, n = 6; **Fig. 12 A and D**), except for a further slowing down in the entry into desensitisation (24 ± 3 s^{-1}, n = 6; **Fig. 12 A and C**). L2 neutralisation was also analysed on the background of L1 chimeras. In γ2, the effect of L2 neutralisation combined with the swap of L1 (L1 γ8 in γ2 L2_GS) was even more striking, leading to a more than 10-fold slower entry into desensitisation compared to GluA2(Q) receptors alone (10 ± 0.4 s^{-1}, n = 7 and 121 ± 16 s^{-1}, n = 9 for L1 γ8 in γ2 L2_GS and GluA2(Q) without TARPs respectively; **Fig. 12 B and C**) and twice as large steady-state current compared to wild-type γ2 (45 ± 3%, n = 7; **Fig. 12 B and D**). Quite remarkable was also the behaviour of the reciprocal γ8 mutant (L1 γ2 in γ8 L2_GS), in which the neutralisation of L2 together with the exchange of L1 determined a 2-fold faster entry into desensitisation in respect to wild-type γ8 (83 ± 7 s^{-1}, n = 6; **Fig. 12 B and C**) and a drop in the steady-state current to the same extent as for unTARPed receptors (5 ± 1%, n = 6; **Fig. 12 B and D**).

3.3.3 Role of Loop1 in AMPA receptor-TARP complex superactivation

The role of TARP extracellular loops was also examined with regard to superactivation of AMPAR-TARP complexes. Upon 7 s application of 10 mM glutamate, the effect of TARP L1 and L2 mutants on the slow augmenting steady-state current of GluA2(Q) channels was measured. TARPs are known to induce a subtype-specific superactivation of GluA2(Q)

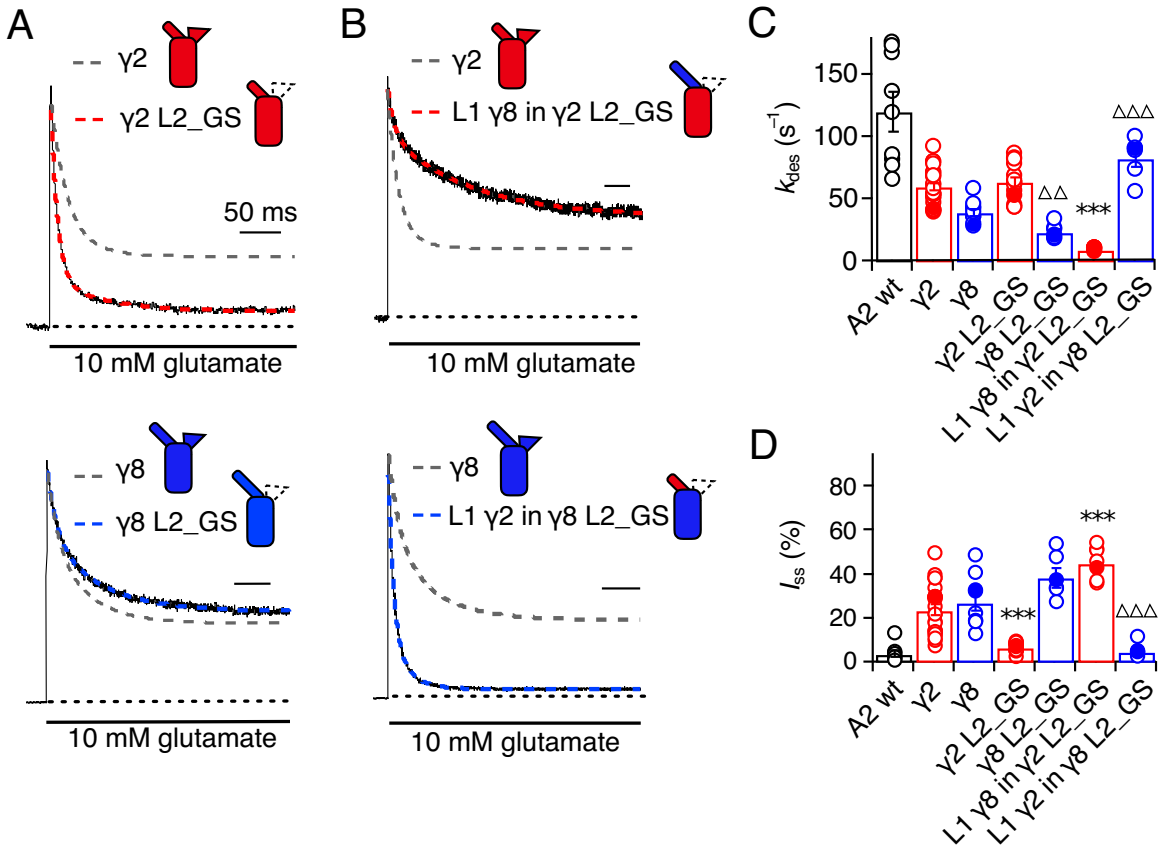

Figure 12. Desensitisation properties of γ2 and γ8 L2 mutants on GluA2(Q). (**A**) Exemplary traces illustrating the effect of L2 neutralisation (with a Gly-Ser, GS, linker) on γ2 (*red*) and γ8 (*blue*) modulation of GluA2(Q) desensitisation, upon 500 ms 10 mM glutamate application. Wild-type TARP traces are shown as grey dotted lines. (**B**) Combining L2 neutralisation with the swap of L1 leads to a great reduction in desensitisation for the L1 γ8 in γ2 L2_GS mutant (*red*) and vice versa to a strong increase in desensitisation for the L1 γ2 in γ8 L2_GS, mutant (*blue*). (**C**) Summary of desensitisation rate and (**D**) steady-state current of γ2 and γ8 L2 mutants. Filled symbols correspond to the traces represented in (**A**) and (**B**). ***p < 0.001 against γ2; ΔΔp < 0.01 and ΔΔΔp < 0.001 against γ8. Currents were recorded at +50 mV in the presence of 50 µM spermine in the pipette solution. From Riva et al., 2017.

homomeric receptors (Kato et al, 2010; Carbone & Plested, 2016). In fact, γ2 generated on average 7 ± 2% (*n* = 10) superactivation, normalised to the peak current amplitude, whereas γ8 about 30 ± 6% (*n* = 4) (**Fig. 13 A, B and C**). Swapping L1 between the two TARP isoforms produced asymmetric results: replacing γ2 L1 with the long L1 of γ8 (L1 γ8 in γ2) transferred the same amount of superactivation of γ8 to γ2 (27 ± 6%, *n* = 10; **Fig. 13 A and C**), but the opposite mutation (L1 γ2 in γ8) did not lower γ8 superactivation to the level of γ2 (16 ± 1%, *n* = 16; **Fig. 13 B and C**). Taking into consideration the strongly enhanced

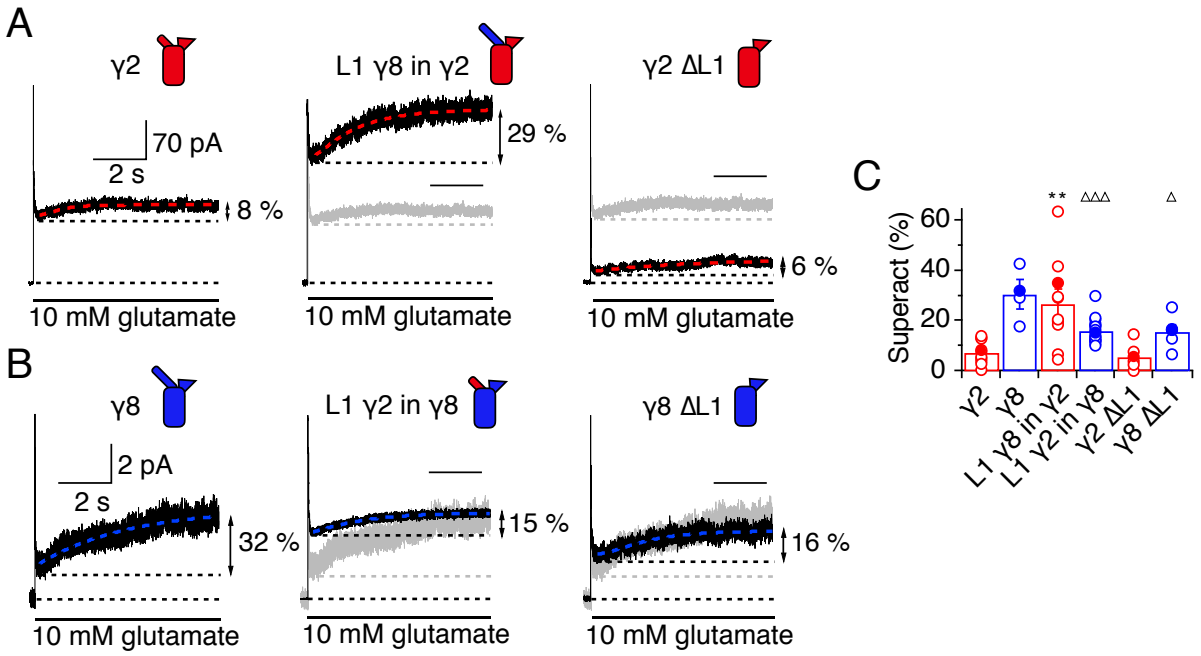

Figure 13. L1 contributes to TARP-mediated GluA2(Q) superactivation. (**A**) Representative superactivation traces of GluA2(Q) with γ2 wt (*left panel*), L1 chimera (*middle panel*) and with L1 deleted (*right panel*), exhibiting the slow augment of steady-state current following desensitisation, upon 7 s exposure to 10 mM glutamate. In grey, the trace of the wt TARP is overlapped to those of the mutants for comparison. Percentages indicate the amount of superactivation of the traces shown. (**B**) Superactivation of A2 complexes induced by wt γ8 (*left panel*) and γ8 L1 mutants (*middle* and *right panels*). (**C**) Bar graph summarising superactivation of γ2 and γ8 L1 mutants. Filled symbols correspond to the traces represented in (**A**) and (**B**). **p < 0.01 against γ2; Δp < 0.05 and ΔΔΔp < 0.001 against γ8. Currents were recorded at +50 mV in the presence of 50 µM spermine in the pipette solution. From Riva et al., 2017.

modulation of GluA2(Q) desensitisation and superactivation altogether by the γ2 mutant harbouring γ8 L1, this chimera was renamed "super TARP". The mutants of γ2 and γ8 with L1 removed (γ2 ΔL1 and γ8 ΔL1) still retained residual levels of superactivation and precisely 6 ± 2% (*n* = 6; **Fig. 13 A and C**) and 16 ± 3% (*n* = 6; **Fig. 13 B and C**) respectively. Again, these results provided evidence that L1 contributes to AMPAR superactivation by TARPs, but also confirmed that other players, possibly L2, must be involved.

3.3.4 Role of Loop2 in AMPA receptor-TARP complex superactivation

TARP L2 mutants were also analysed during long glutamate exposure to reveal the contribution of L2 to superactivation of GluA2(Q) homomeric channels. Neutralisation of L2 in γ2 (γ2 L2_GS) almost totally abolished superactivation of GluA2(Q)-γ2 complexes (1 ± 1%, *n* = 8; **Fig. 14 A and C**), while in γ8 (γ8 L2_GS) it only diminished it roughly to the half (12 ± 2%, *n* = 4; **Fig. 14 B and C**). However, when coupling L2 neutralisation to the swap of L1, γ8 (L1 γ2 in γ8 L2_GS) was no longer able to produce complexes that superactivated (1 ± 1%, *n* = 6; **Fig. 14 B and C**). Given that proper association of L1 γ2 in γ8 L2_GS with

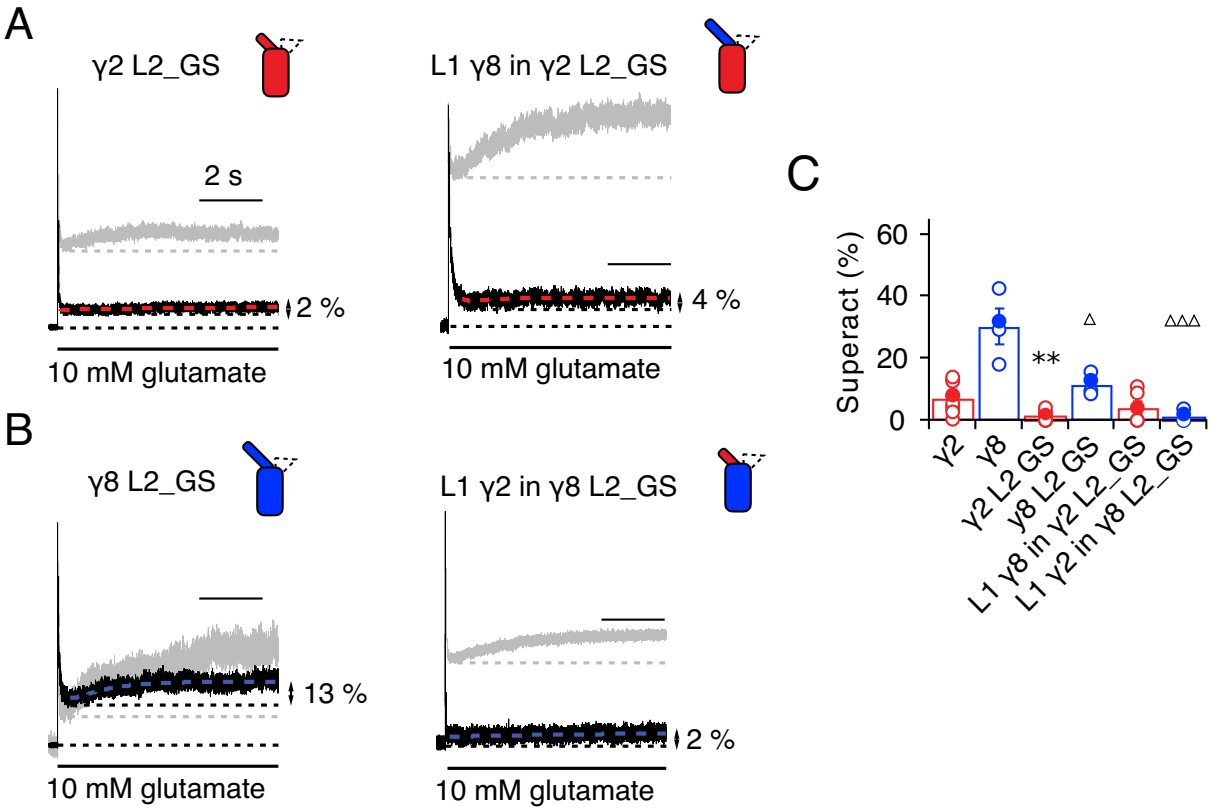

Figure 14. Effect of L2 neutralisation on γ2 and γ8 superactivation of GluA2(Q). (**A**) To the left, representative traces showing the effect of L2 neutralisation on γ2-mediated GluA2(Q) superactivation (*red*) compared to wt γ2 (*grey*), during 7 s application of 10 mM glutamate. To the right, illustration of the effect of L2 neutralisation on the background of L1 substitution (*red*) with respect to L1 substitution alone (*grey*). Percentages indicate the amount of superactivation of the traces shown. (**B**) Same as in (**A**) for γ8 L2 mutants. (**C**) Summary of superactivation of γ2 and γ8 L2 mutants. Filled symbols correspond to the traces represented in (**A**) and (**B**). **p < 0.01 against γ2; Δp < 0.05 and ΔΔΔp < 0.001 against γ8. Currents were recorded at +50 mV in the presence of 50 μM spermine in the pipette solution. From Riva et al., 2017.

GluA2(Q) was beforehand verified, acknowledging the lack of any modulatory effect of this γ8 mutant both on receptor desensitisation and superactivation, it was classified as a kinetically "null γ8". The chimera of γ2 with γ8 L1 and L2_GS (L1 γ8 in γ2 L2_GS) instead still showed a certain level of superactivation (4 ± 2%, n = 6; **Fig. 14 A and C**), even if smaller than that of wild-type γ2, conceivably due to the presence of the powerful positive element of L1 of γ8.

3.3.5 Effect of combined removal of Loop1 and Loop2

The replacement of charged residues in L2 was also combined with the deletion of L1, to observe what occurred to TARP modulation of AMPAR gating when TARPs were deprived of functional extracellular loops. By doing so, a kinetically "null γ2" was also obtained (γ2 ΔL1 L2_GS), deficient in promoting superactivation (0 ± 0%, n = 4; **Fig. 15 C and D**) and in diminishing desensitisation (k_{des} = 81 ± 17 s^{-1} and I_{ss} = 2 ± 1%, n = 5; **Fig. 15 E and F**) of GluA2(Q) receptors, analogously to the gating character of receptors in the absence of auxiliary subunits. Somewhat surprisingly instead, the removal of both L1 and L2 in γ8 (γ8 ΔL1 L2_GS) did not effectively abrogate γ8 modulatory properties and a small degree of GluA2(Q) superactivation (3 ± 1%, n = 2; **Fig. 15 C and D**) and steady-state current (10 ± 5%, n = 5; **Fig. 15 E and F**) could still be measured with this mutant. Perhaps, this retained activity might be explained by the few more amino acids that had to be conserved in γ8 L1 to allow expression of the protein but that may be still interacting with the receptor in some way. Importantly, both γ2 ΔL1 L2_GS and γ8 ΔL1 L2_GS relieved PA block similarly to the respective wild-type TARP (RI (+60/−60) = 0.23 ± 0.10, n = 4 for γ2 ΔL1 L2_GS and 0.14 ± 0.04, n = 4 for γ8 ΔL1 L2_GS; **Fig. 15 A and B**), implying that the extracellular loops are not determinant for complex assembly.

3.3.6 Modulation by the β4-TM2 acidic loop

Multiple cryo-EM structures of the AMPAR-TARP complex predicted the interaction between a conserved electronegative region in the β4-TM2 loop of γ2 (also called 'acidic loop' or 'negative patch', NP; residues 85-95, sequence: EDADYEADTAE), contained together with L1 in the TARP first extracellular segment, and a conserved basic 'KGK' motif on the lower (D2) lobe of GluA2 LBD (residues 697-699) (Twomey et al., 2016; Zhao et al., 2016; Chen et

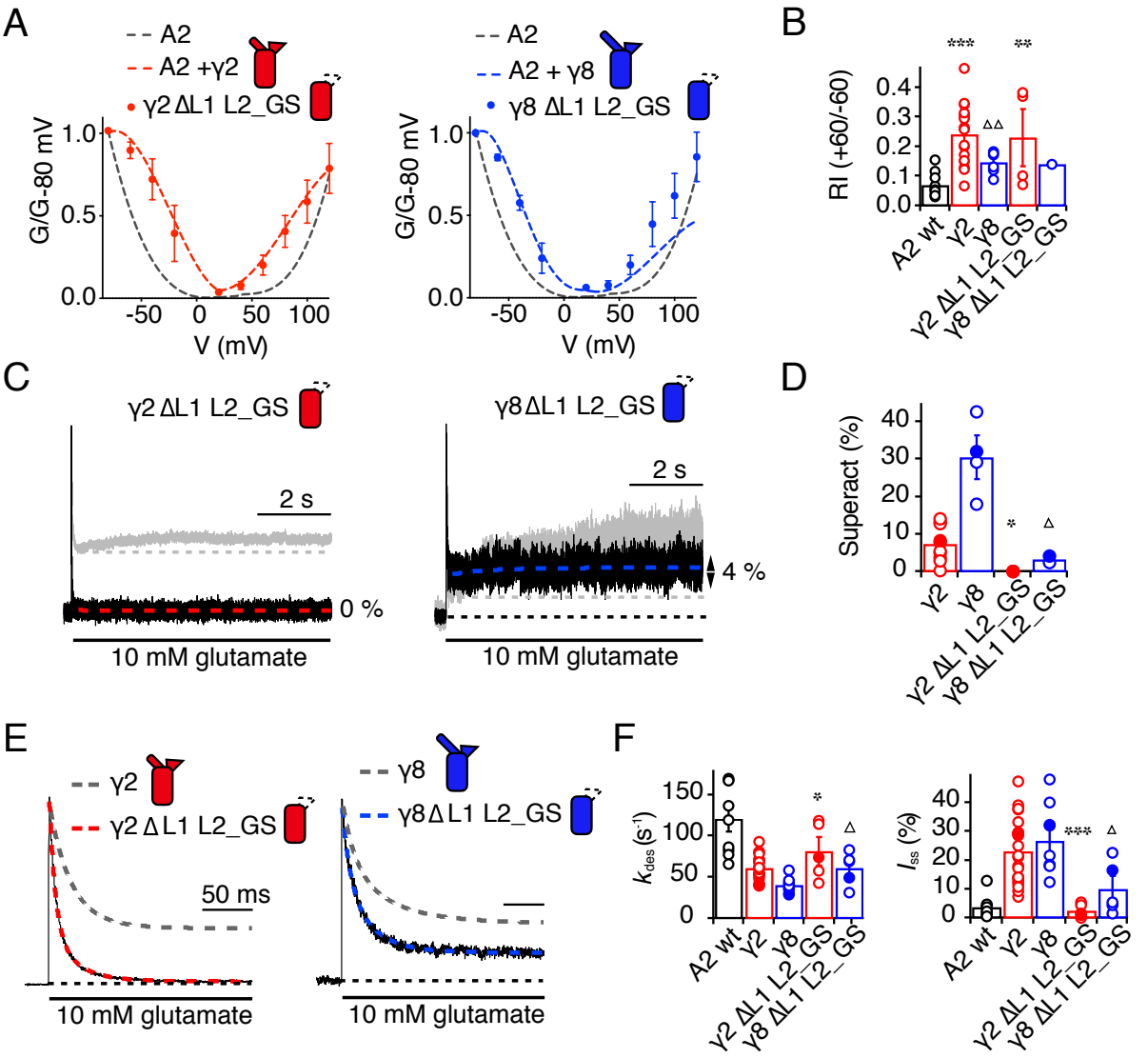

Figure 15. Eliminating L1 and L2 suppresses GluA2(Q) modulation by γ2. (**A**) Normalised G-V curves demonstrating that the mutant γ2 (*left panel, red full circles*) and γ8 (*right panel, blue full circles*) ΔL1 L2_GS relieve PA block of GluA2(Q) receptors similarly to wt γ2 (*left panel*, *red dotted line*) and γ8 (*right panel*, *blued dotted line*), respectively. The G-V curve of A2 alone is shown as a grey dotted line. (**B**) Rectification indices of γ2 ΔL1 L2_GS and γ8 ΔL1 L2_GS in comparison to wt γ2 and γ8 complexes and non-complexed receptors. (**C**) Removing L1 and L2 abolishes γ2 (*left panel*, *red*) but not completely γ8 (*right panel*, *blue*) superactivation of A2 in response to 7 s exposure to the agonist. Exemplary superactivation traces of wt TARPs are overlapped in grey. (**D**) Bar graph summarising the data represented in (**C**), with filled symbols corresponding to the values of the traces shown. (**E**) Effect of L1 and L2 elimination on γ2 (*left panel*, *red*) and γ8 (*right panel*, *blue*) modulation of A2 desensitisation upon 500 ms glutamate application. Wt TARP desensitisation recordings are shown on the background for comparison (*grey dotted lines*). (**F**) Bar graphs summarising k_{des} and I_{ss} of the data represented in (**E**), with filled symbols corresponding to the values of the traces shown.*p < 0.05, **p < 0.01 and ***p < 0.001 against γ2; Δp < 0.05, ΔΔp < 0.01 against γ8. Currents were recorded at +50 mV in the presence of 50 µM spermine in the pipette solution. From Riva et al., 2017.

al., 2017; Zhao et al., April 2019). The KGK motif was previously demonstrated to be a crucial site for GluA2 modulation by γ2 (Dawe et al., 2016). To functionally test this putative interaction, three negatively charged residues of γ2 β4-TM2 loop (Asp88, Glu90 and Asp92) were mutated to neutral Gly-Ser-Gly residues (**Fig. 16 A**). Hence this negative patch mutant

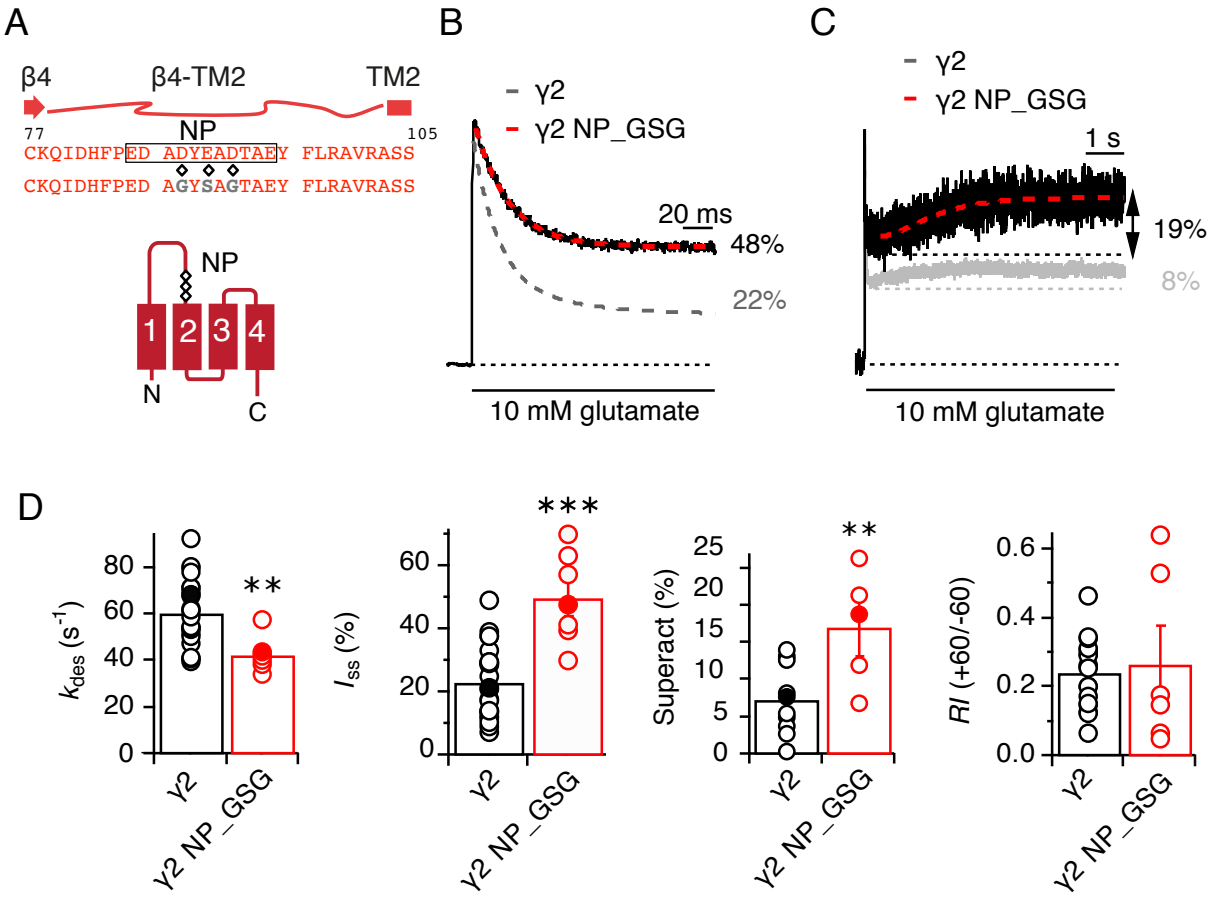

Figure 16. γ2 β4-TM2 loop is a negative modulator of GluA2(Q) gating. (**A**) In the upper panel, the sequence of γ2 β4-TM2 loop is shown with secondary structural elements on the top (*arrow* for β-sheet, *line* for loop and *rectangle* for α-helix); the negative patch (NP) is framed by a black box and the three amino acids that were mutated are marked by diamonds (D88G, E90S and D92G). The sequence of the γ2 NP_GSG mutant is aligned below. In the lower panel, a cartoon with the topology of γ2 is present, indicating the positions of the three residues neutralised within the negative patch. (**B**) Effect of the NP mutation on γ2 desensitisation and (**C**) superactivation properties on GluA2(Q) gating during, respectively, a 500 ms and a 7 s pulse of 10 mM glutamate. (**D**) Bar graphs summarising (*from left to right*) desensitisation rate, steady-state current, superactivation and rectification index of the γ2 NP_GSG mutant. Filled symbols correspond to the traces shown in (**B**) and (**C**). **p < 0.01 and ***p < 0.001 against γ2. Currents were recorded at +50 mV in the presence of 50 µM spermine in the pipette solution. From Riva et al., 2017.

(γ2 NP_GSG) was coexpressed with GluA2(Q) receptors. When activated by 500 ms application of 10 mM glutamate, GluA2(Q) complexes with γ2 NP_GSG showed a significant slowing down in the entry into desensitisation and a more than 2-fold increase in the steady-state current (k_{des} = 43 ± 3 s^{-1} and I_{ss} = 50 ± 6%, n = 7), compared to wild-type GluA2(Q)-γ2 complexes (k_{des} = 61 ± 3 s^{-1} and I_{ss} = 23 ± 2%, n = 24; **Fig. 16 B and D**). Moreover, in response to 7 s glutamate exposure, γ2 NP_GSG induced a robust augment of GluA2(Q) superactivation and specifically from 7 ± 2% (n = 10) for wild-type γ2 to 17 ± 4% (n = 5) for γ2 NP_GSG (**Fig. 16 C and D**). Obviously, also in this case no discrepancy in PA block relief by the mutant vs. wild-type γ2 was primarily verified (*RI* (+60/−60) = 0.24 ± 0.02, n = 18 for wt γ2 and 0.27 ± 0.11, n = 6 for γ2 NP_GSG; **Fig. 16 D**). Based on these data, the TARP β4-TM2 loop seems to interact with the AMPAR as a modulatory element. However, considering the substantial enhancement in GluA2(Q) modulation by the negative patch mutant, an interaction of an inhibitory nature rather than of a positive kind is hypothesised.

3.4 Testing site-specific AMPA receptor-TARP interactions

3.4.1 GluA2(Q) mutants in linkers in close proximity to TARP Loop2

As previously mentioned, according to the structural model that was generated in Riva et al. (2017), TARP L1 was expected to engage the AMPAR LBD layer in multiple interaction sites, including the KGK motif. On the other hand, L2 was unequivocally predicted to be in close proximity to the receptor linkers connecting the LBD and TMD and particularly, the S1-M1 and S2-M4 linkers. These interactions were also suggested by more or less concurrent studies of the GluA2-γ2 complex (Twomey et al., 2016; Chen et al., 2017) and have then been confirmed by the very recent structural data of the aforementioned GluA1/A2_γ8 complex (Herguedas et al., 2019). Observing the sequence of TARP L2, an alternating charge region (for γ2: K166, D168, K170 and K171; for γ8: K190, R191, D192, E193, E194, K195 and K196) was noticed to be mirrored in part of the sequence of the GluA2 linker S1-M1 (Q508, K509 and S510 or 508QKS510; **Fig. 17 A**) and S2-M4 (K781, E782 and K783 or 781KEK783; **Fig. 17 B**). For this reason, 508QKS510 in the S1-M1 linker and 781KEK783 in the S2-M4 linker of GluA2 were neutralised by replacement to GAG and GSG respectively. Therefore, the effects of the receptor LBD-TMD linker mutations on γ2 and γ8

modulation of GluA2(Q) gating were measured and, to prove the site-specificity of this interaction, compared to the effects of TARP L2 mutations.

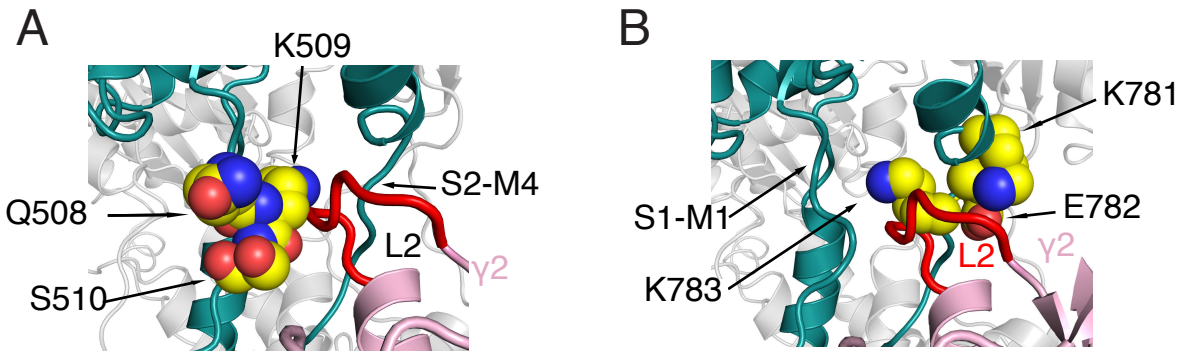

Figure 17. Predicted interactions between γ2 L2 and GluA2 LBD-TMD linkers. (**A**) Charged residues in the GluA2 S1-M1 linker predicted to be in close proximity to γ2 L2 (*red*) are labeled (Gln508, Lys509 and Ser510) and represented as yellow atomic spheres. These residues were neutralised by replacement to GAG. (**B**) Lys781, Glu782 and Lys783 (*yellow atomic spheres*) in the S2-M4 linker of GluA2 were also predicted to be interacting sites with L2 of γ2 and were mutated to GSG. From Riva et al., 2017.

3.4.2 Functionality of GluA2(Q) linker mutants and assembly with TARPs

First of all, the functionality of the GluA2 S1-M1 and S2-M4 linker mutants had to be checked both in terms of gating behaviour and also in terms of formation of TARP complexes. This aspect was quite crucial because earlier works had shown the importance of the linker regions in glutamate receptor gating (Balannik et al., 2005; Schmid et al., 2007; Talukder et al., 2010). Furthermore, in a very new publication unravelling the structure of native AMPA receptors (nAMPARs), contacts between the S2-M4 and the gating-critical M3-S2 linkers from adjacent subunits were identified in all four nAMPAR subunits, pointing out a role of the S2-M4 linker in the receptor gating machinery (Zhao et al., 2019). Nevertheless, somewhat unexpectedly, neutralising the S1-M1 and S2-M4 linkers of GluA2(Q) (flip variant) in the 508QKS510 and 781KEK783 regions did not affect the receptor gating properties to any extent (**Fig. 18 A and B**). Initially, a single-point mutation in the S1-M1 linker was tested, resulting in no differences between the mutant (GluA2 K509A) and the wild-type receptor responses to 10 mM glutamate application (GluA2 wt: k_{des} = 121 ± 16 s^{-1} and I_{ss} = 4 ± 1%, n = 9; GluA2 K509A: k_{des} = 100 ± 6 s^{-1} and I_{ss} = 3 ± 1%, n = 5). Similarly, replacing three

amino acids in a raw on each linker (GluA2 508GAG510, GluA2 781GSG783) and remarkably even on both linkers at the same time (GluA2 GAG/GSG) did not alter the kinetics of receptor activation and desensitisation (GluA2 508GAG510: k_{des} = 146 ± 33 s^{-1} and I_{ss} = 1 ± 1%, n = 3; GluA2 781GSG783: k_{des} = 112 ± 12 s^{-1} and I_{ss} = 2 ± 1%, n = 3; GluA2 GAG/GSG: k_{des} = 153 ± 20 s^{-1} and I_{ss} = 2 ± 1%, n = 5). Once determined that the gating profiles of the receptor linker mutants perfectly coincided with that of the wild-type receptor, association of the linker mutants with TARPs was also evaluated. G-V curves and rectification indices of GluA2 linker mutants with wild-type γ2 and γ8 or L1 chimeras showed no impairment in PA block relief of receptor mutant complexes, in respect to wild-type GluA2-γ2 or -γ8 complexes, indicating that the mutations of the receptor S1-M1 and S2-M4 linkers did not interfere with proper TARP assembly (*RI* (+60/−60) = 0.24 ± 0.02 and n = 18 for GluA2 wt + γ2, 0.21 ± 0.04 and n = 4 for GluA2 K509A + γ2, 0.21 ± 0.04 and n = 4 for GluA2 508GAG510 + γ2, 0.26 ± 0.06 and n = 8 for GluA2 781GSG783 + γ2, 0.31 ± 0.13 and n = 5 for GluA2 GAG/GSG + γ2, 0.43 ± 0.06 and n = 3 for GluA2 GAG/GSG + L1 γ8 in γ2, 0.15 ± 0.02 and n = 6 for GluA2 wt + γ8, 0.28 ± 0.08 and n = 6 for GluA2 GAG/GSG + γ8, 0.24 ± 0.05 and n = 5 for GluA2 GAG/GSG + L1 γ2 in γ8; **Fig. 18 C and D**).

3.4.3 Modulation of GluA2(Q) linker mutants by TARPs

To analyse the consequences of the linker mutations on modulation of receptor gating by TARPs, GluA2 linker mutants were coexpressed with wild-type or chimeric γ2 and γ8 constructs. By replacement of 508QKS510 with GAG in the S1-M1 linker or of 781KEK783 with GSG in the S2-M4 linker, γ2 modulation of GluA2 desensitisation and superactivation was in both cases partially attenuated (**Fig. 19 A, B and G**). In fact, despite the desensitisation rate of these mutant complexes did not differ from that of wild-type GluA2-γ2 complexes (67 ± 6 s^{-1}, n = 4 and 58 ± 5 s^{-1}, n = 9 for GluA2 508GAG510 and GluA2 781GSG783, respectively), the steady-state current was greatly dampened (GluA2 508GAG510: 12 ± 3%, n = 4; GluA2 781GSG783: 9 ± 1%, n = 9) and the superactivation nearly abolished (0 ± 0%, n = 3 for GluA2 508GAG510 and 2 ± 1%, n = 8 for GluA2 781GSG783). In contrast, the mutation of a single amino acid (K509A) in the S1-M1 linker resulted in an enforcement of γ2 positive modulation of GluA2 desensitisation (k_{des} = 30 ± 10 s^{-1} and I_{ss} = 45 ± 3%, n = 5; **Fig. 19 G**), providing indication that a second site was potentially involved. When combining the

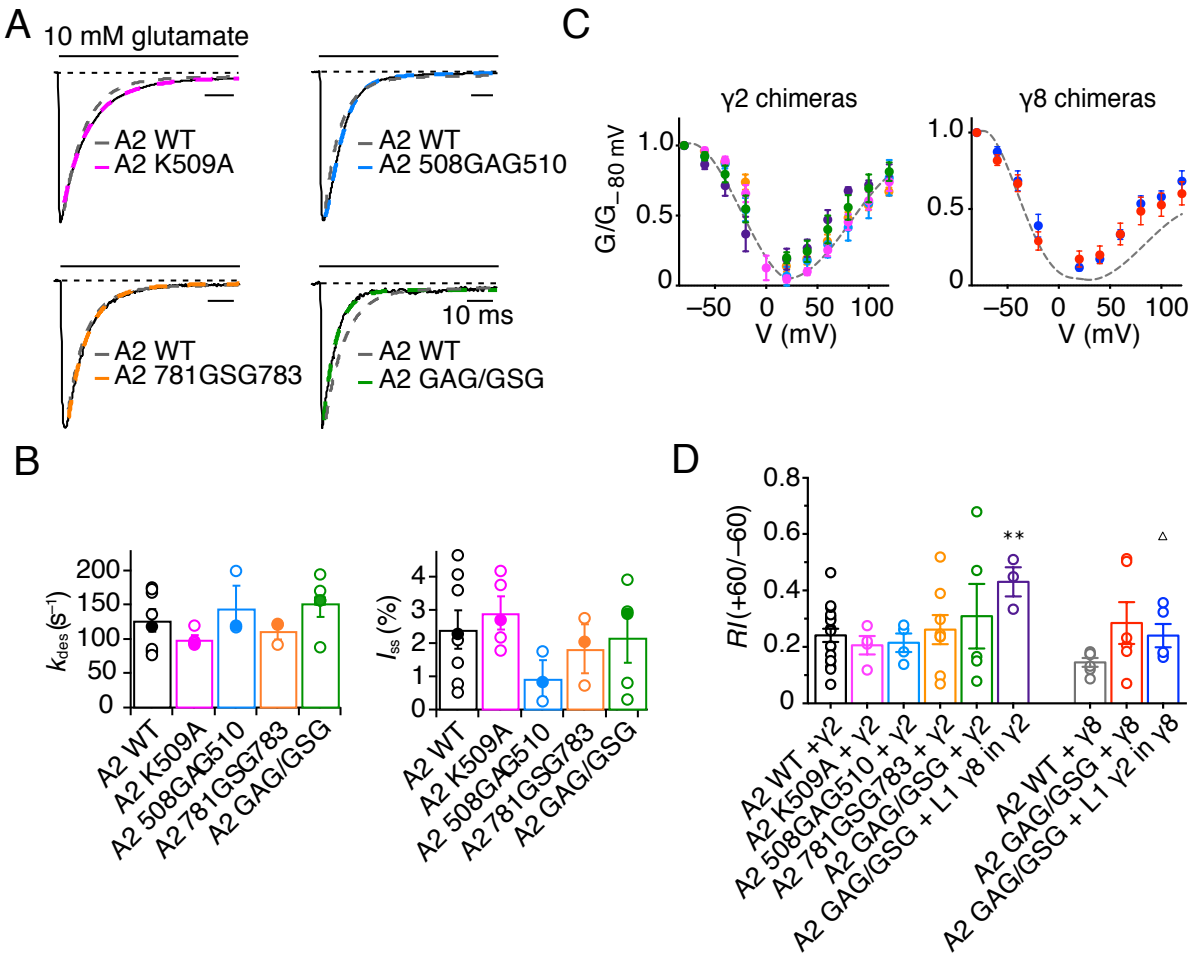

Figure 18. 508GAG510 and 781GSG783 linker mutations do not alter GluA2(Q) gating or assembly with TARPs. (**A**) Representative traces of the single-point mutant GluA2 K509A (*pink*), the triple mutants GluA2 508GAG510 (*light blue*) and GluA2 781GSG783 (*orange*) and the double triple mutant GluA2 GAG/GSG (*green*), during 500 ms application of 10 mM glutamate. Wild-type GluA2 is overlapped for comparison (*grey dotted line*). (**B**) Summary of desensitisation rate and steady-state current of GluA2 linker mutants, colour-coded as in (**A**), showing no significant difference from the wild-type receptor. Filled circles correspond to the representative traces in (**A**). Currents were recorded at −60 mV with PA-free intracellular solution. (**C**) Normalised G-V plots of GluA2 linker mutants in complex, to the left, with wt γ2 or L1 γ8 in γ2 (*purple*) and to the right, with wt γ8 (*red*) or L1 γ2 in γ8 (*blue*). G-V curves of wt GluA2-γ2 or GluA2-γ8 are visible as grey dotted lines. (**D**) Rectification indices of the conditions displayed in (**C**). **p < 0.01 against GluA2 wt + γ2; Δp < 0.05 against GluA2 wt + γ8. Currents were recorded at +50 mV in the presence of 50 µM spermine in the pipette solution. From Riva et al., 2017.

triple mutations in both linkers simultaneously (GluA2 GAG/GSG), in the presence of γ2 the entry into desensitisation of the mutant complexes speeded up (78 ± 8 s^{-1}, n = 8), the steady-state current decreased to the level of wild-type unTARPed receptors (5 ± 1%, n = 8) and the superactivation was completely abrogated (0 ± 0%, n = 4; **Fig. 19 C and G**). Strikingly, this mutant receptor resembled quite closely the effect of the neutralisation of γ2 L2 (k_{des} = 64 ± 4 s^{-1} and I_{ss} = 6 ± 1%, n = 15 and superactivation = 1 ± 1%, n =8; see **Fig. 12 A, C and D** and **Fig. 14 A and C**). To discern wether the loss of γ2 modulation occurred because the LBD-TMD linkers were primary interaction sites or wether the linkers both interacted with TARPs and transmitted distant modulation from sites in the LBD, modulation by γ8 and related chimeras was also assessed. Desensitisation of GluA2 GAG/GSG receptors in complex with γ8 was not much modified with regards to wild-type GluA2-γ8 complexes (k_{des} = 45 ± 2 s^{-1} and I_{ss} = 12 ± 3%, n = 5) and γ8 could still induce on average 23 ± 7% (n = 5) superactivation to these mutant receptors (**Fig. 19 E and G**). This γ8 withheld modulation of receptor lacking the putative interacting sites for TARP L2 might be mediated by the interaction of the long L1 of γ8 with the receptor LBD and might not be visible for γ2 since its L1, being shorter than γ8 L1, is not such a strong LBD modulator (Herguedas et al., 2019). Not surprisingly in fact when γ8 L1 was inserted in γ2 (L1 γ8 in γ2), this chimera powerfully slowed down the entry into desensitisation of the double linker mutant (12 ± 1 s^{-1}, n = 5), even though it could not produce superactivating complexes (2 ± 2%, n = 4; **Fig. 19 D and G**). Consistently with this, the chimera of γ8 with L1 substituted by γ2 L1 (L1 γ2 in γ8) was no longer able to modulate GluA2 GAG/GSG kinetics, reducing the steady-state current (4 ± 1%, n = 5) and the superactivation (1 ± 1%, n = 4) to the same levels as of wild-type GluA2 in the absence of TARPs (**Fig. 19 F and G**). Therefore, without its long L1 γ8 failed to modulate GluA2 when the S1-M1 and S2-M4 interaction sites were disrupted, in coherence with what observed before with the related γ8 L1 chimera lacking L2 interaction sites (L1 γ2 in γ8 L2_GS: k_{des} = 83 ± 7 s^{-1} and I_{ss} = 5 ± 1 %, n = 6 and superactivation = 1 ± 1 %, n = 6; see **Fig. 12 B, C and D** and **Fig. 14 B and C**). These results indicate that the LBD-TMD linkers both transduce upstream TARP modulation, but also function as primary TARP modulatory sites.

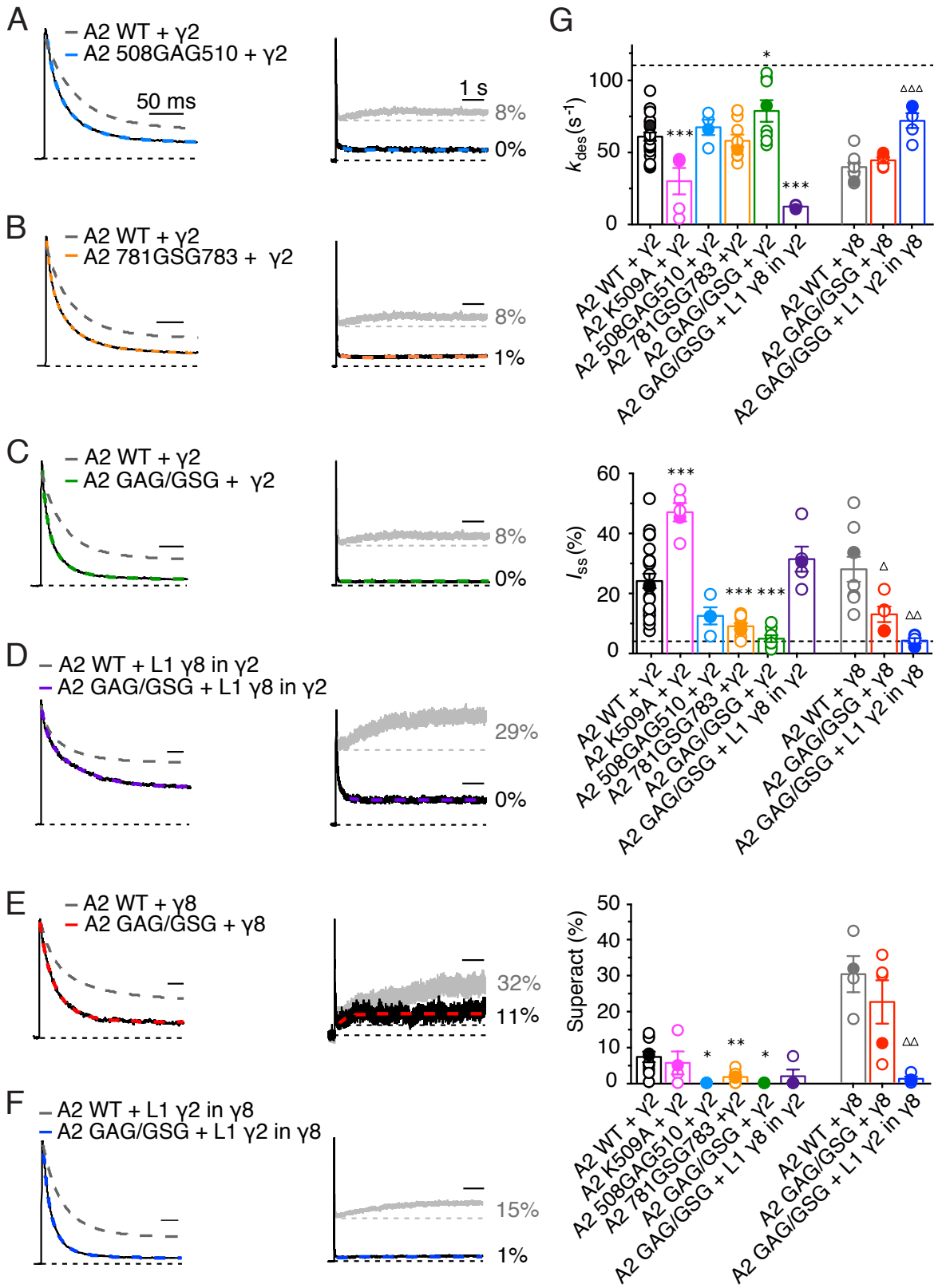
A
A2 WT + γ2
A2 508GAG510 + γ2
50 ms
1 s
8%
0%
B
A2 WT + γ2
A2 781GSG783 + γ2
8%
1%
C
A2 WT + γ2
A2 GAG/GSG + γ2
8%
0%
D
A2 WT + L1 γ8 in γ2
A2 GAG/GSG + L1 γ8 in γ2
29%
0%
E
A2 WT + γ8
A2 GAG/GSG + γ8
32%
11%
F
A2 WT + L1 γ2 in γ8
A2 GAG/GSG + L1 γ2 in γ8
15%
1%
G
k_{des} (s^{-1})
I_{ss} (%)
Superact (%)
A2 WT + γ2
A2 K509A + γ2
A2 508GAG510 + γ2
A2 781GSG783 +γ2
A2 GAG/GSG + γ2
A2 GAG/GSG + L1 γ8 in γ2
A2 WT + γ8
A2 GAG/GSG + γ8
A2 GAG/GSG + L1 γ2 in γ8

Figure 19. LBD-TMD linkers are key sites for GluA2 modulation by TARPs. Exemplary traces showing desensitisation (*left panel*) and superactivation (*right panel*) of GluA2 S1-M1 and S2-M4 linker mutants in complex with wt or mutant γ2 and γ8, during 500 ms for desensitisation and 7 s for superactivation 10 mM glutamate jumps. Currents were recorded at +50 mV in the presence of 50 μM spermine in the pipette solution. Specifically, the following conditions are illustrated: (**A**) the S1-M1 triple mutant GluA2 508GAG510 + γ2, (**B**) the S2-M4 triple mutant GluA2 781GSG783 + γ2, (**C**) the double S1-M1/S2-M4 triple mutant GluA2 GAG/GSG + γ2, (**D**) GluA2 GAG/GSG + L1 γ8 in γ2, (**E**) GluA2 GAG/GSG + γ8 and (**F**) GluA2 GAG/GSG + L1 γ2 in γ8. Overlapping grey traces represent wt GluA2-TARP complexes in (**A**), (**B**), (**C**) and (**E**), while in (**D**) and (**F**) they represent wt GluA2 in complex with the respective L1 chimera. Percentages indicate the amount of superactivation of the different traces shown. (**G**) Bar graphs summarising desensitisation rate, steady-state current and superactivation of the GluA2 linker mutants with wt or mutant γ2 and γ8. Black dotted lines describe the mean values of wt GluA2 without TARPs. Bars are coloured accordingly to the representative traces shown in (**A-F**) and filled symbols in the graphs also correspond to them. *$p < 0.05$, **$p < 0.01$ and ***$p < 0.001$ against GluA2 wt + γ2; $\Delta p < 0.05$, $\Delta\Delta p < 0.01$ and $\Delta\Delta\Delta p < 0.01$ against GluA2 wt + γ8. From Riva et al., 2017.

3.5 Subunit-dependent modulation of AMPA receptor gating by TARPs

3.5.1 Association of TARP modulatory mutants with GluA1 and GluA2(R) homomeric receptors

It is well known that AMPARs in the CNS are mainly present as heterotetrameric channels composed of the four different GluA1-4 subunits rather than as homotetrameric GluA channels. In the recent study by Zhao et al., 2019, using single particle cryo-EM the authors valuably elucidated the architecture of native AMPARs isolated from rat brain, revealing an abundance of triheteromeric GluA1/A2/A3 assemblies. Having demonstrated the importance of TARP extracellular loops in the modulation of GluA2(Q) homomeric receptors, we questioned wether the observed molecular mechanisms might be common to the distinct GluA1-4 AMPAR subunits, or wether TARP modulation might take place in an AMPAR subunit-dependent manner. Some evidence of an AMPAR subunit-specific regulation by TARPs had already been gathered, showing for instance γ2 being ineffective in imparting superactivation to GluA1 receptors (Kato et al., 2010), contrary to what we report for GluA2(Q) receptors (Carbone & Plested, 2016; Riva et al., 2017). In order to further

Construct	k_{des} (s^{-1})	*p*	I_{ss} (%)	*p*	Superact (%)	*p*
A2 wt	120 ± 15 (9)		5 ± 1		–	–
γ2	60 ± 5 (24)		25 ± 2		7 ± 2 (10)	
γ8	40 ± 5 (9)		25 ± 5		30 ± 6 (4)	
γ2 β4 TM2 §	40 ± 5 (7)	0.004	50 ± 5	1×10^{-5}	17 ± 4 (5)	0.009
L1 γ8 in γ2 §	35 ± 5 (30)	5×10^{-6}	50 ± 5	7×10^{-6}	27 ± 6 (10)	0.003
L1 γ2 in γ8 §	45 ± 1 (28)	0.34	25 ± 3	0.86	16 ± 1 (16)	0.001
γ2 ΔL1 §	60 ± 5 (11)	0.90	15 ± 2	0.008	6 ± 2 (6)	0.52
γ8 ΔL1 §	60 ± 5 (15)	0.002	15 ± 3	0.03	16 ± 3 (6)	0.02
γ2 L2_GS §	65 ± 5 (15)	0.49	5 ± 1	1×10^{-6}	1.3 ± 0.6 (8)	0.003
γ8 L2_GS §	25 ± 5 (6)	0.002	40 ± 4	0.07	12 ± 2 (4)	0.01
L1 γ8 in γ2 L2_GS §	10 ± 0.5 (7)	6×10^{-10}	45 ± 3	6×10^{-5}	4 ± 2 (6)	0.19
L1 γ2 in γ8 L2_GS §	85 ± 5 (6)	1×10^{-5}	5 ± 1	0.001	1 ± 0.7 (6)	9×10^{-5}
γ2 ΔL1 L2_GS §	80 ± 20 (5)	0.03	2 ± 1	4×10^{-4}	0 (4)	0.011
γ8 ΔL1 L2_GS §	60 ± 10 (5)	0.02	10 ± 5	0.02	3 ± 1 (4)	0.02
A2 K509A Δ	100 ± 5 (5)	0.34	3 ± 0.5	0.71	–	–
A2 508GAG510 Δ	145 ± 35 (3)	0.42	1 ± 0.5	0.27	–	–
A2 781GSG783 Δ	110 ± 15 (3)	0.76	2 ± 1	0.46	–	–
A2 GAG/GSG Δ	150 ± 20 (5)	0.20	2 ± 1	0.44	–	–
A2 K509A + γ2 #	30 ± 10 (5)	3×10^{-4}	45 ± 3	2×10^{-4}	5 ± 5 (4)	0.59
A2 508GAG510 + γ2 #	70 ± 5 (4)	0.39	10 ± 5	0.07	0 (3)	0.03
A2 781GSG783 + γ2 #	60 ± 5 (9)	0.60	10 ± 1	0.001	2 ± 0.5 (8)	0.005
A2 GAG/GSG + γ2 #	80 ± 5 (8)	0.01	5 ± 1	9×10^{-5}	0 (4)	0.01
A2 GAG/GSG + L1 γ8 in γ2 #	12 ± 0.5 (5)	4×10^{-8}	30 ± 5	0.21	2 ± 2 (4)	0.065
A2 GAG/GSG + γ8 #	45 ± 2 (5)	0.30	12 ± 3	0.03	25 ± 5 (5)	0.37
A2 GAG/GSG + L1 γ2 in γ8 #	72 ± 5 (5)	8×10^{-5}	4 ± 1	0.001	1 ± 1 (4)	0.001
A2 GAG/GSG + γ2 L2_GS #	90 ± 10 (9)	3×10^{-4}	2 ± 1	5×10^{-6}	0 (4)	0.01

Table 1. Kinetic properties of TARP extracellular loop and GluA2 linker mutants. List of desensitisation rate (k_{des}), steady-state current (I_{ss}) and superactivation (Superact) values of all the wild-type and mutant γ2, γ8 and GluA2 constructs tested. The values are shown as mean ± SEM. The number of recordings for each condition is indicated in brackets. *p* values (from Student's *t*-test) were calculated as follows: § against the parent TARP, Δ against GluA2 wt, # against GluA2 wt + parent TARP. To record currents in the presence of TARPs, outside-out patches were voltage-clamped at +50 mV and the intracellular solution contained 50 μM spermine. In the absence of TARPs, currents were recorded at the holding potential of –60 mV with spermine-free intracellular solution. From Riva et al., 2017.

investigate this aspect, TARP L1 and L2 mutants, and in particular those that exhibited either a lack (γ2 ΔL1 L2_GS or "null γ2" and L1 γ2 in γ8 L2_GS or "null γ8") or a potentiation (L1 γ8 in γ2 or "super TARP") of GluA2(Q) modulation, were tested on GluA1 and GluA2(R) subunits both as homomeric and heteromeric receptors. With the intent to analyse a more physiological scenario, inwardly rectifying PA-sensitive mRNA-unedited GluA2(Q) receptors were replaced by non-inwardly rectifying PA-insensitive mRNA-edited GluA2(R) receptors, which constitute about 99% of the total GluA2 subunits throughout the brain (Wright & Vissel, 2012). In the first place again association of the TARP modulatory mutants with GluA1 and GluA2(R) receptors was examined. The current-voltage (I-V) curve of GluA1 homomers without TARPs showed inward rectification caused by the voltage-dependent block due to the presence of intracellular spermine. GluA1 PA block was similarly attenuated by wild-type γ2 and the null γ2 and super TARP mutants, as also confirmed by the rectification index values, implying unaltered assembly of GluA1 receptors with the TARP mutants compared to wild-type γ2 (*RI* (+60/−60) = 0.04 ± 0.00 and *n* = 3 for GluA1, 0.26 ± 0.13 and *n* = 6 for GluA1 + γ2, 0.21 ± 0.08 and *n* = 5 for GluA1 + null γ2, 0.22 ± 0.06 and *n* = 2 for GluA1_super TARP; **Fig. 20 A**). In the case of GluA2(R) homomers instead, the PA block relief test was not an unequivocal indication of TARP association, being GluA2(R)-containing AMPARs not sensitive to the block. As a consequence, the I-V relationship of unTARPed or TARPed GluA2(R) complexes results to be almost linear. Data of GluA2(R) receptors alone actually could not be collected, since this subunit very hardly expresses at the cell membrane unless in the presence of other AMPAR subunits or auxiliary proteins. However, the I-V curves of GluA2(R) with wild-type γ2 or with the γ2 mutants appeared to perfectly overlap and their rectification indices to be comparable. Therefore, unaffected assembly of the mutant complexes could be assumed also for GluA2(R) homomeric receptors (*RI* (+60/−60) = 0.66 ± 0.06 and *n* = 5 for GluA2(R) + γ2, 0.67 ± 0.05 and *n* = 6 for GluA2(R) + null γ2, 0.67 ± 0.07 and *n* = 4 for GluA2(R) + super TARP; **Fig. 20 B**).

3.5.2 TARP mutants modulation of GluA1 and GluA2(R) homomers desensitisation

After establishing that mutations of TARP extracellular loops do not interfere with complexes formation not only of GluA2(Q) but also of GluA1 and GluA2(R) receptors, the effect of the null γ2 and the super TARP mutants on gating of homomeric channels of these AMPAR

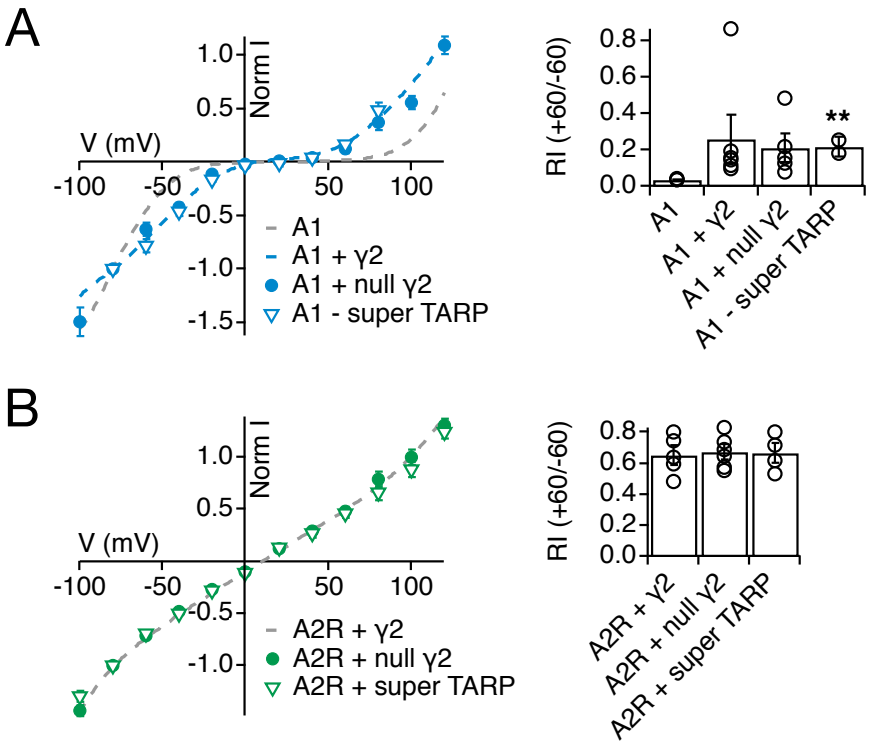

Figure 20. Unaltered association of γ2 modulatory mutants with GluA1 and GluA2(R) homomers. (**A**) To the left, normalised I-V plots of GluA1 homomers displaying attenuated inward rectification and PA block similarly by wild-type and mutant γ2 (γ2 ΔL1 L2_GS or "null γ2" and L1 γ8 in γ2 or "super TARP", *blue*), in comparison to GluA1 alone (*grey*); to the right, bar graphs with the corresponding rectification indices. (**B**) Almost linear I-V curves of non-inwardly rectifying PA block-insensitive GluA2(R) homomers in complex with wild-type γ2 (*grey*) or with γ2 modulatory mutants (*green*; *left panel*); summary of the rectification indices of GluA2(R) complexes (*right panel*). **p < 0.01 against GluA1 without TARPs. Currents were recorded using 50 μM spermine in the pipette solution.

subtypes was inspected. Analogously to what seen with GluA2(Q) homomers, the removal of both L1 and L2 from γ2 resulted in a reduced modulation by the regulatory protein of the kinetics of both GluA1 and GluA2(R) homomers. This was particularly evident for GluA2(R) receptors, whose association with wild-type γ2 produced a very large steady-state current (46 ± 3%, n = 7), that was markedly thinned by the null γ2 mutant (9 ± 1%, n = 6; **Fig. 21 C and D**). Besides this, the entry into desensitisation of GluA2(R)-null γ2 complexes was significantly faster with regards to GluA2(R)-wild-type γ2 complexes (65 ± 6 s^{-1}, n = 6 and 40 ± 5 s^{-1}, n = 7 for GluA2(R) + null γ2 and + wt γ2 respectively). Also the entry into

desensitisation of GluA1 receptors turned out to be much faster with the null γ2 mutant compared to wild-type γ2 (241 ± 26 s^{-1}, *n* = 6 for GluA1 + null γ2 and 173 ± 18 s^{-1}, *n* = 7 for GluA1 + wt γ2; **Fig. 21 A and B**). Although γ2 did not induce a big augment of GluA1 steady-state current and thus the effect of the null mutant was not as striking as for GluA2(R), null γ2 determined a decrease in the steady-state current nearly to the same level as unassociated GluA1 homomers (2 ± 1%, *n* = 6 for GluA1 + null γ2 and 1 ± 0%, *n* = 6 for GluA1 alone). The super TARP mutant instead behaved somehow unexpectedly with these AMPAR subunits: the strongly enhanced modulation given by the insertion of γ8 L1 that was noticed for GluA2(Q) was only partially enhanced for GluA1 and GluA2(R) receptors. In fact, the super TARP did not really determine any change in GluA1 and GluA2(R) desensitisation with respect to wild-type γ2 (I_{ss} = 9 ± 3% and *n* = 6 for GluA1_super TARP, 6 ± 3% and *n* =7 for GluA1 + γ2, 51 ± 2% and *n* = 3 for GluA2(R) + super TARP), except for a slowing down in the entry into desensitisation of the complexes (91 ± 10 s^{-1}, *n* = 6 and 18 ± 4 s^{-1}, *n* = 3 for GluA1 and GluA2(R) respectively with the super TARP; **Fig. 21 A-D**). Noteworthy though was the effect of the super TARP on the decay of GluA2(R) currents at the end of the jump in the glutamate solution and therefore during the phase in which the ligand unbinds from the receptor. This decay was considerably slower compared to that of currents mediated by GluA2(R)-wild type γ2 complexes and was not visible for GluA1-super TARP complexes, possibly meaning a stronger affinity to glutamate of GluA2(R) receptors in the presence of the super TARP.

3.5.3 TARP mutants modulation of GluA1 and GluA2(R) homomers superactivation

The slow superactivating current rising upon long glutamate exposure was also quantified for GluA1 and GluA2(R) homomeric complexes with the TARP modulatory mutants null γ2 and super TARP. As supposed, no superactivation was measured for GluA1 together with the null γ2 (0 ± 0%, *n* = 3). However, GluA1 did not undergo any superactivation also in the presence of the wild-type γ2, excluding one case out of three recordings (2 ± 2%, *n* = 3; **Fig. 22, A and B**). This result was coherent with what shown in previous work from other people (Kato et al., 2010) that similarly could not detect superactivation (slow augmenting current, synonymous with “resensitisation”) for GluA1 coexpressed with γ2 in HEK 293 cells, but observed a big extent of superactivation when GluA1 was coexpressed with TARP γ8. In our hands though,

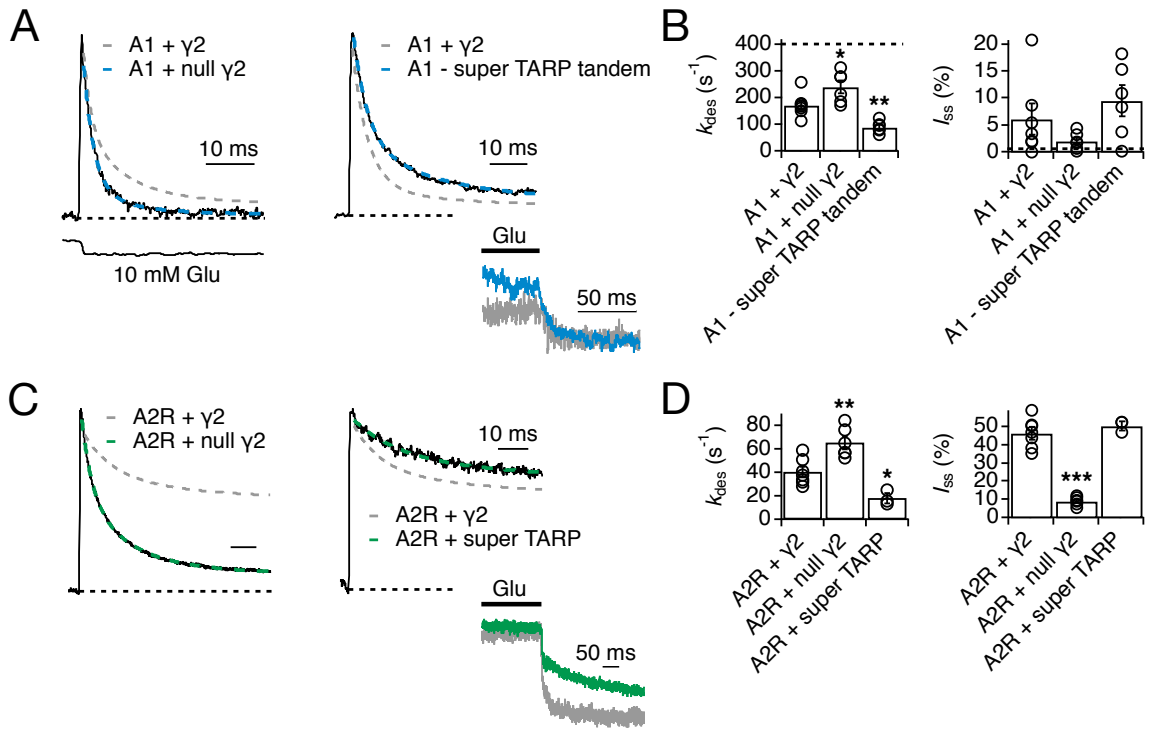

Figure 21. Desensitisation of GluA1 and GluA2(R) homomeric complexes with γ2 modulatory mutants. (**A**) Effect of the null γ2 (*left panel*) and the super TARP (*right panel*) mutants on desensitisation of GluA1 homomeric channels (*blue)* in response to 500 ms 10 mM glutamate application. Traces of GluA1 with wild-type γ2 are overlapped in grey for comparison. Solution exchange measured at the open tip is also illustrated. (**B**) Bar graphs with k_{des} and I_{ss} values for GluA1 complexes with wt and mutant γ2; black dotted lines represent mean values for GluA1 without TARPs. (**C**) Desensitisation properties of null γ2 (*left panel*) and super TARP (*right panel*) on GluA2(R) homomers (*green*) during a 500 ms pulse of 10 mM glutamate. GluA2(R) + wt γ2 is shown in grey. Insets in (**A**) and (**C**) represent the decay of GluA1 and GluA2(R) currents at the end of glutamate application in the presence of the super TARP (*blue* and *green* respectively), compared to in the presence of wild-type γ2 (*grey*). (**D**) Bar graphs collecting desensitisation data for GluA2(R)-wt or mutant γ2 complexes. *p < 0.05, **p < 0.01 and ***p < 0.001 against GluA + wild-type γ2. When TARPs were present currents were recorded at +50 mV with 50 μM spermine in the pipette solution, otherwise at –60 mV with PA-free intracellular solution.

the super TARP, endowed with the strong positive modulatory element of γ8 L1, was as well unable to induce superactivation of GluA1 complexes (0 ± 0%, *n* = 3). Controversially then according to our data GluA1, oppositely to GluA2(Q), seemed overall not prone to sustain TARP-evoked superactivation. The effects of the TARP modulatory mutants on GluA2(Q)

superactivation were not precisely reflected also on GluA2(R). In fact, a small degree of superactivation was recorded for GluA2(R) in complex with wild-type γ2 (2 ± 2%, *n* = 3), but strangely also with the null γ2 (1 ± 2%, *n* = 5; **Fig. 22 C and D**). Nonetheless, even if not proportionate to the almost 30% that was measured for GluA2(Q) (see **Fig. 13 A and C**), also in this case and compared to the other conditions the super TARP mediated a noticeable increase in superactivation of GluA2(R) complexes (6 ± 4%, *n* = 3).

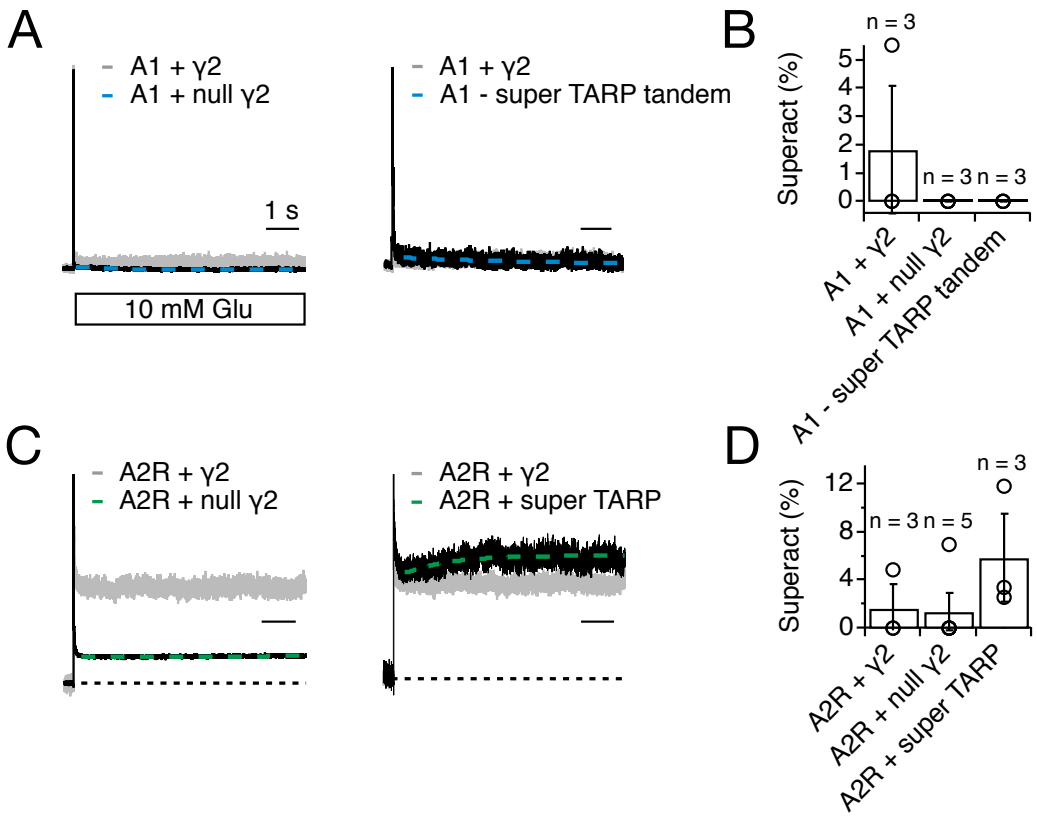

Figure 22. GluA1 is refractory to superactivation by the super TARP. (**A**) Representative traces of currents evoked by 10 mM glutamate applied for 7 s to GluA1-wt γ2 (*grey*), GluA1-null γ2 (*blue*, *left panel*) and GluA1-super TARP (*blue*, *right panel*) complexes. (**B**) Summary of the data represented in (**A**). (**C**) Exemplary responses of GluA2(R) in complex with wt γ2 (*grey*), null γ2 (*green*, *left panel*) or super TARP (*green*, *right panel*) to long glutamate application, displaying super TARP-induced superactivation. (**D**) Bar graphs recapitulating GluA2(R) superactivation data. Currents were recorded at +50 mV in the presence of 50 µM spermine in the pipette solution.

3.5.4 Association of TARP modulatory mutants with GluA1/A2(R) heteromeric receptors

Similarly to GluA2(R) homomers, heteromers of GluA1/A2(R) subunits are not subject to the voltage-dependent block by intracellular PAs that is partially relieved by the association with TARPs. Therefore, the I-V relationships of GluA1/A2(R) complexes are almost linear and it is difficult to interpret TARP assembly based on them. However, again equally to GluA2(R) homomers, the I-V curves of null γ2, super TARP and additionally null γ8 (that was the chimera of γ8 with L2 neutralised, L1 γ2 in γ8 L2_GS) were fairly overlapping with that of wild-type γ2. Thus, also in this case it could be assumed that mutating TARP extracellular loops did not disturb formation of complexes with AMPARs (**Fig. 23 A**). Interestingly, the I-V curves of the heteromeric complexes with wild-type or mutant TARPs were all slightly less linear than the I-V curve of the heteromers in the absence of TARPs. This discrepancy also emerged through the rectification indices, showing TARPed GluA1/A2(R) complexes altogether a bit lower *RI* (+60/–60) values than GluA1/A2(R) without TARPs (0.58 ± 0.07, n = 11 for GluA1/A2(R) + γ2, 0.66 ± 0.09, n = 11 for GluA1/A2(R) + null γ2, 0.61 ± 0.07, n = 13 for GluA1/A2(R) + super TARP, 0.52 ± 0.03, n = 4 for GluA1/A2(R) + null γ8 and 0.83 ± 0.08, n = 4 for GluA1/A2(R) alone; **Fig. 23 B**). Despite this, some contamination with unTARPed complexes in the other heteromeric conditions could not be completely excluded.

3.5.5 TARP mutants modulation of GluA1/A2(R) heteromer desensitisation

When analysing the desensitisation properties of the TARP modulatory mutants on GluA1/A2(R) complexes, the null γ2 mutant appeared to effectively behave as a numb modulator of the heteromer kinetics. This outcome was analogous to what observed before for the respective homomeric subunits and also for GluA2(Q) homomers. The desensitisation rate was strongly increased with respect to wild-type γ2 (108 ± 14 s^{-1}, n = 6 and 64 ± 7 s^{-1}, n = 8 for GluA1/A2(R)/null γ2 and GluA1/A2(R)/wt γ2 respectively) and the steady-state current reduced almost to the level of the heteromers without regulatory proteins (4 ± 1%, n = 6 for GluA1/A2(R)/null γ2 and 1 ± 0%, n = 4 for GluA1/A2(R) alone; **Fig. 24 B, C and F**). Likewise, modulation of GluA1/A2(R) heteromer desensitisation was weakened by the null γ8 chimera, in which the vigorous effect of γ8 L1 was wiped out by γ2 L1 and simultaneously L2 was neutralised. This combination resulted in a not much faster entry into desensitisation (91 ± 18 s^{-1}, n = 4), but in a significantly diminished steady-state current relatively to GluA1/

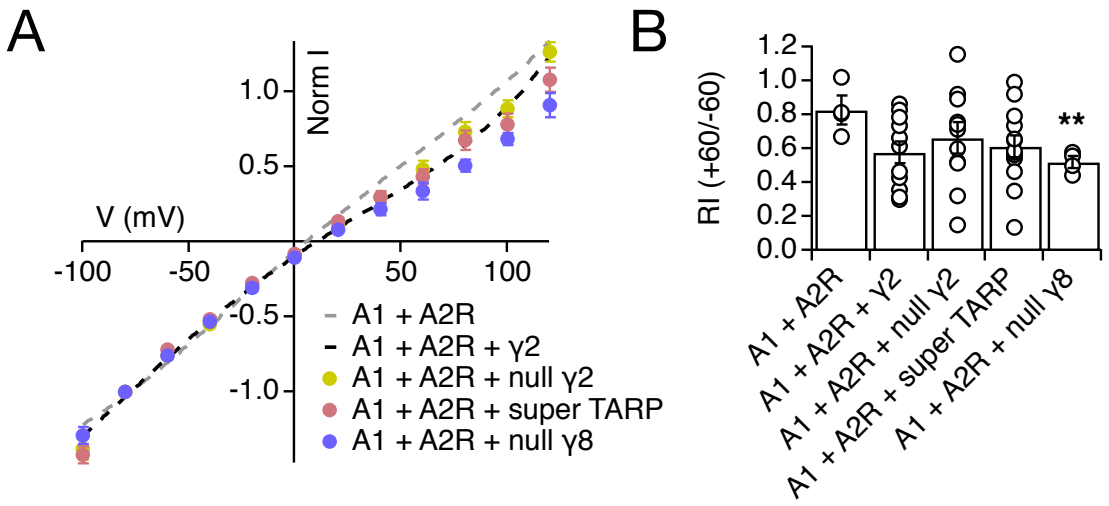

Figure 23. TARP modulatory mutants form complexes with heteromeric GluA1/A2(R) receptors. (**A**) Normalised I-V curves of heteromeric GluA1/A2(R) complexes without TARPs (*grey dotted line*), with wild-type γ2 (*black dotted line*), with null γ2 (*yellow circles*), with super TARP (*pink circles*) and with null γ8 (L1 γ2 in γ8 L2_GS, *purple circles*). (**B**) Bar graph summarising the rectification indices of the different conditions illustrated in (**A**). **p < 0.01 against GluA1/A2(R) alone. Currents were recorded using 50 μM spermine in the pipette solution.

A2(R)/wt γ2 complexes (7 ± 2%, n = 4 and 18 ± 1%, n = 8 respectively for GluA1/A2(R)/null γ8 and GluA1/A2(R)/wt γ2; **Fig. 24 C, E and F**). For correctness, this mutant γ8 condition should have been tested against the tripartite GluA1/A2(R)/wt γ8 and not γ2 complex. Being though this sort of experiment quite challenging and laborious, for the sake of simplicity it was initially omitted with the intention to be completed in the future. Regarding the super TARP instead, results on GluA1/A2(R) heteromers appeared much more persuasive than the homomers results, showing this mutant to be once again an effective potentiator of AMPAR kinetics and blocker of desensitisation. Similarly to GluA2(Q) indeed, the introduction of γ8 L1 in γ2 more than doubled the steady-state current of GluA1/A2(R) complexes in comparison to wild-type γ2 and the rate of desensitisation was approximately halved (I_{ss} = 45 ± 2% and k_{des} = 37 ± 5 s^{-1}, n = 9; **Fig. 24 C, D and F**). Moreover, as already noticed for GluA2(R) homomers, the super TARP remarkably slowed down the current decay of GluA1/A2(R) heteromers during the phase of glutamate unbinding, suggesting an implication of this mutant not only in potentiation of gating but also of agonist affinity.

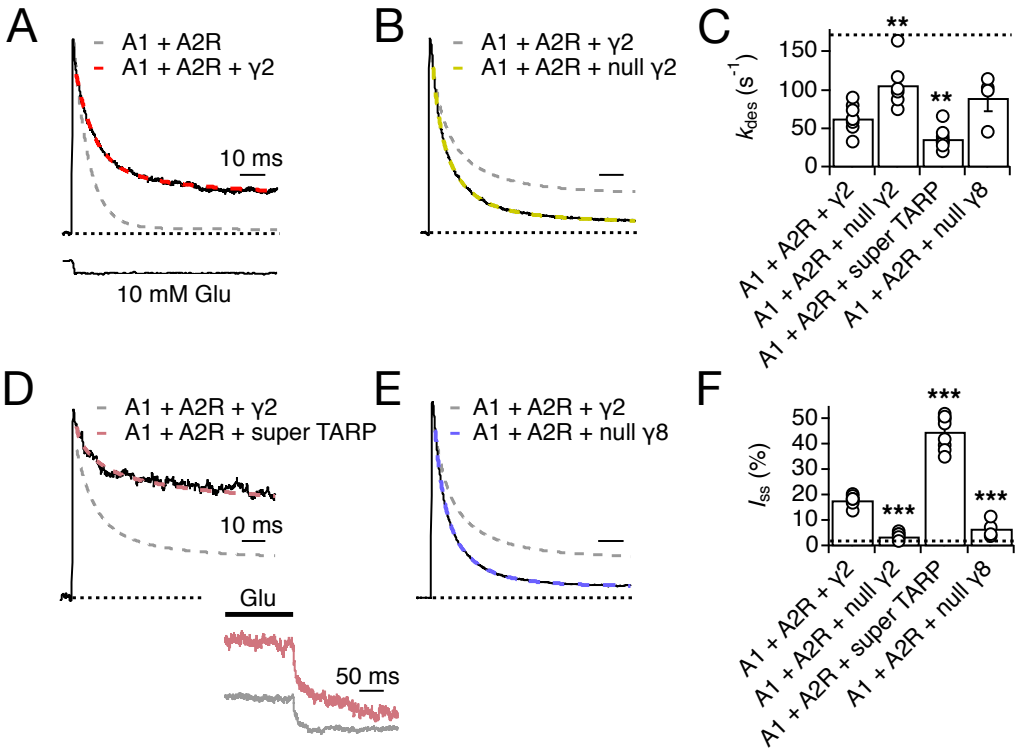

Figure 24. Desensitisation properties of GluA1/A2(R) heteromeric complexes with TARP modulatory mutants. (**A**) Effect of TARP γ2 (*red*) on the desensitisation of GluA1/A2(R) heteromers (in grey without TARPs), following activation with 10 mM glutamate. Solution exchange measured at the open tip is illustrated below. (**B**) Representative desensitisation trace of GluA1/A2(R) heteromers with null γ2 (*yellow*), compared to wild-type γ2 (*grey*). (**C**) Bar graph summarising the desensitisation rates of the different heteromeric conditions. (**D**) Exemplary desensitisation traces of GluA1/A2(R) complexes with the super TARP (*pink*) and, overlapped, with wild-type γ2 (*grey*). The inset shows the current decay during glutamate wash-out at the end of its application. (**E**) Desensitisation of GluA1/A2(R)/null γ8 complexes (*purple*); for comparison GluA1/A2/γ2 is represented in grey. (**F**) Bar graph recapitulating the steady-state current values of the heteromeric TARP complexes. Black dotted lines in (**C**) and (**F**) represent mean values for the heteromers without TARPs. **p < 0.01 and ***p < 0.001 against GluA1/A2(R) alone. When TARPs were present currents were recorded at +50 mV with 50 µM spermine in the pipette solution, otherwise at –60 mV with PA-free intracellular solution.

3.5.6 TARP mutants modulation of GluA1/A2(R) heteromer deactivation

The effect of the TARP modulatory mutants was also evaluated on the deactivation of GluA1/A2(R) heteromeric complexes following activation by a short (1 ms) pulse of glutamate. This kinetic parameter is of particular relevance because it mimics the decay of AMPAR-mediated synaptic currents in response to fast neurotransmitter release. Therefore, it seemed more

meaningful to be taken into account for the more physiological heteromeric condition rather than for the homomeric ones. Wild-type GluA1/A2(R)/γ2 complexes deactivated with a rate of approximately 222 ± 22 s^{-1} (n = 5). The elimination of both L1 and L2 in γ2 (null γ2) and the combination of L1 swap and L2 neutralisation in γ8 (null γ8) accelerated the deactivation rate more than 2-fold, to 482 ± 72 s^{-1} (n = 6) and 546 ± 77 s^{-1} (n = 3) respectively (**Fig. 25 A, B and D**). In the opposite direction the effect of the super TARP was even more impressive: the presence of the long L1 of γ8 in γ2 determined an about 5-fold slowing down in the deactivation rate of the heteromeric complexes in comparison to wild-type γ2 (43 ± 21 s^{-1}, n = 4; **Fig. 25 C and D**).

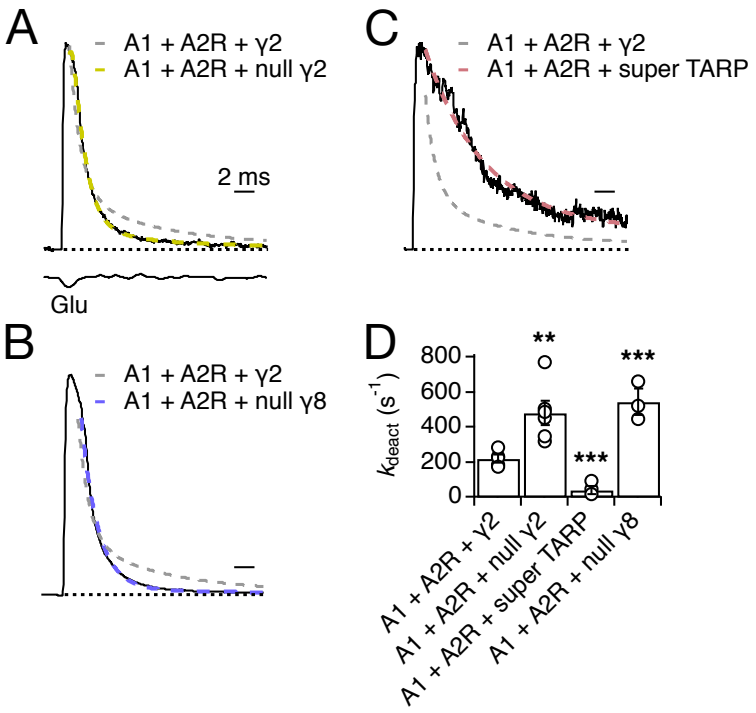

Figure 25. Deactivation kinetics of GluA1/A2(R) heteromers modulated by null and super TARPs. (**A**) Representative traces showing the effect of the mutants null γ2 (*yellow*), (**B**) null γ8 (*purple*) and (**C**) super TARP (*pink*) on the deactivation of GluA1/A2(R) heteromers, following a 1 ms pulse of 10 mM glutamate. Exemplary deactivation trace of wild-type GluA1/A2(R)/γ2 complexes is overlapped in grey for comparison. (**D**) Summary of the deactivation rates of the wild-type and mutant tripartite species. **p < 0.01 and ***p < 0.001 against GluA1/A2(R)/γ2. Currents were recorded at +50 mV in the presence of 50 μM spermine in the pipette solution.

3.5.7 TARP mutants modulation of GluA1/A2(R) heteromer superactivation

Also in terms of superactivation the effects of the TARP mutants on GluA1/A2(R) heteromers segregated quite well accordingly to the type of extracellular loop mutations. Wild-type γ2 evoked on average about 2 ± 1% (n = 7) superactivation of the heteromeric complexes. This did not constitute a really sizeable response and in fact just for two patches out of seven 4 and 7% superactivation could be measured, whereas for the other five none was detected. Nevertheless, the null mutants, both γ2 and γ8, did not show in any of the attempted recordings any trace of superactivation (0 ± 0%, n = 4 for null γ2 and 0 ± 0%, n = 3 for null γ8; **Fig. 26 A, B and D**), correspondingly to what found for GluA2(Q) homomeric complexes (see **Fig. 14 B and C** for null γ8 or L1 γ2 in γ8 L2_GS and **Fig. 15 C and D** for null γ2 or γ2 ΔL1 L2_GS). On the contrary, the super TARP mutant increased the amount of GluA1/A2(R) superactivation to approximately the double of wild-type γ2 (4 ± 2%, n = 6; **Fig. 26 C and D**). It is worth noticing that this chimera similarly potentiated superactivation of homomeric GluA2(R) receptors. The GluA1 subunit, instead, in the homomeric condition resulted to be refractory to superactivation. However, in the heteromeric condition, super TARP-mediated potentiation was restored, hinting at a possibly dominant role of the GluA2(R) subunit in GluA1/GluA2(R) heteromers.

3.5.8 Fast train responses of heteromeric GluA1/A2(R) complexes with TARPs

Superactivation is a very interesting property to look at when studying TARP regulation of AMPA receptor gating, since it represents a TARP-induced accumulation of AMPAR complexes in a high conductance state. This potentiating effect could obviously have important implications at a synaptic level, where plasticity of AMPARs is finely tuned. However, the experimental time during which superactivation is observed (several seconds) does not correspond to the ultra fast kinetics of synaptic signalling (in the range of 1-100 milliseconds approximately). Thus, another way to capture superactivation, that would be more representative of the physiological situation of intense neurotransmitter release, is through application of trains of short (1 ms) pulses of glutamate. It was demonstrated in fact that train stimulation at different frequencies can boost responses of GluA2(Q) homomeric receptors in the presence of TARP γ2 or γ8, specifically noticeable as an increase of the peak current following desensitisation and as a substantial pedestal current slowly developing over

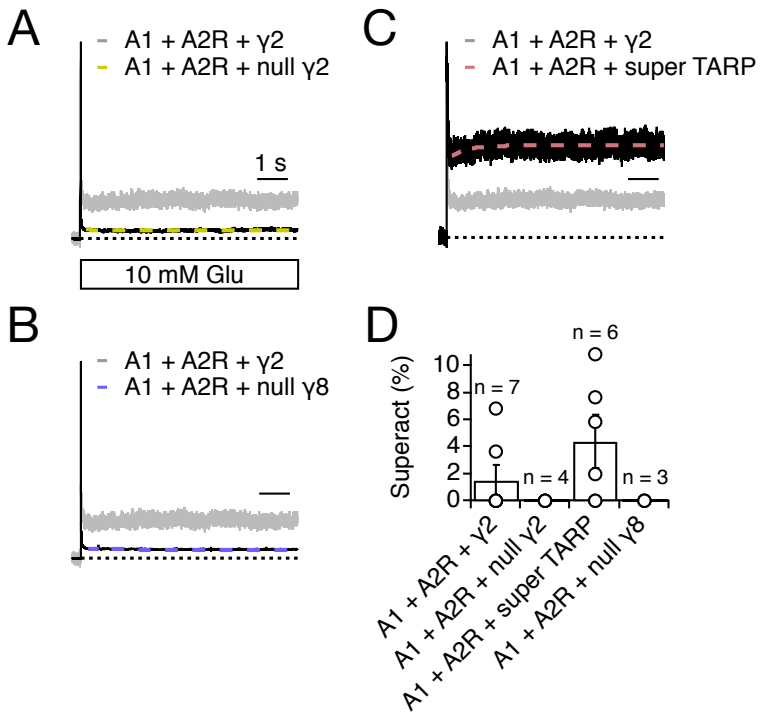

Figure 26. Super TARP-mediated superactivation is restored in GluA1/A2(R) complexes. (**A**) Upon long (7 s) 10 mM glutamate exposure, no superactivation was measured for GluA1/A2(R) heteromers in complex with the null γ2 (*yellow*) or (**B**) the null γ8 (*purple*). When wild-type γ2 was present (*grey*), in a few cases a small level of GluA1/A2(R) superactivation was recorded. (**C**) γ2-induced superactivation was doubled by the super TARP mutant (*pink*).(**D**) Bar graph collecting all the superactivation measurements of the analysed heteromeric conditions. Currents were recorded at +50 mV in the presence of 50 μM spermine in the pipette solution.

time during the train (Carbone & Plested, 2016). Therefore, train responses of GluA1/A2(R) heteromeric receptors in complex with wild-type and mutant TARPs were also analysed. At 10, 20 and 50 Hz frequencies neither wild-type GluA1/A2(R)/γ2 or mutant complexes showed an increase of the peak current after the trough of desensitisation (**Fig. 27 A and B**). Nonetheless, only for the super TARP heteromeric condition a pedestal current was visualised and, even if not really pronouncedly, it seemed to gradually increase during the train. Moreover, the charge transfer of the train responses was calculated. Since the postsynaptic membrane must be depolarised by charging, the charge transfer is a crucial parameter for defining how synaptic transmission might get stronger. The charge transfer, normalised to the initial peak current, of GluA1/A2(R) heteromers with the null γ2 or γ8 mutant was significantly lower at all frequencies (10, 20 and 50 Hz), in comparison to the heteromers

Construct	k_{des} (s^{-1})	*p*	I_{ss} (%)	*p*	Superact (%)	*p*
A1 wt	400 ± 40 (6)		1 ± 0.2		–	–
A1 + γ2	170 ± 20 (7)		6 ± 3		2 ± 2 (3)	
A1 + null γ2 §	240 ± 30 (6)	0.04	2 ± 1	0.2	0 (3)	0.4
A1 + super TARP §	90 ± 10 (6)	0.002	9 ± 3	0.4	0 (3)	0.4
A2(R) wt	–	–	–	–	–	–
A2(R) + γ2	40 ± 5 (7)		45 ± 5		2 ± 2 (3)	
A2(R) + null γ2 Δ	65 ± 5 (6)	0.003	9 ± 1	4×10^{-7}	1 ± 2 (5)	0.9
A2(R) + super TARP Δ	20 ± 5 (3)	0.01	50 ± 2	0.4	6 ± 4 (3)	0.3
A1/A2(R) wt	170 ± 30 (4)		1 ± 0.4		–	
A1/A2(R) + γ2	65 ± 5 (8)		18 ± 1		2 ± 1 (7)	
A1/A2(R) + null γ2 #	110 ± 15 (6)	0.006	4 ± 1	4×10^{-9}	0 (4)	0.3
A1/A2(R) + null γ8 #	90 ± 20 (4)	0.08	7 ± 2	2×10^{-5}	0 (3)	0.4
A1/A2(R) + super TARP #	35 ± 5 (9)	0.002	45 ± 2	9×10^{-9}	4 ± 2 (6)	0.2

Table 2. Kinetic properties of null and super TARP mutants on GluA1 and GluA2(R) homomers and heteromers. List of desensitisation rate (k_{des}), steady-state current (I_{ss}) and superactivation (Superact) values of GluA1 and GluA2(R) homomers and heteromers, alone or in complex with wild-type γ2, null or super TARP mutants. The values are shown as mean ± SEM. The number of recordings for each condition is indicated in brackets. *p* values (from Student's *t*-test) were calculated as follows: § against GluA1 + γ2 wt, Δ against GluA2(R) + γ2 wt, # against GluA1/A2(R) + γ2 wt. To record currents in the presence of TARPs, outside-out patches were voltage-clamped at +50 mV and the intracellular solution contained 50 µM spermine. In the absence of TARPs, currents were recorded at the holding potential of –60 mV with spermine-free intracellular solution.

with wild-type γ2 (at 10 Hz: 0.11 ± 0.00 pC/pA and n = 2 for GluA1/A2(R)/null γ2, 0.13 ± 0.01 pC/pA and n = 3 for GluA1/A2(R)/null γ8, 0.22 ± 0.03 pC/pA and n = 2 for GluA1/A2(R)/γ2; at 20 Hz: 0.19 ± 0.03 pC/pA and n = 2 for GluA1/A2(R)/null γ2, 0.21 ± 0.02 pC/pA and n = 3 for GluA1/A2(R)/null γ8, 0.36 ± 0.02 pC/pA and n = 3 for GluA1/A2(R)/γ2; at 50 Hz: 0.21 ± 0.04 pC/pA and n = 4 for GluA1/A2(R)/null γ2, 0.28 ± 0.04 pC/pA and n = 2 for GluA1/A2(R)/null γ8, 0.58 ± 0.05 pC/pA and n = 4 for GluA1/A2(R)/γ2; **Fig. 27 C**). For the super TARP mutant instead, at 10 Hz frequency the charge transfer was apparently higher (0.61 ± 0.54 pC/pA, n = 2), while at 20 and 50 Hz perhaps slightly higher than wild-type γ2 (0.41 pC/pA, n = 1 and 0.64 pC/pA, n = 1 at 20 and 50 Hz respectively), but further

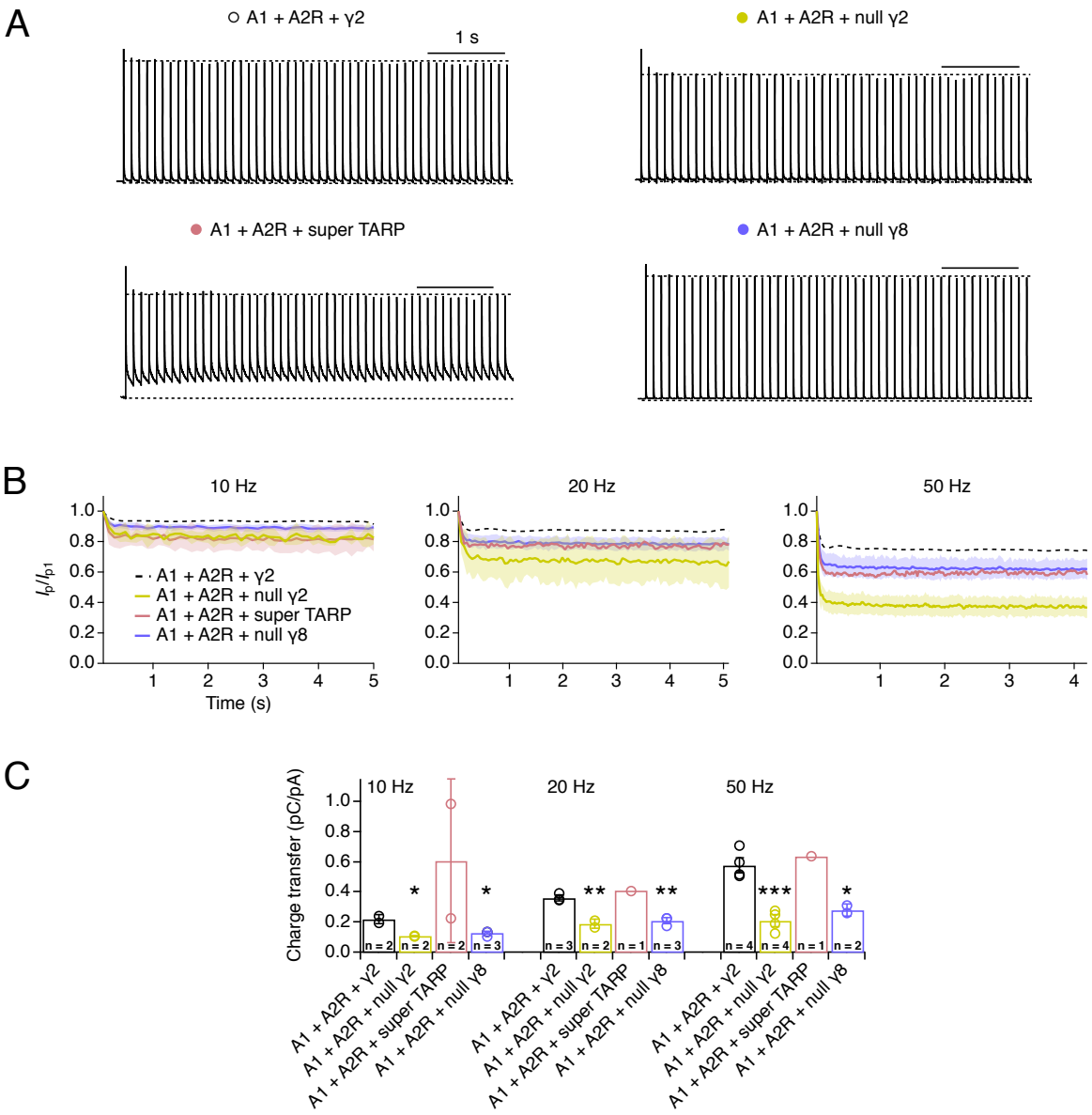

Figure 27. Train responses of GluA1/A2(R)/super TARP complexes show pedestal current. (**A**) Exemplary responses of GluA1/A2(R) heteromers together with, in clockwise order, wild-type γ2, null γ2, null γ8 and super TARP to 10 Hz train pulses (1 ms pulse width) of 10 mM glutamate. Coloured symbols appearing next to the titles refer to the colour-code in the following panels. (**B**) Plots of the peak current increase over the train duration at 10 (*left panel*), 20 (*middle panel*) and 50 (*right panel*) Hz frequency for the aforementioned conditions. (**C**) The charge transfer of GluA1/A2(R) heteromers, calculated as the integrated area of the whole train normalised to the first peak amplitude, is decreased by both the null γ2 (*yellow*) and γ8 (*purple*) mutants at 10, 20 and 50 Hz and at least at 10 Hz it seems to augment in the presence of the super TARP mutant (*pink*), in comparison to wt γ2 (*black*). Numbers inside the bars indicate the number of patches for each condition. *p < 0.05, **p < 0.01 and ***p < 0.001 against GluA1/A2(R)/wt γ2. Currents were recorded at +50 mV in the presence of 50 µM spermine in the pipette solution.

experiments are definitely needed to confirm. Overall anyway these results suggested that the TARP null modulatory mutants could hinder AMPAR-mediated synaptic transmission by disfavouring depolarisation of the postsynaptic membrane. On the other hand, the strong positive modulation by the super TARP mutant seemed to play a potentiating role on AMPA receptor heteromeric train responses, that might be related to what earlier observed as superactivation and altogether constitute the substrate for synaptic plasticity potentiation.

3.5.9 Model for abundance of tripartite complexes

When cotransfecting two AMPAR subtypes, such as GluA1 and GluA2(R), together with a TARP subunit with the intention of studying the behaviour of the heteromeric AMPAR-TARP complex, it is actually not possible to isolate purely the triple complexes. For example, in the case of GluA1, GluA2(R) and γ2 five species are expected to assemble at the plasma membrane: GluA1, GluA1/A2(R), GluA1/γ2, GluA2(R)/γ2 and the tripartite complex GluA1/A2(R)/γ2. As already mentioned, GluA2(R) alone is very unlikely to express at the cell membrane. GluA1 homomers instead can express, but at +50 mV they are almost completely blocked by the presence of intracellular spermine. Therefore, even if their share could be omitted, it is assumed to be really low. To overcome this issue, a statistical model was created to predict the abundance of wild-type GluA1/A2(R)/γ2 and mutant GluA1/A2(R)/super TARP complexes, based on gating and trafficking effects of the other respective non-tripartite four species that these cotransfections permit. The kinetic profile of bipartite heteromeric GluA1/A2(R) complexes without TARPs is characterised by a very fast entry into desensitisation (168 s^{-1}) and almost absent steady-state current (1%), quite in contrast with the extremely slow desensitisation and high steady-state current level of tripartite GluA1/A2(R)/super TARP (k_{des} = 37 s^{-1} and I_{ss} = 45%) but also GluA1/A2(R)/γ2 (k_{des} = 64 s^{-1} and I_{ss} = 18%) complexes. Furthermore, as previously noted, wild-type and mutant TARP tripartite complexes are equally more rectifying than A1/A2(R) heteromers alone (*RI* = 0.58 for GluA1/A2(R)/γ2, 0.61 GluA1/A2(R)/super TARP and 0.83 for GluA1/A2(R) without TARPs). On the basis of these data, we reasoned that the contribution of unTARPed GluA1/A2(R) species to the total complex mixture could not be too prevalent. Between the two remaining bipartite species that may preponderate from the triple cotransfection, GluA1/γ2 and GluA2(R)/γ2, the gating behaviour of GluA2(R)/γ2 (k_{des} = 40 s^{-1} and I_{ss} = 46%) resulted much closer, i.e. less

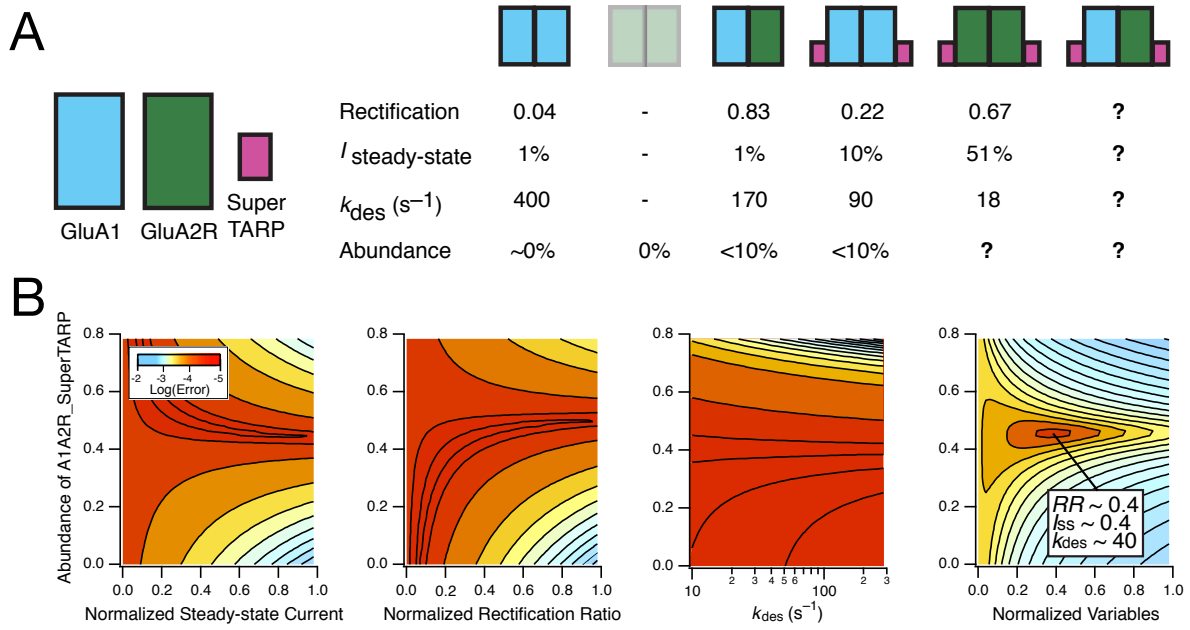

Figure 28. Predicted abundance of the triple complex GluA1/A2(R)/super TARP. (**A**) Scheme illustrating the experimentally measured parameters of rectification ratio (RR), steady-state current (I_{ss}) and desensitisation rate (k_{des}) of the different species allowed to form at the plasma membrane following the triple transfection of GluA1 (*light blue*), GluA2(R) (*green*) and the super TARP mutant (*purple*). GluA2(R) homomers are faded because mainly retained in the endoplasmic reticulum. RR, I_{ss}, k_{des} and relative abundance of the tripartite GluA1/A2(R)/super TARP complex are questioned. (**B**) Individual contours showing the probabilities for the RR, I_{ss} and k_{des} properties of the tripartite complex. Combining the contours (*right panel*) revealed that the error is lowest (*red*) when abundance of the tripartite complex is approximately 50% of the total. The white box displays the corresponding estimated RR, I_{ss} and k_{des} properties.

desensitising, than that of GluA1/γ2 (k_{des} = 173 s^{-1} and I_{ss} = 6%) to the properties of the tripartite condition. As this observation was valid also in the case of the super TARP mutant (GluA2(R)/super TARP: k_{des} = 18 s^{-1} and I_{ss} = 51%; GluA1/super TARP: k_{des} = 91 s^{-1} and I_{ss} = 9%), we hypothesised that the GluA2(R) subunit might play a dominant role in the gating of the heteromeric receptors. The abundance of the tripartite mutant complex GluA1/A2(R)/ super TARP was predicted by the model based on rectification index (or rectification ratio, RR), steady-state current and desensitisation rate of the four non-tripartite conditions GluA1, GluA1/A2(R), GluA1/super TARP and GluA2(R)/super TARP, with initial guesses for the GluA2(R)/super TARP fraction in order to take into account asymmetries in trafficking as an

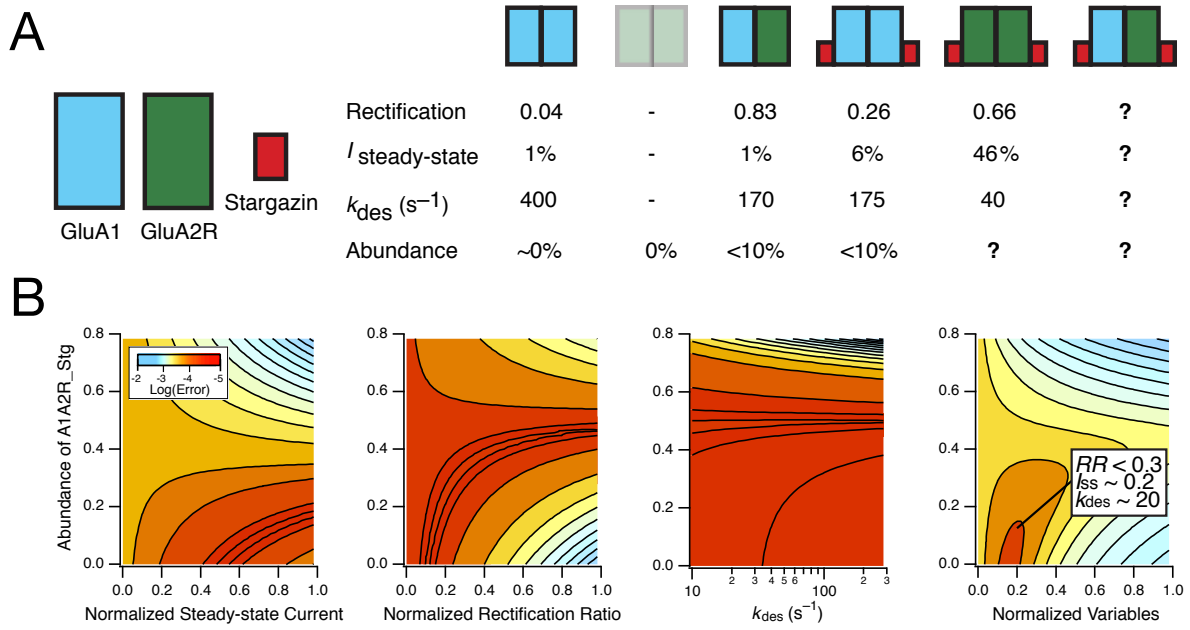

Figure 29. Predicted abundance of the triple complex GluA1/A2(R)/γ2. (**A**) Same as in Fig. 28, but for the triple transfection of GluA1 (*light blue*), GluA2(R) (*green*) and wild-type γ2 (*red*). (**B**) Contrary to the super TARP model, in this case combining the contours (*right panel*) did not produce a definitive answer. However, the error is small (*orange-red*) when abundance of the GluA1/A2(R)/γ2 complex is below 40%. The corresponding estimated properties are indicated in the white box.

explanation for GluA2(R) dominance (**Fig. 28**). The combination of the probabilities for the three variables together (RR, I_{ss} and k_{des}) revealed that the error was lowest when GluA1/A2(R)/super TARP abundance was around 50% of the total. Additionally, as experimentally observed, the triple complex was predicted to be more rectifying than GluA1/A2(R) heteromers without TARPs ($RR_{estimated} \sim 0.4$) and its estimated gating properties approximated really well the measured ones ($I_{ss\_estimated} \sim 40\%$ vs. $I_{ss\_measured} = 45\%$ and $k_{des\_estimated} \sim 40$ s^{-1} vs. $k_{des\_measured} = 37$ s^{-1}). Unfortunately, repeating the same procedure for wild-type γ2 did not produce such a definitive, unambiguous answer (**Fig. 29**). The most likely abundance for tripartite GluA1/A2(R)/γ2 complexes appeared to be less than 40% of the total. Although the estimated desensitisation rate was much slower than the measured one ($k_{des\_estimated} \sim 20$ s^{-1} vs. $k_{des\_measured} = 64$ s^{-1}), the steady-state current levels fairly coincided ($I_{ss\_estimated} \sim 20\%$ vs. $I_{ss\_measured} = 18\%$). Moreover, also in this case very high rectification ratio values resulted implausible, speaking in favour of a small contamination from unTARPed GluA1/A2

assemblies, instead defined by a higher rectification ratio, in both the wild-type γ2 and the super TARP mutant triple complex conditions. Even without accurately determining the abundances, or properties, this analysis confirmed that the tripartite complexes are more rectifying than heteromers without γ2. Therefore, while TARPs attenuate the rectification of GluA2(R)-lacking, GluA1 and GluA2(Q), AMPARs and have no effect on non-rectifying GluA2(R) homomeric receptors, they curiously seem to introduce a small extent of rectification in heteromeric forms of GluA2(R)-containing AMPARs.

3.6 Single-Cell Electroporation of TARP mutants in organotypic hippocampal slices

3.6.1 Overexpression of wild-type and mutant TARPs in CA1 pyramidal neurons

In order to further investigate AMPAR modulation by TARPs from the heterologous system of HEK 293 cells to a system that would better approximate the real brain environment, TARP constructs were overexpressed in organotypic brain slice cultures using Single-Cell Electroporation (SCE) with the aim to analyse their effect on AMPAR-mediated synaptic transmission. In particular, since TARPs are quite abundant in the hippocampus (and within the TARP family γ8 is the most plentiful, Tomita et al., 2003) and synaptic circuits in this brain region are well described, organotypic slices were prepared from the hippocampi of mouse pups at postnatal day 6 to 9 (P6-9) and SCE pyramidal neurons in the CA1 area were transfected (**Fig. 30 A and B**). Via western blotting it was shown that γ2 and γ8 (and γ3) are expressed at low levels in the cerebral cortex of newborn and neonatal rats and that they increase to reach high levels in the adult starting from about P16 (Tomita et al., 2003). Nevertheless, another study demonstrated that even if present at low levels in early postnatal mice γ8 is already functional to regulate AMPAR responses in CA1 pyramidal neurons of acute hippocampal slices (Menuz et al., 2009). The SCE procedure was tested by injecting CA1 neurons with an empty EGFP plasmid DNA and the day after the slices were checked for EGFP-fluorescent cells (**Fig. 30 C and D**). Once established the electroporating system, being aware of the strong toxicity of γ8 DNA in HEK 293 cells, the super TARP (L1 γ8 in γ2) mutant was overexpressed as a surrogate of γ8 in the hippocampus and compared to wild-type γ2 overexpression. In general, SCE worked with a yield of approximately 40-50%, meaning

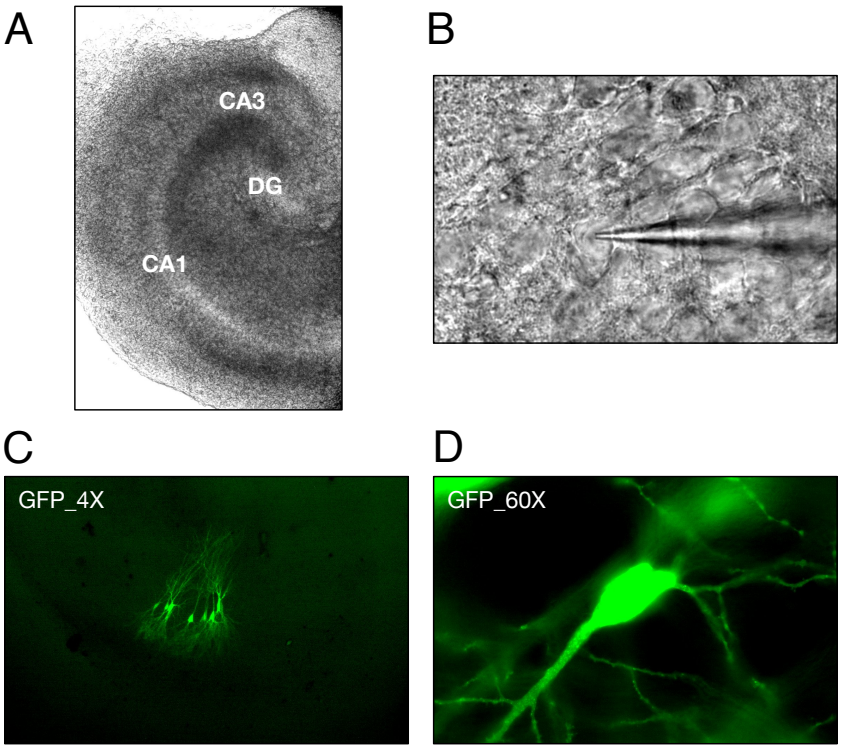

Figure 30. SCE of hippocampal CA1 pyramidal neurons. (**A**) Organotypic hippocampal slice at days in vitro 2 (DIV2) from a postnatal day 7 (P7) mouse pup. The positions of the hippocampus areas CA1, CA3 and dentate gyrus (DG) are marked; the brighter stripe in the middle of the slice represents the pyramidal cell layer. The image was acquired using a 4X objective and a Differential Interference Contrast (DIC) system. (**B**) CA1 pyramidal neurons visualised with DIC and 60X objective during SCE. A patch-clamp pipette filled with DNA-containing intracellular solution is shown while approaching the plasma membrane of a cell (DIV7, P8). (**C**) CA1 pyramidal neurons expressing EGFP (30 ng/µL) 1 day after SCE (DIV10, P7). (**D**) Focus on one of the transfected neurons displayed in (**C**).

that by electroporating around 10 neurons per slice when successful perhaps 4-5 neurons resulted transfected, rarely more and sometimes less. Wild-type γ2 DNA was initially transfected with an IRES (Internal Ribosome Entry Site) sequence before the DNA of the DsRed fluorescent protein (γ2 IRES-DsRed-Max); this produced a quite homogenous red fluorescence signal both in the cell body and in the dendrites of CA1 transfected neurons (**Fig. 31 A and B**). Electroporation of the super TARP mutant instead, also followed by the IRES and DsRed sequences (Super TARP IRES-DsRed-Max), generated a spread red fluorescent signal especially over the cell body, but on the top of it the neurons were decorated by little dots of more intense fluorescence (**Fig. 32 A and B**). In other cases, a very bright signal

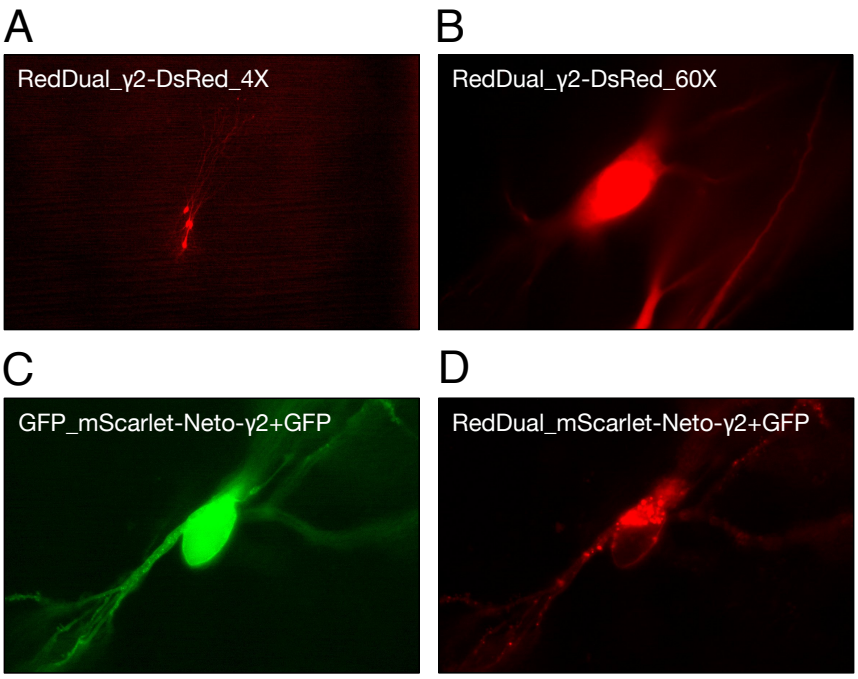

Figure 31. Heterogeneous expression of wild-type γ2 constructs. (**A**) Organotypic slice from mouse hippocampus (DIV10, P7) electroporated with γ2 IRES-DsRed-Max DNA (30 ng/µL) and imaged with 4X and (**B**) 60X objective 1 day after SCE. (**C**) CA1 pyramidal neuron (DIV10, P9) cotransfected with EGFP and (**D**) γ2 in fusion with an extracellular mScarlet fluorophore (mScarlet-Neto2-γ2) using a DNA concentration of 20 ng/µL each, 1 day after SCE.

deriving from the soma and a complete dimness in correspondence of the dendrites suggested a retained accumulation of super TARP and DsRed proteins in this part of the neuron and a lack of expression at the more interesting postsynaptic sites (**Fig. 32 D**). However, given the presence of an IRES sequence between the TARP DNA and the DsRed fluorophore and not being the two proteins directly fused together, the distribution of the fluorescence signal could have been not colocalising with the TARP distribution. For this reason, another γ2 construct was tested in which γ2 N-terminus was extracellularly labelled with another brighter red fluorescent protein (mScarlet) via fusion to the single transmembrane protein Neto2 (mScarlet-Neto2-γ2). Neto2 is an auxiliary subunit of kainate receptors, not interacting with AMPARs (Zhang et al., 2009). This construct was previously overexpressed in HEK 293 cells and proved to produce the typical effects expected by γ2 on GluA2(Q)-mediated glutamate-activated currents (data not shown). Following electroporation, mScarlet-Neto2-γ2-transfected neurons displayed a decent level of fluorescence diffused throughout the whole

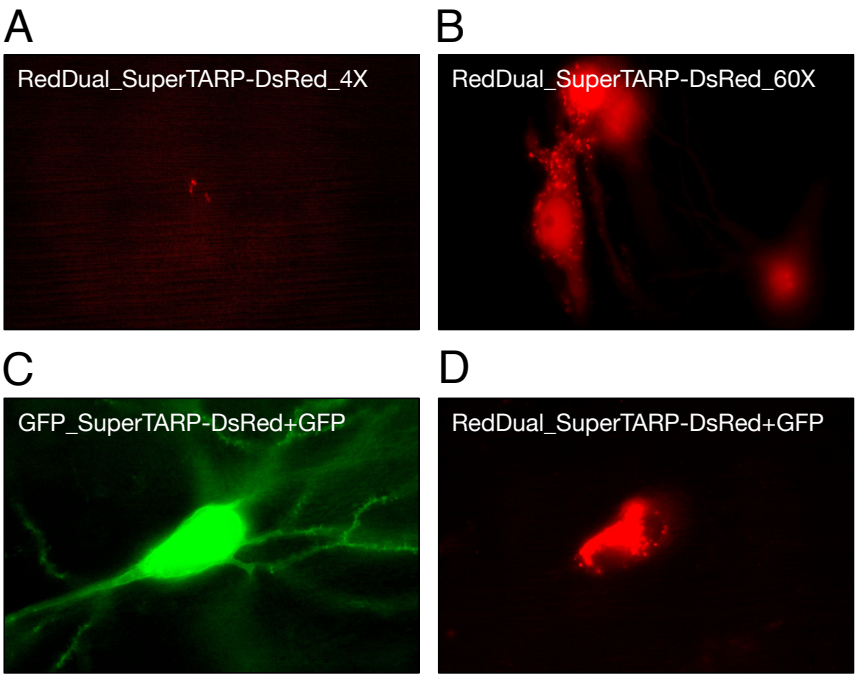

Figure 32. Super TARP-associated fluorescence concentrates in the soma. (**A**) Organotypic hippocampal slice (DIV13, P9) transfected with Super TARP IRES-DsRed-Max DNA (30 ng/µL) visualised 3 days after SCE with a 4X objective. (**B**) 60X magnification on the fluorescent neurons depicted in (**A**) reveals a diffused bright signal in the cell body and dots of more intense fluorescence all over it. (**C**) CA1 pyramidal neuron (DIV13, P8) coexpressing EGFP and (**D**) Super TARP-DsRed 1 day after electroporation, using a DNA concentration of 20 ng/µL each. The strong red fluorescent signal suggests an accumulation of the super TARP protein in the soma and a lack of expression in the dendritic regions.

neuronal structure and an higher level of fluorescence clustered probably in proximity of the nucleus and outlining the plasma membrane (**Fig. 31 D**). Moreover, similarly to the super TARP transfection little dots of intense fluorescence were also visible, but in this condition they seemed more distributed along the dendrites and less concentrated in the soma. Sometimes, since TARP-associated DsRed or mScarlet fluorescence was not always easily detectable, an EGFP plasmid was cotransfected to help the visualisation (**Fig. 31 C and 32 C**). How to exactly interpret this heterogeneity of TARP overexpression patterns is still unclear and certainly more data need to be collected in the different experimental conditions, but for sure a critical factor is represented by the amount of TARP DNA being electroporated. In the above-described experiments 20 and 30 ng/µL total TARP DNA was used, but lower amounts could as well be considered. Eventually, as initially mentioned, the main purpose of

SCE in organotypic hippocampal slices will be to use these TARP, and particularly γ8, modulatory mutants as tools to study through electrophysiology the effects of TARP modulation on AMPAR-mediated synaptic activity.

4. DISCUSSION

4.1 Mutations of TARP γ2 and γ8 extracellular loops

4.1.1 TARP extracellular loops are not involved in association with AMPA receptors

In the framework of this study, the molecular mechanisms underlying the interactions between the AMPAR and its auxiliary subunits TARPs have been investigated, with a particular focus on the role of TARP extracellular loops in the modulation of AMPAR gating. To address this issue, the extracellular loops L1 and L2 of TARP γ2 and γ8 were mutated by deletion or exchange between the two TARP subunits (L1), by replacement with a neutral linker (L2), or by a combination of these modifications.

TARP γ2, also known as stargazin, and γ8 are highly expressed throughout the mammalian brain, with peak levels respectively in the cerebellum and hippocampus, where they are part of native AMPAR complexes (Tomita et al., 2003). Within the TARP family (γ2, γ3, γ4, γ5, γ7 and γ8), γ2 and γ8 have been grouped, together with γ3 and γ4, into the type I TARPs sub-family. The classification into type I and type II TARPs (including γ5 and γ7) has both phylogenetic and functional bases. Nevertheless, even within the same subgroup, each TARP subtype is endowed with specific structural features and regulatory properties on the AMPAR function. In fact, although γ2 and γ8 both act to potentiate AMPAR responses, γ8 determines a slower entry into the desensitised state (**Fig. 11 C**) and a more profound superactivation (**Fig. 13**) of the receptor complexes compared to γ2. Another difference lies in the structure of γ2 and γ8 extracellular regions and especially in the much larger L1, that is contained in the TARP first extracellular segment, of γ8 in respect to that of γ2 (approximately 30 and 20 residues, respectively; **Fig. 5**). Seeking for a possible correlation between these functional and structural aspects, γ2 and γ8 L1, and additionally L2, mutants were overexpressed in HEK 293 cells together with the homomeric mRNA-unedited GluA2(Q) receptor and characterised through electrophysiology. In the first place, proper assembly of the mutant TARPs with GluA2(Q) was assessed. It was previously observed that TARP cotransfection gives rise to a mosaic population of receptors, in which some receptors are associated with a variable number of TARP subunits and some others lack any TARPs (Carbone & Plested, 2016). A way to purely isolate AMPAR-TARP complexes takes advantage of the voltage-dependent

block by intracellular polyamines to which Ca^{2+}-permeable (i.e. GluA2-lacking or GluA2(Q)-containing) AMPARs are subject. TARP association attenuates intracellular polyamine (such as spermine) block (Soto et al., 2007), resulting in a less rectifying I-V relationship and in a higher rectification index of TARPed versus unTARPed Ca^{2+}-permeable channels. Remarkably, all L1 and L2 mutants showed relief of spermine block and within each series of γ2 or γ8 mutants the degree of relief was comparable to that of the relative wild-type TARP (**Fig. 10** and **Fig. 15 A and B**). Similarly, mutating γ2 β4-TM2 acidic loop, included together with L1 in the TARP first extracellular segment, did not impair the ability of this γ2 mutant to attenuate GluA2(Q) block by intracellular spermine (**Fig. 16 D**). These findings imply that formation of GluA2(Q)-TARP complexes is not hindered by modifications of TARP extracellular loops, thus indicating that these elements are not determinant of TARP association with AMPARs.

4.1.2 Characterisation of the role of TARP Loop1 and Loop2 in GluA2(Q) gating

The various effects of TARP regulation on the AMPAR function have been ascribed to distinct structural domains of the auxiliary subunits. For instance, different studies that made use of chimeric TARP mutants demonstrated that the first extracellular segment is involved in modulation of AMPAR desensitisation and deactivation kinetics (Tomita et al., 2005; Turetsky et al., 2005; Cho et al., 2007). In line with these works, swapping L1 between γ2 and γ8 (L1 γ8 in γ2, L1 γ2 in γ8) or deleting it from both (γ2 ΔL1, γ8 ΔL1) altered modulation of GluA2(Q) rate of desensitisation and steady-state current by γ2 and γ8 (**Fig. 11**). In particular, L1 of γ8 in γ2 emerged as a very strong positive GluA2(Q) modulator, capable of markedly slowing the receptor entry into desensitisation (**Fig. 11 C**), increasing γ2 steady-state current to an even higher level than that of γ8 (**Fig. 11 D**) and transferring the same amount of γ8 superactivation to γ2 (**Fig. 13 C**). On the basis of this enhanced modulation of GluA2(Q) agonist-evoked responses, L1 γ8 in γ2 was reasonably appointed as the "super TARP" mutant. Given though that the exchange of L1 did not lead to symmetric effects and that its removal did not entirely abolish γ2 or γ8 influence on GluA2(Q) desensitisation, other TARP elements were considered as potential contributors. The neutralisation of the alternating charge residues in the short L2 (L2_GS) coupled with the deletion of L1 in γ2 produced a kinetically null mutant (γ2 ΔL1 L2_GS) that, although still associating with GluA2(Q), appeared deficient in

modulating receptor desensitisation as well as superactivation, as if no TARP subunit was present (**Fig. 15**). Strikingly, this outcome was not paralleled by the γ8 ΔL1 L2_GS mutant, still retaining some extent of modulation (**Fig 15**) probably due to few more L1 amino acids that had to be conserved in γ8 in order to allow functional expression of the auxiliary protein (**Fig 6**). Confirming the powerful role of L1 of γ8, modulation of GluA2(Q) desensitisation and superactivation by γ8 was indeed suppressed by replacement of γ8 L1 with that of γ2 on the background of L2 neutralisation (L1 γ2 in γ8 L2_GS, **Fig. 12 B-D** and **Fig. 14 B and C**). Even though TARP extracellular loops could not be completely resolved in any structure of the AMPAR-TARP complex to date, recent cryo-EM data of the heteromeric GluA1/A2 AMPAR associated with γ8 (Herguedas et al., 2019) suggest that γ8 L1 is able to reach the upper (D1) lobe of the receptor LBD. γ2 L1 instead would span a shorter distance and interact with sites that are located further down, perhaps in the LBD lower (D2) lobe. The length of its L1 might therefore enable γ8 to contact more extensive regions of the LBD and explain the more dramatic impact of γ8 control on AMPAR gating in comparison to γ2. In support of this kind of interaction, contact regions between the first extracellular segment (and also the second, or L2) of both γ2 and γ8 and the LBD of GluA2 were previously identified by another study that used peptide arrays to map AMPAR-TARP interaction sites (Cais et al., 2014).

By mutating γ2 and γ8 extracellular loops, null or super TARP mutants were obtained, that still showed the ability to assemble with homomeric GluA2(Q) AMPARs, but also displayed a loss or an enhancement of modulation of receptor desensitisation and superactivation. These results proved that TARP L1 and L2 concerted action is necessary and sufficient to account for the TARP-dependent effects on AMPAR gating.

4.1.3 Inhibitory role of γ2 β4-TM2 loop in GluA2(Q) gating

Several structural analyses of the AMPAR-TARP complex predicted an interaction between a basic motif (KGK) in the lower lobe of GluA2 LBD and an acidic patch in the β4-TM2 loop contained in the first extracellular segment of γ2. The KGK motif in GluA2 was already demonstrated to be crucial for γ2-mediated prolongation of the channel activation time course (Dawe et al., 2016). Intriguingly, the interaction between GluA2 KGK motif and γ2 β4-TM2 acidic patch was only proposed for the receptor subunits B/D, that have been described as the ion channel gating-dominant positions (Chen et al., 2014). Analogously to L1 and L2, the

structure of the β4-TM2 loop in the cryo-EM complexes appears to be disordered, most likely because of the high intrinsic flexibility of these extracellular regions. In some cases, when a direct contact between the β4-TM2 loop and the receptor LBD could not be assumed, it was rather speculated that lowering of the LBD layer upon receptor activation could enable such interaction (Zhao et al., 2016) or alternatively that the β4-TM2 loop might play an important role in structural transitions leading to receptor activation (Twomey et al., 2017). To test these hypotheses, the acidic patch in the β4-TM2 loop of γ2 was mutated by neutralisation of putative interacting negatively charged residues (**Fig. 16 A**) and this mutant (γ2 NP_GSG) was once again coexpressed with homomeric GluA2(Q) receptors in HEK 293 cells. Surprisingly, in response to fast (500 ms) and long (7s) glutamate exposure, the neutralisation of the acidic patch substantially doubled γ2 potentiation of GluA2(Q) steady-state and superactivating currents and significantly slowed the receptor entry into desensitisation (**Fig. 16 B-D**). Thus, these results proved that TARP β4-TM2 loop contributes to regulation of AMPAR gating, but contrary to what excepted from the structural data, this interaction seems to be of inhibitory nature limiting rather than promoting receptor activation. This observation contradicts the idea of an interaction of the β4-TM2 loop with the KGK motif in GluA2, which has been established to be required for the typical positive modulation of the receptor gating by stargazin, and other sites of the TARP, perhaps L1, are more probably involved. Moreover, it raises the possibility that distinct TARP domains may be responsible not only for different but sometimes also for opposing functional effects, further broadening the spectrum of roles that TARPs play on the AMPAR function.

4.1.4 LBD-TMD linker region is critical for GluA2(Q) modulation by TARPs

The LBD-TMD linkers of glutamate receptors (namely the S1-M1, M3-S2 and S2-M4 linkers) are the structural elements responsible for mediating allosteric coupling of ligand binding events and opening of the channel pore. The M3-S2 linker is known to play a critical role in receptor activation, directly transducing LBD movements into channel gating (Sobolevsky et al., 2009). Mutagenesis studies of the other two, S1-M1 and S2-M4, linkers established the importance also of these regions in the control of iGluRs gating, defining them as part of a fine-tuned structural element in which transient gating-dependent interactions can stabilise or destabilise the channel open or closed state (Balannik et al., 2005; Schmid et al.,

2007; Talukder et al., 2010). Moreover, on the basis of recent structural data elucidating the architecture of native AMPAR complexes, it was determined that the S2-M4 linker makes direct contact with the gating-critical M3-S2 linkers from adjacent receptor subunits (Zhao et al., 2019).

Whereas it is difficult to pinpoint the exact contact sites of TARP L1 on the receptor LBD, structural modelling of the GluA2 complex with two γ2 and two γ8 TARPs unequivocally predicted TARP L2 to engage, four times in the same way for each receptor subunit, the receptor S1-M1 and S2-M4 linkers (Riva et al., 2017). Coherently, such interactions have also been suggested by current cryo-EM structures of the AMPAR-TARP complex and in particular in one of these (Herguedas et al., 2019) contact of γ8 L2 with the residue Lys511 in the S1-M1 linker of GluA2 was detected. According to the GluA2-γ2-γ8 model though, Lys511 appears to be positioned in the S1-M1 linker below the interface of interaction with L2 and residues located further up (that are Gln508, Lys509 and Ser510) seem more likely to be involved (**Fig. 9 C**). Analogously, the model spotted putative L2 contact sites on the S2-M4 linker. Therefore, in order to prove the hypothetic AMPAR-TARP interactions both the GluA2 S1-M1 and S2-M4 linkers were mutated at the positions of interest. Despite the above-mentioned vulnerability of these sites, the joint mutation of three electrically charged residues to neutral ones in the S1-M1 or in the S2-M4 linker (respectively, 508QKS510 to GAG and 781KEK783 to GSG) resulted to be harmless on the function of GluA2(Q) AMPARs (**Fig. 7** and **Fig. 18 A and B**). Even merging the two triple linker mutations onto the same receptor (GluA2 GAG/GSG) produced desensitising currents that kinetically perfectly resembled those of wild-type GluA2(Q) receptors. Importantly, the linker mutations did not affect also the assembly of the receptors with wild-type or chimeric TARP subunits (**Fig 18 C and D**), again indicating that the extracellular regions tested, neither of the AMPAR nor of the TARP, are determinant of complex formation. When disrupting the supposed interactions of the LBD-TMD linkers with L2, the desensitisation and superactivation of this double linker mutant receptor were resistant to modulation by γ2 (**Fig. 19 C and G**). The fact that γ8 instead still preserved some modulation of GluA2 GAG/GSG receptors (**Fig. 19 E and G**) might be again attributed to the powerful effect of its long L1. Conceivably, the extensive upstream interaction of γ8 L1 with the receptor LBD could be transmitted via the linkers to the ion channel, even when the linkers are disabled from directly interacting with TARPs. Vice versa,

the shorter L1 of γ2 may not be as effective in propagating LBD modulation downstream to the channel gate, or perhaps γ2 actually requires intact linker interactions in order to express its modulatory properties on the receptor. To address this aspect, L1 of γ8 was substituted with that of γ2. Modulation of the desensitisation and superactivation kinetics of the double linker mutant by this chimeric γ8 was indeed reduced to the level of receptors without TARPs (**Fig. 19 F and G**). On the other hand, the chimeric γ2 incorporating L1 of γ8 did not produce superactivating GluA2 GAG/GSG complexes, but it hold the slow desensitising behaviour due to the presence of γ8 L1 (**Fig. 19 D and G**). Furthermore, the loss of TARP modulation deriving from the mutations of the receptor S1-M1 and S2-M4 linkers showed a very close resemblance to the effects of TARP L2 neutralisation (**Fig. 12** and **Fig. 14**), strongly reinforcing the idea of a site-specific interaction of this kind. Together these results demonstrate that the AMPAR LBD-TMD linkers are primary TARP interaction sites and, at least in the case of γ8, they also act to transduce modulation by TARPs taking place above in the LBD layer. It is worth noticing that, although the DNA ratio used for AMPAR:TARP cotransfection would lead to assume that the receptors were fully saturated with auxiliary subunits, a preferential stoichiometry of association might account for some functional discrepancy between γ2 and γ8. It was indeed reported that γ8 preferentially associate with the AMPAR in a two-TARP stoichiometry, while four γ2 subunits appear to associate per receptor tetramer at least in overexpression (Hastie et al., 2013).

4.1.5 Proposed mechanism of AMPA receptor modulation by TARPs

Based on the results obtained, a molecular mechanism for AMPAR modulation by TARPs was tentatively proposed. Despite the strong evidence in favour of an interaction between the TARP extracellular loop β4-TM2 and the AMPAR LBD D2 lobe, the highly enhanced modulation of GluA2 gating by γ2 following the neutralisation of a major part of the loop rules out a dominant role of this element in TARP modulation. TARP extracellular L1 and L2 and the receptor LBD-TMD linker regions were shown to account for all the modifications of AMPAR gating by TARPs. Previous work suggested L1 and L2 interactions with the receptor ATD and a prominent role of the ATD-LBD linker region in modulation of AMPARs by TARPs (Cais et al., 2014). However, according to the structural data such interactions do not appear physically-plausible, the unstructured loops being too short, and the proposed

interactions are more proximal to the channel gate. These mechanisms might be shared by AMPAR transmembrane auxiliary proteins other than TARPs, such as GSG1L, whose structure recalls that of TARPs and first extracellular segment was similarly found to be involved in regulation of the AMPAR function, although apparently of a negative kind (Gu et al., 2016). Whilst for γ2 the collaboration of L1 and L2 seems to be necessary for the expression of γ2-dependent effects on AMPAR desensitisation and superactivation, in the case of γ8 the disruption of L2 interaction sites in the receptor still enables the propagation of some modulation by L1 at the level of the receptor LBD. Upon activation, glutamate binding to the LBD induces conformational rearrangements in the receptor that are transduced via the LBD-TMD linkers to open the ion channel pore. During such transition, the linkers are expected to

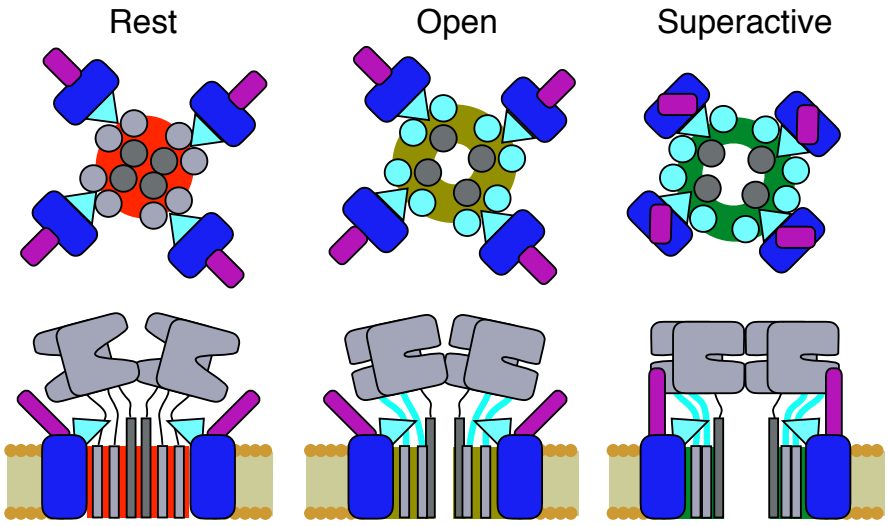

Figure 33. A proposed mechanism for TARP modulation. Cartoon illustrating a model of AMPAR (*grey*) modulation by TARPs (*blue*), proposing state-dependent interactions of TARP L1 (*purple*) and L2 (*cyan*) with the receptor LBD and LBD-TMD linker regions. TARP β4-TM2 loop has been omitted. The receptor pore forming M3 domains are coloured in dark grey. The AMPAR-TARP complex is represented from the top (*upper panel*) and in side view (*lower panel*) in the resting/closed pore (*red*), active/open pore (*olive green*) and superactive/high open probability (*dark green*) states. In the resting state, TARP L2 is positioned in close proximity to the receptor S1-M1 and S2-M4 LBD-TMD linkers. Upon activation, the movement of the linkers away from the central pore axis allows L2 to wedge between the S1-M1 and S2-M4 linkers and modulate gating. Superactivation is thought to be mediated by the stabilisation of the LBD layer by L1 together with the interaction of L2 with the linkers. From Riva et al., 2017.

move away from the overall pore axis and engage L2 through state-dependent interactions. Particularly, we hypothesise that L2 could act as a wedge between the S1-M1 and S2-M4 linkers to modulate the receptor gating (**Fig. 33**). Reaching up to the LBD layer, L1 is instead predicted to create extensive contacts with multiple sites in the LBD and consistently with its flexible structure, to adopt multiple conformations to stabilise separate functional states of the receptor.

4.2 Subtype-dependency of TARP modulation

4.2.1 TARP association with GluA2(R)-lacking and GluA2(R)-containing AMPARs

After studying the effects of TARP extracellular loop mutations on homomeric GluA2(Q) receptors, the investigation of AMPAR-TARP interactions was extended to other AMPAR types and specifically to the GluA1 and GluA2(R) subunits. In order to tackle the possibility of subunit-dependent mechanisms of TARP modulation, TARP extracellular loop mutants that showed either a loss (null γ2 and null γ8) or an enhanced (super TARP) modulation of GluA2(Q) gating were coexpressed with homomeric GluA1 and GluA2(R) channels. It is known for example that type II TARPs γ5 and γ7 modulate with unique properties preferentially certain AMPAR assemblies, including GluA1/A4 for γ5 (Soto et al., 2009) and GluA1 or GluA2 for γ7 (Kato et al., 2008). Also within type I TARPs, it has been shown that homologous TARP isoforms can impart specific AMPAR subtypes with different kinetic features. Although both stargazing and γ8 are able to induce superactivation of GluA2(Q) receptors, γ8 but not stargazin can superactivate GluA1 complexes (Kato et al., 2010).

Additionally, to examine a more physiological condition, null and super TARP mutants were tested on heteromeric GluA1/A2(R) channels. In the adult brain homomeric forms of AMPARs are quite uncommon and the major AMPAR populations are composed of diheteromeric GluA1/A2 and GluA2/A3 assemblies (Wenthold et al., 1996; Zhao et al., 2019). More precisely, GluA1/A2 heteromers are the dominant AMPAR subtype at CA1 cell synapses in the hippocampus, where synaptic AMPAR subunit composition fundamentally underlies the mechanisms of synaptic plasticity (Lu et al., 2009). In this regard, another influential determinant of synaptic AMPARs behaviour is the impermeability to Ca^{2+} of GluA2-containing AMPARs, that is conferred by an arginine (R) instead of a glutamine (Q) in

the pore region of the large majority (about 99%) of GluA2 subunits following mRNA editing at this site (Wright & Vissel, 2012).

When inspecting the association of the TARP extracellular loop mutants with GluA1 homomeric receptors, similarly to GluA2(Q), both null and super TARPs were found to attenuate the block by intracellular spermine equally to wild-type γ2. As a result, the I-V relationship of GluA1-TARP complexes appears less rectifying than that of GluA1 receptors without TARPs (**Fig. 20 A**). Initially, the super TARP mutant was tested in the TARP tandem configuration, where the C-terminus of GluA1 was fused to the N-terminus of the super TARP. Since no difference in polyamine block relief emerged between this GluA1_super TARP tandem condition and the cotransfections of the wild-type and null γ2 constructs with GluA1, for the sake of simplicity the consecutive experiments were all based on the contransfection of AMPAR and TARP subunits. Conversely to GluA1, TARP association with GluA2(R)-containing AMPARs can not be assessed based on the I-V profile. In fact, together with the Ca^{2+} impermeability, the presence of the arginine at the Q/R site of edited GluA2 subunits prevents GluA2(R)-containing AMPARs from being sensitive to the intracellular polyamine block. Consequently, the I-V relationship of GluA2(R)-containing receptors, such as GluA2(R) homomers and GluA1/A2(R) heteromers, does not show rectification and is almost linear both when TARPs are included and are not (**Fig. 20 B** and **Fig. 23**). Noteworthy though is that the I-V curve of GluA2(R) or GluA1/A2(R) complexes with each TARP mutant is quite well overlapping with that of the respective receptor assembly with wild-type γ2, thus leading to the assumption that the mutations of L1 and L2 do not alter TARP association also with these typologies of AMPARs. Moreover, in GluA1/A2(R) heteromers TARPs seem to induce some extent of rectification, as their I-V curves uniformly appear slightly less linear in comparison to the I-V of the heteromers without TARPs. This observation is somehow in contrast with the commonly believed effect of TARPs in relieving AMPARs from the polyamine block, but it has been reported before in literature perhaps without attracting the appropriate attention (Cho et al., 2007). Our analysis of tripartite complexes suggested the introduction of rectification by TARPs is more profound than the G-V of the mixture suggests. Indeed, TARPs specify an “intermediate” block state, whether they associate with homomers (normally strongly blocked) or heteromers (normally insensitive). Intriguingly, in neurons AMPAR-mediated responses show some rectification that so far has generally been

related to the content of polyamine-sensitive, GluA2-lacking AMPARs (Rozov & Burnashev, 1999; Terrier et al., 2016). Our finding now points to TARPs introduction of rectification as a possible alternative explanation.

4.2.2 Loss of modulation of homomeric and heteromeric GluA1 and GluA2(R) receptors by null TARP mutants

The null γ2 mutant, devoid of both L1 and L2 (γ2 ΔL1 L2_GS), resulted unable to modulate superactivation and desensitisation of GluA2(Q) receptors as if no TARP was associated, despite having proven that complexes formation was unaffected (**Fig. 15**). A similar outcome was obtained with GluA1 and GluA2(R) subunits in both homomeric and heteromeric forms, all showing a significant increase in the desensitisation rate, a drop in the steady-state current comparable to the level of receptors without auxiliary subunits and, with exception of one out of five GluA2(R)/null γ2 recordings, a general annulment of the superactivation (**Fig. 21**, **Fig. 22**, **Fig. 24 B, C and F** and **Fig. 26 A and D**). The lack of superactivation of GluA1 complexes with null γ2 was actually quite expected, given that GluA1, save one case out of three, did not undergo superactivation even in the presence of wild-type γ2 (**Fig. 22 A and B**; Kato et al., 2010). The same was observed for GluA2(R)/γ2 complexes (1/3 recording with approximately 5% superactivation and the rest without any; **Fig. 22 D**), while γ2 in GluA1/A2(R) complexes induced on average 2% superactivation (**Fig. 26 D**). Compared to unedited GluA2(Q) receptors, of which γ2 promoted about 7% superactivation (**Fig. 13 C**), these AMPAR subtypes thus displayed to be less prone to stargazin-mediated superactivation, suggesting that this TARP property does depend on the specific AMPAR subunit composition. Considering then that GluA1/A2/γ8 assemblies represent the most common pool of AMPAR complexes in the hippocampus, the effect of the kinetically null γ8, with the long L1 of γ8 exchanged with that of γ2 and L2 neutralised (L1 γ2 in γ8 L2_GS), was also tested on GluA1/A2(R) heteromers. Like the null γ2, the null γ8 mutant determined a strong decrease in the steady-state current and the absence of superactivation of GluA1/A2(R) heteromeric complexes (**Fig. 24 C, E and F** and **Fig. 26 B and D**). These measurements have temporarily been confronted to those of GluA1/A2(R) heteromers with wild-type γ2 and still have to be analysed in comparison to more adequate wild-type γ8 control experiments. It is important to mention that, not being possible to strictly rely upon the polyamine block test for TARP

association, a contamination from GluA1/A2(R) receptors alone in the other heteromeric conditions with TARPs can not be completely excluded. This is obviously particularly critical for those TARP mutants that lack of modulatory properties on the receptor and whose behaviour therefore mirrors that of receptors not in complex with TARPs. Despite this, the fairly moderate desensitisation kinetics of all the heteromeric TARP complexes compared to the much faster kinetics of non-complexed heteromeric receptors speak in favour of a small degree of contamination with GluA1/A2(R) receptors alone in the other species (**Fig. 24 C**). For GluA1/A2(R) heteromers, the rate of deactivation following a 1 ms pulse of saturating glutamate was also calculated, to approximate synaptic transmission during which the glutamate transient decays in about 1 ms (Clements et al., 1992). With respect to wild-type γ2, both null γ2 and null γ8 accelerated more than 2-fold the deactivation rate of GluA1/A2(R) complexes (**Fig. 25 A, B and D**). Hence, modifications of γ2 and γ8 extracellular loops seem to similarly dictate the loss of TARP modulation of GluA1 and GluA2 subunits, regardless of the homomeric or heteromeric receptor composition and editing of the Q/R site in GluA2.

4.2.3 GluA1 resistance to potentiation by the super TARP and GluA2(R) dominance in heteromeric TARP complexes

The replacement of L1 of γ2 with γ8 L1, that proved to be such a powerful modulator of GluA2(Q) gating, did not produce identical effects on homomeric receptors of GluA1 and GluA2(R) subunits. This super TARP mutant (L1 γ8 in γ2) slowed the entry into desensitisation of both GluA1 and GluA2(R) homomers, without significantly changing the steady-state current level that, especially for GluA2(R), was almost indistinguishable from that of the homomers with wild-type γ2 (**Fig. 21**). Nonetheless, compared to wild-type γ2 the super TARP caused a dramatic slowing down in the decay of GluA2(R) currents following the end of the glutamate pulse, whereas GluA1 currents similarly decayed in the presence of the super TARP or of wild-type γ2 (**Fig. 21 A and C**). In addition, the almost null superactivation of GluA2(R)/γ2 complexes was augmented by effect of the super TARP mutant (**Fig. 22 C and D**), but GluA1 even in complex with the super TARP oddly did not sustain any extent of superactivation (**Fig. 22 A and B**). In GluA1/A2(R) heteromers, potentiation by the super TARP, to which GluA1 alone seems to be refractory, is restored. In fact, in relation to wild-type γ2 not only decreased the super TARP the rate of desensitisation and more than doubled

the steady-state current of the heteromeric complexes (**Fig. 24 C, D and F**), but, like for GluA2(R) alone, it also elicited bigger superactivation responses and robustly slowed down the current decay (**Fig. 26 C and D** and **Fig. 24 D**). Editing of the Q/R site in GluA2 is known to play a dominant role on the other GluA subunits in terms of permeation properties such as Ca^{2+} permeability and affinity to intracellular polyamines. Our data now indicate that in heteromeric GluA1/A2(R) receptors, GluA2(R) is dominant also in TARP-mediated gating properties. Besides this, oppositely to the effect of the null TARP mutants, the insertion of γ8 L1 in γ2 determined an about 5-fold slowing down in the deactivation kinetics of GluA1/A2(R) heteromers by the super TARP in comparison to γ2 (**Fig. 25 C and D**).

4.2.4 Super TARP facilitation of GluA1/A2(R) responses during train stimulation

Repetitive synaptic stimulation can be mimicked in heterologous system by exposure of the outside-out patches to trains of short pulses of saturating glutamate. Outside-out patches from HEK 293 cells overexpressing GluA1/A2(R) heteromeric receptors with or without wild-type γ2 or the null or super TARP mutants were recorded during train stimulation of 1 ms pulses of 10 mM glutamate at 10, 20 and 50 Hz frequencies. Thus, the activity of the heteromeric channels during stimulation was analysed in terms of increase in the peak amplitude after desensitisation and charge transfer. As a rule of thumb, the amplitude of the excitatory postsynaptic currents (EPSCs) largely reflects the number of postsynaptic AMPARs, whereas the charge transfer is the cumulative ion flow through open receptor channels (Bidinosti et al., 2010). TARPs are known to enhance the charge transfer through synaptic AMPAR channels by slowing down the time course and increasing the size of the synaptic currents (Greger et al., 2017). However, TARPs tend to have only a small influence on the receptor rise times and to rather regulate the decay kinetics. A recent study though, by using a laser-pulse glutamate photolysis technique to measure GluA4 channel-opening and -closing rates, showed that γ2 and γ4 similarly both slow down the formation and prolong the duration of GluA4 open-channel, overall leading to a higher volume of ionic flux and thus charge transfer through the open channel (Pierce & Niu, 2019). Charge transfer and deactivation are measures that define the onset and offset of glutamatergic activity and are therefore directly relevant to the propagation of synaptic transmission and plasticity (Ward et al., 2017). As already discussed, the effect of the TARP mutants on GluA1/A2(R) deactivation following 1 ms glutamate

application segregated quite well accordingly to the type of extracellular loop mutations, with the null γ2 and γ8 accelerating and the super TARP greatly decelerating the deactivation rate of the heteromers (**Fig. 25**). In coherence with these results, the charge transfer, determined by integrating the current trace over time and normalising it to the initial peak current, of GluA1/A2(R) heteromers with both the null γ2 or γ8 mutants was significantly lower at all frequencies in comparison to the heteromers with wild-type γ2 (**Fig. 27 C**). On the other hand, preliminary data with the super TARP pointed to a more pronounced increase in GluA1/A2(R) charge transfer by the super TARP compared to wild-type γ2. Given that the postsynaptic membrane must be depolarised by charging, the increase in charge is a decisive parameter for synaptic transmission strengthening. Additionally, in the presence of the super TARP, but not of wild-type γ2, the slowed deactivation decay at the end of each 1 ms application prevented the complete decay of each response before the next application. Consequently, this incomplete decay promoted the appearance of a substantial, sustained inward current during the trains referred to as "pedestal" current (**Fig. 27 A**). The onset of the pedestal current was not paralleled though by an increase in the peak current subsequent to the desensitisation trough (**Fig. 27 A and B**). It was previously observed that train stimulation induces a potentiation, in the form of pedestal current and peak current increase, of GluA2(Q) responses that is dependent on the coexpression of the receptors with TARP γ2 or γ8, with γ8 potentiating more than γ2 (Carbone & Plested, 2016). Interestingly, it has been speculated that the pedestal current arises primarily from a population of TARP-associated receptors gating in the high-open probability (P_{open}) mode (Devi et al., 2016; Tomita et al., 2005). Using outside-out patches from tsA201 cells expressing GluA1/A2 heteromers, Devi and coauthors showed that the high-P_{open} mode of AMPARs in complex with γ2 was resistant to NBQX and selectively blocked by pentobarbital (with inhibition being greater for GluA2(R)- than for GluA2(Q)-containing receptors). The profile of these recombinant receptors strikingly coincided with that of the late component of the train EPSC evoked by parallel fibre stimulation to Purkinje cells in cerebellar slices, that appeared to be characterised by a small initial amplitude and a facilitation throughout the train. The early and late phases of the train EPSC presented different functional features as well as synaptic distribution and were therefore imputed to two distinct classes of synaptic AMPARs, of which the "late phase" one was hypothesised to be recruited from low-release probability or silent synapses during longer

bursts of activity (Devi et al., 2016). Even though in our hands train stimulation did not lead to facilitation of GluA1/A2(R)/γ2 responses, the pedestal current that was generated in the presence of the super TARP mutant might correspond to an accumulation of AMPAR complexes in the high-P_{open} gating mode, that is thought be the mechanism underlying the phenomenon of superactivation. In this regard, it seems consistent that wild-type γ2 did not result much effective in producing superactivating GluA1/A2(R) complexes, while the super TARP mutant induced a 2-fold bigger superactivation. By favouring the accumulation of AMPAR complexes in a superactive state, strongly slowing the currents decay and increasing the charge transfer during train stimulation, this chimera of γ2 endowed with γ8 L1 might contribute to a postsynaptic mechanism for synaptic transmission potentiation. Oppositely, modifications of TARP extracellular loops that convert γ2 and γ8 into numb modulators of AMPAR desensitisation, also impede AMPAR complexes from superactivating, accelerate the receptors deactivation kinetics and decrease the charge transfer upon stimulation, overall presumably hampering TARP contribution to the enhancement of synaptic AMPARs function.

4.2.5 Predicting abundance of tripartite GluA1/A2(R)/TARP complexes

As aforementioned, the cotransfection of the AMPAR subunits GluA1 and GluA2(R) together with a TARP construct does not guarantee the mere isolation of the intended triple GluA1/A2(R)/TARP complex. In fact, mono- and binary complexes could collaterally form at the plasma membrane. In order to estimate the abundance of the triple complex from such cotransfection, a statical model was created on the basis of presumed abundances and experimentally measured properties (that are desensitisation rate, steady-state current and rectification ratio) of the other, mono- and binary, obtainable species (**Fig. 28** and **Fig. 29**). The observation of the separately measured parameters for each of the species allowed by the cotransfection lead to hypothesise a gating-dominant role for GluA2(R)/TARP assemblies in the tripartite complexes. To assess wether this consideration might be rather explained by a preponderance of surface GluA2(R)/TARP complexes, the model included in the calculations a range of GluA2(R)/TARP abundances. GluA2(R) dominance of gating resulted to be robust to asymmetries in trafficking, thus emphasising the idea that the GluA2(R) subunit might act as dominant in GluA1/A2(R) heteromeric complexes not only in terms of permeation but also of gating. Notably, in their recent study elucidating the architecture of the heteromeric GluA1/

A2(R) AMPAR complex with TARP γ8, with γ8 in tandem with GluA2(R), Herguedas et al. (2019) demonstrated preferential placement of the GluA2 subunits in the pore-distal functionally dominant B/D positions. Moreover, although perhaps expected by the use of the tandem configuration, γ8 appears to primarily engage the GluA2 subunits, reasonably enabling itself to exert a greater control over the receptor gating-dominant positions. Save the case of the GluA1_super TARP tandem, that exhibited a degree of polyamine block relief similar to that of the other GluA1/TARP cotransfections (**Fig. 20 A**), in the course of this work no tandem AMPAR_TARP construct has been used mainly for three reasons. Firstly, because of the much easier handling of the cotransfections. Secondarily, not to influence the stoichiometry of association of the heteromeric complexes. Lastly, because it was previously shown that at +50 mV, holding potential of all the performed recordings in the presence of TARPs, the gating properties of stargazin in tandem or cotransfected with GluA2 are quite closely resembling each other (Carbone & Plested, 2016). For triheteromeric GluA1/A2(R) complexes with the super TARP mutant the model produced a very univocal estimate, strikingly similar to the experimentally measured values, in correspondence with an approximate abundance of 50% of the total (**Fig. 28**). With wild-type γ2 instead, such a definitive answer was not obtained and the estimated properties only partially approximated the measured ones (**Fig. 29**). Nonetheless, for both the super TARP and the wild-type γ2 tripartite complexes the model predicted high rectification ratios to be least probable, contrary to what observed for GluA1/A2(R) receptors not associated to TARPs (**Fig. 23 B**). This result again hints at a surprising, opposite to what expected, slightly rectifying effect of TARPs on heteromeric AMPARs, whose function still remains to be clarified and which would be worth further analysing in other heteromeric forms. At the same time, the unlikelihood of high rectification values rules out a strong presence of heteromeric species without TARPs in the tripartite GluA1/A2(R)/TARP condition.

5. FUTURE PERSPECTIVES: investigating the effects of TARP modulation on AMPA receptor-mediated synaptic transmission

This work has produced mutant TARPs that both lack modulatory properties and also those that have greatly enhanced modulation of the gating of RNA-unedited or -edited, homomeric or heteromeric forms of AMPARs. In addition, AMPAR mutants mirroring the loss of modulation of some "null" TARP mutants were obtained, providing evidence of the existence of specific AMPAR-TARP interactions. Common as well as subunit-dependent mechanisms of AMPAR modulation by TARPs have been unveiled and a model based on the key role of TARP extracellular loops L1 and L2 and the AMPAR LBD and LBD-TMD linker regions has been proposed.

The present study has focused on two type I TARPs, γ2 and γ8, as representatives of TARP function on the kinetics of AMPAR gating. It might be likewise intriguing to question the mechanisms of modulation of type II TARPs, γ5 and γ7, that have been shown to exert unique regulatory properties on the receptor and whose extracellular loops structure deviates from that of γ2 and γ8.

Furthermore and most importantly, we now reason that "null" and "super" TARP mutants might represent useful tools to investigate TARP action in synapses. In fact, thank to several knockout mouse model studies, a lot has been learned about the relative contribution of the different TARP subtypes to the synaptic anchoring of AMPAR complexes. On the contrary, the consequences of TARP kinetic modulation of AMPAR gating on synaptic transmission, and particularly in terms of short-term plasticity, have never been thoroughly addressed. In this context, we have already started overexpressing TARP mutants of interest in CA1 pyramidal neurons from organotypic hippocampal slice cultures, with the aim of studying their effect on AMPAR-mediated spontaneous synaptic activity. In parallel, we intend to analyse also evoked AMPAR responses by stimulation of CA3 pyramidal cells projecting through the Schaffer collaterals to CA1 cell inputs, one of the most extensively studied glutamatergic synapses in the brain constituting the seat of memory formation. In this framework, we would like to attempt to define the physiological relevance, if any, of the TARP-dependent phenomenon of AMPAR superactivation. It was demonstrated that hippocampal AMPARs do not exhibit superactivation and that this might be due to a

counteraction of another AMPAR auxiliary subunit, CNIH-2 (Kato et al., 2010). However, we hypothesise that superactivation might account for important modifications in the gating mode of TARP-associated AMPARs possibly at the basis of a postsynaptic mechanism for synaptic facilitation.

Obviously, when scaling up from recombinant AMPAR complexes to native assemblies in the brain multiple levels of complexity must be taken into account, including the preferential TARP stoichiometry and the presence of auxiliary subunits of different kinds that might hinder or compensate for the altered function of our TARP mutants. Again though, the coexpression of AMPAR and TARP subunits with third party auxiliary proteins in heterologous system might help to understand the interplay between distinct AMPAR auxiliary proteins and to dissect their respective roles in multipartite AMPAR complexes.

APPENDIX

```
import numpy as np
import matplotlib.pyplot as plt

#abundance = xrange(0, 1, 50)
components = ["A1", "A2R", "Stg"]

class receptor:
    def __init__(self, properties):
        #initialise with a dictionary of properties to
preserve clean namespace
        self.properties = properties
        self.abundance = 0

    def build(self, components):
        self.components = components

class measurement:
    def __init__(self, value):
        self.value = value
    #should be done as function of a matrix
    def error(self, calculated):
        return np.power(np.subtract(calculated, self.value),2)

# generate weighted value across population

def set_abundances (receptors, preset):

    abundance = xrange(0, 1, 50)

def weighted(receptors, obs):
    #address either with "RR", "Iss" or "kdes"
    weighted = 0

    for r in receptors:
        v = r.properties.obs
        w = r.abundance

        weighted += v * w

    return weighted

TARP = "wt"
TARP = "superTARP"

a1homo = receptor({"RR": 0.04, "Iss": 0.01, "kdes": 400})
a1homo.build("A1")
```

```
#new values from Irene 190710
a1a2R = receptor({"RR": 0.83, "Iss": 0.01, "kdes": 170})
a1a2R.build(["A1", "A2R"])

#true values unknown
a1_a2R_stg = receptor({"RR": 0, "Iss": 0, "kdes": 0})
a1_a2R_stg.build(["A1", "A2R", "Stg"])

if TARP == "wt":
    #normal Stg
    #new values from Irene 190710
    a1_stg = receptor({"RR": 0.26, "Iss": 0.0, "kdes": 175})
    a1_stg.build(["A1", "Stg"])

    a2R_stg = receptor({"RR": 0.66, "Iss": 0.46, "kdes": 40})
    a2R_stg.build(["A2R", "Stg"])

    #triple condition mixture measurements
    measured_RR = measurement(.58)
    measured_Iss = measurement(.18)
    measured_kdes = measurement(64)

elif TARP == "superTARP":
    #Super TARP
    a1_stg = receptor({"RR": 0.22, "Iss": 0.1, "kdes": 90})
    a1_stg.build(["A1", "Stg"])

    a2R_stg = receptor({"RR": 0.67, "Iss": 0.51, "kdes": 18})
    a2R_stg.build(["A2R", "Stg"])

    #triple condition mixture measurements
    measured_RR = measurement(.61)
    measured_Iss = measurement(.45)
    measured_kdes = measurement(37)

receptors = [a1homo, a1a2R, a1_stg, a1_a2R_stg, a2R_stg]
#preset = {a1homo: 0.1, a1a2R: 0.1, a1_Stg: 0.1}

#make a grid of values for triple complex abundance versus the
property in question
#Assume low abundance of other complexes and fill gap with A2R
+ Stg

a1homo.abundance = 0            #can't be detected in either
triple condition
a1_stg.abundance = 0.1
a1a2R.abundance = 0.1
step = 0.02
```

```
fixed = a1homo.abundance + a1_stg.abundance + a1a2R.abundance
v_abund = np.arange(0, 1 - fixed, step * (1-fixed))
v_RR = np.arange(0, 1, step)
v_Iss = np.arange(0, 1, step)
v_kdes = np.arange(0, 2.5, step * 2.5)
v_kdes = np.power(10, v_kdes)
#grids of values
gaR, gR = np.meshgrid(v_abund, v_RR, sparse=True)
gaI, gI = np.meshgrid(v_abund, v_Iss, sparse=True)
gaK, gK = np.meshgrid(v_abund, v_kdes, sparse=True)

z_RR = gaR * gR + (1 - gaR - fixed) * a2R_stg.properties["RR"]
+ a1_stg.properties["RR"] * a1_stg.abundance +
a1homo.properties["RR"] * a1homo.abundance +
a1a2R.properties["RR"] * a1a2R.abundance

z_Iss = gaI * gI + (1 - gaI - fixed) *
a2R_stg.properties["Iss"] + a1_stg.properties["Iss"] *
a1_stg.abundance + a1homo.properties["Iss"] * a1homo.abundance
+ a1a2R.properties["Iss"] * a1a2R.abundance

z_kdes = gaK * gK + (1 - gaK - fixed) *
a2R_stg.properties["kdes"] + a1_stg.properties["kdes"] *
a1_stg.abundance + a1homo.properties["kdes"] *
a1homo.abundance + a1a2R.properties["kdes"] * a1a2R.abundance

z_RR_error = measured_RR.error(z_RR)
RR_error_plot = plt.contourf (v_abund, v_RR, z_RR_error , 25)
#plt.show()

z_Iss_error = measured_Iss.error(z_Iss)
Iss_error_plot = plt.contourf (v_abund, v_Iss, z_Iss_error ,
25)
#plt.show()

z_kdes_error = measured_kdes.error(z_kdes)
kdes_error_plot = plt.contourf (v_abund, v_kdes,
z_kdes_error , 25)
#plt.show()

#"normalise" error matrices so elements sum to 1
z_RR_err_norm = z_RR_error / np.sum(z_RR_error)
z_Iss_err_norm = z_Iss_error / np.sum(z_Iss_error)
z_kdes_err_norm = z_kdes_error / np.sum(z_kdes_error)
z_combi_error = z_RR_err_norm + z_Iss_err_norm +
z_kdes_err_norm
#write error matrices
np.savetxt(TARP + "RR.txt", z_RR_err_norm)
```

```
np.savetxt(TARP + "Iss.txt", z_Iss_err_norm)

np.savetxt(TARP + "kdes.txt", z_kdes_err_norm)

np.savetxt(TARP + "combi.txt", z_combi_error)
axes = [v_abund, v_RR, v_Iss, v_kdes]

    #for v in axes:
#print (len(v))
#print (v)

np.savetxt("axes.txt", np.column_stack((v_abund, v_RR, v_Iss,
v_kdes)), header = "abund\tRR\tIss\tkdes")
```

BIBLIOGRAPHY

Amin, J. B., Leng, X., Gochman, A., Zhou, H. X. & Wollmuth, L. P. (2018). A conserved glycine harboring disease-associated mutations permits NMDA receptor slow deactivation and high Ca2+ permeability. *Nature Communications, 9*(1): 3748.

Amin, J. B., Salussolia, C. L., Chan, K., Regan, M. C., Dai, J., Zhou, H. X., … Wollmuth, L. P. (2017). Divergent roles of a peripheral transmembrane segment in AMPA and NMDA receptors. *The Journal of General Physiology, 149*(6), 661-680.

Armstrong, N. & Gouaux, E. (2000). Mechanisms for activation and antagonism of an AMPA-sensitive glutamate receptor: crystal structures of the GluR2 ligand binding core. *Neuron, 28*(1), 165-181.

Armstrong, N., Sun, Y., Chen, G. Q. & Gouaux, E. (1998). Structure of a glutamate-receptor ligand-binding core in complex with kainate. *Nature, 395*(6705), 913-917.

Ayalon, G., Segev, E., Elgavish, S. & Stern-Bach, Y. (2005). Two regions in the N-terminal domain of ionotropic glutamate receptor 3 form the subunit oligomerization interfaces that control subtype-specific receptor assembly. *The Journal of Biological Chemistry, 280*(15), 15053-15060.

Balannik, V., Menniti, F. S., Paternain, A. V., Lerma, J. & Stern-Bach, Y. (2005). Molecular mechanism of AMPA receptor noncompetitive antagonism. *Neuron, 48*(2), 279-288.

Baranovic, J., Chebli, M., Salazar, H., Carbone, A. L., Faelber, K., Lau, A. Y., … Plested, A. J. (2016). Dynamics of the Ligand Binding Domain Layer during AMPA Receptor Activation. *Biophysical Journal, 110*(4), 896-911.

Barria, A., Derkach, V. & Soderling, T. (1997). Identification of the Ca2+/calmodulin-dependent protein kinase II regulatory phosphorylation site in the alpha-amino-3-hydroxyl-5-methyl-4-isoxazole-propionate-type glutamate receptor. *The Journal of Biological Chemistry, 272*(52), 32727-32730.

Bats, C., Groc, L. & Choquet, D. (2007). The interaction between Stargazin and PSD-95 regulates AMPA receptor surface trafficking. *Neuron, 53*(5), 719-734.

Bedoukian, M. A., Whitesell, J. D., Peterson, E. J., Clay, C. M. & Partin, K. M. (2008). The stargazin C terminus encodes an intrinsic and transferable membrane sorting signal. *The Journal of Biological Chemistry, 283*(3), 1597-1600.

Beneyto, M. & Meador-Woodruff, J. H. (2006). Lamina-specific abnormalities of AMPA receptor trafficking and signaling molecule transcripts in the prefrontal cortex in schizophrenia. *Synapse, 60*(8), 585-598.

Bidinosti, M., Ran, I., Sanchez-Carbente, M. R., Martineau, Y., Gingras, A. C., Gkogkas, C., … Sonenberg, N. (2010). Postnatal deamidation of 4E-BP2 in brain enhances its association with raptor and alters kinetics of excitatory synaptic transmission. *Molecular Cell, 37*(6), 797-808.

Bliss, T. V. & Lomo, T. (1973). Long-lasting potentiation of synaptic transmission in the dentate area of the anaesthetized rabbit following stimulation of the perforant path. *The Journal of Physiology, 232*(2), 331-356.

Bowie, D. & Mayer, M. L. (1995). Inward rectification of both AMPA and kainate subtype glutamate receptors generated by polyamine-mediated ion channel block. *Neuron, 15*(2), 453-462.

Buonarati, O. R., Hammes, E. A., Watson, J. F., Greger, I. H. & Hell, J. W. (2019). Mechanisms of postsynaptic localization of AMPA-type glutamate receptors and their regulation during long-term potentiation. *Science Signaling, 12*(562).

Burgess, D. L., Davis, C. F., Gefrides, L. A. & Noebels, J. L. (1999). Identification of three novel Ca(2+) channel gamma subunit genes reveals molecular diversification by tandem and chromosome duplication. *Genome Research, 9*(12), 1204-1213.

Burgess, D. L., Gefrides, L. A., Foreman, P. J. & Noebels, J. L. (2001). A cluster of three novel Ca2+ channel gamma subunit genes on chromosome 19q13.4: evolution and expression profile of the gamma subunit gene family. *Genomics, 71*(3), 339-350.

Burnashev, N., Khodorova, A., Jonas, P., Helm, P. J., Wisden, W., Monyer, H., … Sakmann, B. (1992). Calcium-permeable AMPA-kainate receptors in fusiform cerebellar glial cells. *Science, 256*(5063), 1566-1570.

Cais, O., Herguedas, B., Krol, K., Cull-Candy, S. G., Farrant, M. & Greger, I. H. (2014). Mapping the interaction sites between AMPA receptors and TARPs reveals a role for the receptor N-terminal domain in channel gating. *Cell Reports, 9*(2), 728-740.

Carbone, A. L. & Plested, A. J. (2016). Superactivation of AMPA receptors by auxiliary proteins. *Nature Communications, 7*:10178.

Chen, L., Chetkovich, D. M., Petralia, R. S., Sweeney, N. T., Kawasaki, Y., Wenthold, R. J., … Nicoll, R. A. (2000). Stargazin regulates synaptic targeting of AMPA receptors by two distinct mechanisms. *Nature, 408*(6815), 936-943.

Chen, L., Dürr, K. L. & Gouaux, E. (2014). X-ray structures of AMPA receptor-cone snail toxin complexes illuminate activation mechanism. *Science, 345*(6200), 1021-1026.

Chen, L., El-Husseini, A., Tomita, S., Bredt, D. S. & Nicoll, R. A. (2003). Stargazin differentially controls the trafficking of alpha-amino-3-hydroxyl-5-methyl-4-isoxazolepropionate and kainate receptors. *Molecular Pharmacology, 64*(3), 703-706.

Chen, S., Zhao, Y., Wang, Y., Shekhar, M., Tajkhorshid, E. & Gouaux, E. Activation and Desensitization Mechanism of AMPA Receptor-TARP Complex by Cryo-EM. *Cell, 170*(6), 1234-1246.

Cho, C. H., St-Gelais, F., Zhang, W., Tomita, S. & Howe, J. R. (2007). Two families of TARP isoforms that have distinct effects on the kinetic properties of AMPA receptors and synaptic currents. *Neuron, 55*(6), 890-904.

Choquet, D. (2018). Linking Nanoscale Dynamics of AMPA Receptor Organization to Plasticity of Excitatory Synapses and Learning. *The Journal of Neuroscience, 38*(44), 9318-9329.

Choquet, D. & Triller, A. (2003). The role of receptor diffusion in the organization of the postsynaptic membrane. *Nature Reviews Neuroscience, 4*(4), 251-265.

Chung, H. J., Xia, J., Scannevin, R. H., Zhang, X. & Huganir, R. L. (2000). Phosphorylation of the AMPA receptor subunit GluR2 differentially regulates its interaction with PDZ domain-containing proteins. *The Journal of Neuroscience, 20*(19), 7258-7267.

Clements, J. D., Lester, R. A., Tong, G., Jahr, C. E. & Westbrook, G. L. (1992). The time course of glutamate in the synaptic cleft. *Science, 258*(5087), 1498-1501.

Cokić, B. & Stein, V. (2008). Stargazin modulates AMPA receptor antagonism. *Neuropharmacology, 54*(7), 1062-1070.

Coombs, I. D., MacLean, D. M., Jayaraman, V., Farrant, M. & Cull-Candy, S. G. (2017). Dual Effects of TARP γ-2 on Glutamate Efficacy Can Account for AMPA Receptor Autoinactivation. *Cell Reports, 20*(5), 1123-1135.

Coombs, I. D., Soto, D., McGee, T. P., Gold, M. G., Farrant, M. & Cull-Candy, S. G. (2019). Homomeric Q/R edited AMPA receptors conduct when desensitized. *BioRxiv,* doi: 10.1101/595009.

Dakoji, S., Tomita, S., Karimzadegan, S., Nicoll, R. A. & Bredt, D. S. Interaction of transmembrane AMPA receptor regulatory proteins with multiple membrane associated guanylate kinases. (2003). *Neuropharmacology, 45*(6), 849-856.

Dawe, G. B., Kadir, M. F., Venskutonytė, R., Perozzo, A. M., Yan, Y., Alexander, R. P. D., … Bowie, D. (2019). Nanoscale Mobility of the Apo State and TARP Stoichiometry Dictate the Gating Behavior of Alternatively Spliced AMPA Receptors. *Neuron, 102*(5), 976-992.

Dawe, G. B., Musgaard, M., Aurousseau, M. R. P., Nayeem, N., Green, T., Biggin, P. C. & Bowie, D. (2016). Distinct Structural Pathways Coordinate the Activation of AMPA Receptor-Auxiliary Subunit Complexes. *Neuron, 89*(6), 1264-1276.

Derkach, V., Barria, A. & Soderling, T. R. (1999). Ca2+/calmodulin-kinase II enhances channel conductance of alpha-amino-3-hydroxy-5-methyl-4-isoxazolepropionate type glutamate receptors. *Proceedings of the National Academy of Sciences of the United States of America, 96*(6), 3269-3274.

Devi, S. P., Howe, J. R. & Auger, C. (2016). Train stimulation of parallel fibre to Purkinje cell inputs reveals two populations of synaptic responses with different receptor signatures. *The Journal of Physiology, 594*(13), 3705-3027.

Diamond, J. S. (2002). A broad view of glutamate spillover. *Nature Neuroscience, 5*(4), 291-292.

Díaz-Alonso, J., Sun, Y. J., Granger, A. J., Levy, J. M., Blankenship, S. M. & Nicoll, R. A. (2017). Subunit-specific role for the amino-terminal domain of AMPA receptors in synaptic targeting. *Proceedings of the National Academy of Sciences of the United States of America, 114*(27), 7136-7141.

Dong, H., O'Brien, R. J., Fung, E. T., Lanahan, A. A., Worley, P. F. & Huganir, R. L. (1997). GRIP: a synaptic PDZ domain-containing protein that interacts with AMPA receptors. *Nature. 386*(6622), 279-284.

Dong, H., Zhang, P., Song, I., Petralia, R. S., Liao, D. & Huganir, R. L. (1999). Characterization of the glutamate receptor-interacting proteins GRIP1 and GRIP2. *The Journal of Neuroscience, 19*(16), 6930-6941.

Dürr, K. L., Chen, L., Stein, R. A., De Zorzi, R., Folea, I. M., Walz, T., … Gouaux, E. (2014). Structure and dynamics of AMPA receptor GluA2 in resting, pre-open, and desensitized states. *Cell, 158*(4), 778-792.

Esteban, J. A., Shi, S. H., Wilson, C., Nuriya, M., Huganir, R. L. & Malinow, R. (2003). PKA phosphorylation of AMPA receptor subunits controls synaptic trafficking underlying plasticity. *Nature Neuroscience, 6*(2), 136-143.

Everett, K. V., Chioza, B., Aicardi, J., Aschauer, H., Brouwer, O., Callenbach, P., … Gardiner, M. (2007). Linkage and association analysis of CACNG3 in childhood absence epilepsy. *European Journal of Human Genetics, 15*(4), 463-472.

Farrow, P., Khodosevich, K., Sapir, Y., Schulmann, A., Aslam, M., Stern-Bach, Y., … von Engelhardt, J. (2015). Auxiliary subunits of the CKAMP family differentially modulate AMPA receptor properties. *Elife, 4*.

Fisher, J. L. & Mott, D. D. (2012). The auxiliary subunits Neto1 and Neto2 reduce voltage-dependent inhibition of recombinant kainate receptors. *The Journal of Neuroscience, 32*(37), 12928-12933.

Fukata, Y., Tzingounis, A. V., Trinidad, J. C., Fukata, M., Burlingame, A. L., Nicoll, R. A. & Bredt, D. S. (2005). Molecular constituents of neuronal AMPA receptors. *The Journal of Cell Biology, 169*(3), 399-404.

Fukaya, M., Yamazaki, M., Sakimura, K. & Watanabe, M. (2005). Spatial diversity in gene expression for VDCCgamma subunit family in developing and adult mouse brains. *Neuroscience Research, 53*(4), 376-383.

Gao, C., Sun, X. & Wolf, M. E. (2006). Activation of D1 dopamine receptors increases surface expression of AMPA receptors and facilitates their synaptic incorporation in cultured hippocampal neurons. *The Journal of Neurochemistry, 98*(5), 1664-1677.

Gleason, S. D., Kato, A., Bui, H. H., Thompson, L. K., Valli, S. N., Stutz, P. V., … Witkin, J. M. (2015). Inquiries into the Biological Significance of Transmembrane AMPA Receptor Regulatory Protein (TARP) γ-8 Through Investigations of TARP γ-8 Null Mice. *CNS & Neurological Disorders Drug Targets, 14*(5), 612-626.

Granger, A. J. & Nicoll, R. A. (2014). LTD expression is independent of glutamate receptor subtype. *Frontiers in Synaptic Neuroscience, 6*:15.

Granger, A. J., Shi, Y., Lu, W., Cerpas, M. & Nicoll, R. A. (2013). LTP requires a reserve pool of glutamate receptors independent of subunit type. *Nature, 493*(7433), 495-500.

Greger, I. H., Watson, J. F. & Cull-Candy, S. G. (2017). Structural and Functional Architecture of AMPA-Type Glutamate Receptors and Their Auxiliary Proteins. *Neuron, 94*(4), 713-730.

Grof, P., Duffy, A., Cavazzoni, P., Grof, E., Garnham, J., MacDougall, M., … Alda, M. (2002). *The Journal of Clinical Psychiatry, 63*(10), 942-947.

Gu, X., Mao, X., Lussier, M. P., Hutchison, M. A., Zhou, L., Hamra, F. K., … Lu, W. (2016). GSG1L suppresses AMPA receptor-mediated synaptic transmission and uniquely modulates AMPA receptor kinetics in hippocampal neurons. *Nature Communications, 7*:10873.

Hashimoto, K., Fukaya, M., Qiao, X., Sakimura, K., Watanabe, M. & Kano, M. (1999). Impairment of AMPA receptor function in cerebellar granule cells of ataxic mutant mouse stargazer. *The Journal of Neuroscience, 19*(14), 6027-6036.

Hastie, P., Ulbrich, M. H., Wang, H. L., Arant, R. J., Lau, A. G., Zhang, Z., … Chen, L. (2013). AMPA receptor/TARP stoichiometry visualized by single-molecule subunit counting. *Proceedings of the National Academy of Sciences of the United States of America, 110*(13), 5163-5168.

He, K., Song, L., Cummings, L. W., Goldman, J., Huganir, R. L. & Lee, H. K. (2009). Stabilization of Ca2+-permeable AMPA receptors at perisynaptic sites by GluR1-S845 phosphorylation. *Proceedings of the National Academy of Sciences of the United States of America, 106*(47), 20033-20038.

Henley, J. M. & Wilkinson K. A. (2016). Synaptic AMPA receptor composition in development, plasticity and disease. *Nature Reviews Neuroscience, 17*(6), 337-350.

Herguedas, B., Watson, J. F., Ho, H., Cais, O., García-Nafría, J. & Greger, I. H. (2019). Architecture of the heteromeric GluA1/2 AMPA receptor in complex with the auxiliary subunit TARP γ8. *Science, 364*(6438).

Hibi, S., Ueno, K., Nagato, S., Kawano, K., Ito, K., Norimine, Y., … Yonaga, M. (2012). Discovery of 2-(2-oxo-1-phenyl-5-pyridin-2-yl-1,2-dihydropyridin-3-yl)benzonitrile

(perampanel): a novel, noncompetitive α-amino-3-hydroxy-5-methyl-4-isoxazolepropanoic acid (AMPA) receptor antagonist. *The Journal of Medicinal Chemistry, 55*(23), 10584-10600.

Honoré, T., Davies, S. N., Drejer, J., Fletcher, E. J., Jacobsen, P., Lodge, D. & Nielsen, F. E. (1988). Quinoxalinediones: potent competitive non-NMDA glutamate receptor antagonists. *Science, 241*(4866), 701-703.

Hosokawa, T., Mitsushima, D., Kaneko, R. & Hayashi, Y. (2015). Stoichiometry and phosphoisotypes of hippocampal AMPA-type glutamate receptor phosphorylation. *Neuron, 85*(1), 60-67.

Iino, M., Goto, K., Kakegawa, W., Okado, H., Sudo, M., Ishiuchi, S., … Ozawa, S. (2001). Glia-synapse interaction through Ca2+-permeable AMPA receptors in Bergmann glia. *Science, 292*(5518), 926-929.

Isaac, J. T., Ashby, M. C. & McBain, C. J. (2007). The role of the GluR2 subunit in AMPA receptor function and synaptic plasticity. *Neuron, 54*(6), 859-871.

Jackson, A. C. & Nicoll, R. A. (2011). Stargazin (TARP gamma-2) is required for compartment-specific AMPA receptor trafficking and synaptic plasticity in cerebellar stellate cells. *The Journal of Neuroscience, 31*(11), 3939-3952.

Jackson, A. C. & Nicoll, R. A. (2011). The expanding social network of ionotropic glutamate receptors: TARPs and other transmembrane auxiliary subunits. *Neuron, 70*(2), 178-199.

Jin, R., Banke, T. G., Mayer, M. L., Traynelis, S. F. & Gouaux, E. (2003). Structural basis for partial agonist action at ionotropic glutamate receptors. *Nature Neuroscience, 6*(8), 803-810.

Jin, R., Horning, M., Mayer, M. L. & Gouaux, E. (2002). Mechanism of activation and selectivity in a ligand-gated ion channel: structural and functional studies of GluR2 and quisqualate. *Biochemistry, 41*(52), 15635-15643.

Jonas, P. & Burnashev, N. (1995). Molecular mechanisms controlling calcium entry through AMPA-type glutamate receptor channels. *Neuron, 15*(5), 987-990.

Kaae, B. H., Harpsøe, K., Kastrup, J. S., Sanz, A. C., Pickering, D. S., Metzler, B., … Madsen, U. (2007). Structural proof of a dimeric positive modulator bridging two identical AMPA receptor-binding sites. *Chemistry & Biology, 14*(11), 1294-1303.

Kalashnikova, E., Lorca, R. A., Kaur, I., Barisone, G. A., Li, B., Ishimaru, T., … Díaz, E. (2010). SynDIG1: an activity-regulated, AMPA- receptor-interacting transmembrane protein that regulates excitatory synapse development. *Neuron, 65*(1), 80-93.

Kamboj, S. K., Swanson, G. T. & Cull-Candy, S. G. (1995). Intracellular spermine confers rectification on rat calcium-permeable AMPA and kainate receptors. *The Journal of Physiology, 486*(Pt 2), 297-303.

Kang, M. G., Chen, C. C., Felix, R., Letts, V. A., Frankel, W. N., Mori, Y. & Campbell, K. P. (2001). Biochemical and biophysical evidence for gamma 2 subunit association with neuronal voltage-activated Ca2+ channels. *The Journal of Biological Chemistry, 276*(35), 32917-32924.

Kato, A. S., Burris, K. D., Gardinier, K. M., Gernert, D. L., Porter, W. J., Reel, J., … Witkin, J. M. (2016). Forebrain-selective AMPA-receptor antagonism guided by TARP γ-8 as an antiepileptic mechanism. *Nature Medicine, 22*(12), 1496-1501.

Kato, A. S., Gill, M. B., Ho, M. T., Yu, H., Tu, Y., Siuda, E. R., … Bredt, D. S. (2010). Hippocampal AMPA receptor gating controlled by both TARP and cornichon proteins. *Neuron, 68*(6), 1082-1096.

Kato, A. S., Siuda, E. R., Nisenbaum, E. S. & Bredt, D. S. (2008). AMPA receptor subunit-specific regulation by a distinct family of type II TARPs. *Neuron, 59*(6), 986-996.

Kato, A. S., Zhou, W., Milstein, A. D., Knierman, M. D., Siuda, E. R., Dotzlaf, J. E., … Bredt, D. S. (2007). New transmembrane AMPA receptor regulatory protein isoform, gamma-7, differentially regulates AMPA receptors. *The Journal of Neuroscience, 27*(18), 4969-4977.

Kessels, H. W. & Malinow, R. (2009). Synaptic AMPA receptor plasticity and behavior. *Neuron, 61*(3), 340-350.

Kim, C. H., Chung, H. J., Lee, H. K. & Huganir, R. L. (2001). Interaction of the AMPA receptor subunit GluR2/3 with PDZ domains regulates hippocampal long-term depression. *Proceedings of the National Academy of Sciences of the United States of America, 98*(20), 11725-11730.

Kim, K. S., Yan, D. & Tomita, S. (2010). Assembly and stoichiometry of the AMPA receptor and transmembrane AMPA receptor regulatory protein complex. *The Journal of Neuroscience, 30*(3), 1064-1072.

Klugbauer, N., Dai, S., Specht, V., Lacinová, L., Marais, E., Bohn, G. & Hofmann, F. (2000). A family of gamma-like calcium channel subunits. *FEBS Letters, 470*(2), 189-197.

Knight, H. M., Maclean, A., Irfan, M., Naeem, F., Cass, S., Pickard, B. S., … Ayub, M. (2008). Homozygosity mapping in a family presenting with schizophrenia, epilepsy and hearing impairment. *European Journal of Human Genetics, 16*(6), 750-758.

Koh, D. S., Burnashev, N. & Jonas, P. (1995). Block of native Ca(2+)-permeable AMPA receptors in rat brain by intracellular polyamines generates double rectification. *The Journal of Physiology, 486*(Pt 2), 305-312.

Körber, C., Werner, M., Kott, S., Ma, Z. L. & Hollmann, M. (2007). The transmembrane AMPA receptor regulatory protein gamma 4 is a more effective modulator of AMPA receptor function than stargazin (gamma 2). *The Journal of Neuroscience, 27*(31), 8442-8447.

Kott, S., Sager, C., Tapken, D., Werner, M. & Hollmann, M. (2009). Comparative analysis of the pharmacology of GluR1 in complex with transmembrane AMPA receptor regulatory proteins gamma2, gamma3, gamma4, and gamma8. *Neuroscience, 158*(1), 78-88.

Kott, S., Werner, M., Körber, C. & Hollmann, M. (2007). Electrophysiological properties of AMPA receptors are differentially modulated depending on the associated member of the TARP family. *The Journal of Neuroscience, 27*(14), 3780-3789.

Lee, H. K., Barbarosie, M., Kameyama, K., Bear, M. F. & Huganir, R. L. (2000). Regulation of distinct AMPA receptor phosphorylation sites during bidirectional synaptic plasticity. *Nature, 405*(6789), 955-959.

Lee, H. K., Takamiya, K., Han, J. S., Man, H., Kim, C. H., Rumbaugh, G., … Huganir, R. L. (2003). Phosphorylation of the AMPA receptor GluR1 subunit is required for synaptic plasticity and retention of spatial memory. *Cell, 112*(5), 631-643.

Letts, V. A., Felix, R., Biddlecome, G. H., Arikkath, J., Mahaffey, C. L., Valenzuela, A., … Frankel, W. N. (1998). The mouse stargazer gene encodes a neuronal Ca2+-channel gamma subunit. *Nature Genetics, 19*(4), 340-347.

Letts, V. A., Mahaffey, C. L., Beyer, B. & Frankel, W. N. (2005). A targeted mutation in Cacng4 exacerbates spike-wave seizures in stargazer (Cacng2) mice. *Proceedings of the National Academy of Sciences of the United States of America, 102*(6), 2123-2128.

Liu, Y. L., Fann, C. S., Liu, C. M., Chen, W. J., Wu, J. Y., Hung, S. I., … Hwu, H. G. (2008). RASD2, MYH9, and CACNG2 genes at chromosome 22q12 associated with the subgroup of schizophrenia with non-deficit in sustained attention and executive function. *Biological Psychiatry, 64*(9), 789-796.

Lu, H. C., She, W. C., Plas, D. T., Neumann, P. E., Janz, R. & Crair, M. C. (2003). Adenylyl cyclase I regulates AMPA receptor trafficking during mouse cortical 'barrel' map development. *Nature Neuroscience, 6*(9), 939-947.

Lu, W., Shi, Y., Jackson, A. C., Bjorgan, K., During, M. J., Sprengel, R., … Nicoll, R. A. (2009). Subunit composition of synaptic AMPA receptors revealed by a single-cell genetic approach. *Neuron, 62*(2), 254-268.

Lüscher, C. & Malenka, R. C. (2012). NMDA receptor-dependent long-term potentiation and long-term depression (LTP/LTD). *Cold Spring Harbor Perspectives in Biology, 4*(6).

Lüschner, W. D. & Hoch, W. (1999). Subtype-specific assembly of alpha-amino-3-hydroxy-5-methyl-4-isoxazole propionic acid receptor subunits is mediated by their n-terminal domains. *The Journal of Biological Chemistry, 274*(24), 16907-16016.

Lynch, G. S., Dunwiddie, T. & Gribkoff, V. (1977). Heterosynaptic depression: a postsynaptic correlate of long-term potentiation. *Nature, 266*(5604), 737-739.

Maccaferri, G. & Dingledine, R. (2002). Complex effects of CNQX on CA1 interneurons of the developing rat hippocampus. *Neuropharmacology, 43*(4), 523-529.

Maclean, D. M. & Bowie, D. (2011). Transmembrane AMPA receptor regulatory protein regulation of competitive antagonism: a problem of interpretation. *The Journal of Physiology, 589*(Pt 22), 5383-5890.

Mah, S. J., Cornell, E., Mitchell, N. A. & Fleck, M. W. (2005). Glutamate receptor trafficking: endoplasmic reticulum quality control involves ligand binding and receptor function. *The Journal of Neuroscience, 25*(9), 2215-2225.

Malenka, R. C. (1994). Synaptic plasticity in the hippocampus: LTP and LTD. *Cell, 78*(4), 535-538.

Malenka, R. C. & Bear, M. F. (2004). LTP and LTD: an embarrassment of riches. *Neuron, 44*(1), 5-21.

Malinow, R. & Malenka, R. C. (2002). AMPA receptor trafficking and synaptic plasticity. *Annual Review of Neuroscience, 25*, 103-126.

Man, H. Y., Sekine-Aizawa, Y., & Huganir, R. L. (2007). Regulation of {alpha}-amino-3-hydroxy-5-methyl-4-isoxazolepropionic acid receptor trafficking through PKA phosphorylation of the Glu receptor 1 subunit. *Proceedings of the National Academy of Sciences of the United States of America, 104*(9), 3579-3584.

Martin, S. J., Grimwood, P. D. & Morris, R. G. (2000). Synaptic plasticity and memory: an evaluation of the hypothesis. *Annual Review of Neuroscience, 23*, 649-711.

McBain, C. J., Eaton, J. V., Brown, T. & Dingledine, R. (1992). CNQX increases spontaneous inhibitory input to CA3 pyramidal neurones in neonatal rat hippocampal slices. *Brain research, 592*(1-2), 255-260.

Meng, Y., Zhang, Y. & Jia, Z. (2003). Synaptic transmission and plasticity in the absence of AMPA glutamate receptor GluR2 and GluR3. *Neuron, 39*(1), 163-176.

Menuz, K. & Nicoll, R. A. (2008). Loss of inhibitory neuron AMPA receptors contributes to ataxia and epilepsy in stargazer mice. *The Journal of Neuroscience, 28*(42), 10599-10603.

Menuz, K., Kerchner, G. A., O'Brien, J. L. & Nicoll, R. A. (2009). Critical role for TARPs in early development despite broad functional redundancy. *Neuropharmacology, 56*(1), 22-29.

Menuz, K., O'Brien, J. L., Karmizadegan, S., Bredt, D. S. & Nicoll, R. A. (2008). TARP redundancy is critical for maintaining AMPA receptor function. *The Journal of Neuroscience, 28*(35), 8740-8746.

Menuz, K., Stroud, R. M., Nicoll, R. A. & Hays, F. A. (2007). TARP auxiliary subunits switch AMPA receptor antagonists into partial agonists. *Science, 318*(5851), 815-817.

Meyerson, J. R., Chittori, S., Merk, A., Rao, P., Han, T. H., Serpe, M. … Subramaniam, S. (2016). Structural basis of kainate subtype glutamate receptor desensitization. *Nature, 537*(7621), 567-571.

Meyerson, J. R., Kumar, J., Chittori, S., Rao, P., Pierson, J., Bartesaghi, A., … Subramaniam, S. (2014). Structural mechanism of glutamate receptor activation and desensitization. *Nature, 514*(7522), 328-334.

Miladinovic, T., Nashed, M. G. & Singh, G. (2015). Overview of Glutamatergic Dysregulation in Central Pathologies. *Biomolecules, 5*(4), 3112-3141.

Milstein, A. D. & Nicoll, R. A. (2008). Regulation of AMPA receptor gating and pharmacology by TARP auxiliary subunits. *Trends in Pharmacological Sciences, 29*(7), 333-339.

Milstein, A. D., Zhou, W., Karimzadegan, S., Bredt, D. S. & Nicoll, R. A. (2007). TARP subtypes differentially and dose-dependently control synaptic AMPA receptor gating. *Neuron, 55*(6), 905-918.

Miranda, A., Shekhtman, T., McCarthy, M., DeModena, A., Leckband, S. G. & Kelsoe, J. R. (2019). Study of 45 candidate genes suggests CACNG2 may be associated with lithium response in bipolar disorder. *Journal of Affective Disorders, 248*, 175-179.

Morimoto-Tomita, M., Zhang, W., Straub, C., Cho, C. H., Kim, K. S., Howe, J. R. & Tomita, S. (2009). Autoinactivation of neuronal AMPA receptors via glutamate-regulated TARP interaction. *Neuron, 61*(1), 101-112.

Mosbacher, J., Schoepfer, R., Monyer, H., Burnashev, N., Seeburg, P. H. & Ruppersberg, J. P. (1994). A molecular determinant for submillisecond desensitization in glutamate receptors. *Science, 266*(5187), 1059-1062.

Möykkynen, T., Coleman, S. K., Semenov, A. & Keinänen, K. (2014). The N-terminal domain modulates α-amino-3-hydroxy-5-methyl-4-isoxazolepropionic acid (AMPA) receptor desensitization. *The Journal of Biological Chemistry, 289*(19), 13197-13205.

Nakagawa, T., Cheng, Y., Ramm, E., Sheng, M. & Walz, T. (2005). Structure and different conformational states of native AMPA receptor complexes. *Nature, 433*(7025), 545-549.

Newpher, T. M. & Ehlers, M. D. (2008). Glutamate receptor dynamics in dendritic microdomains. *Neuron, 58*(4), 472-497.

Noebels, J. L., Qiao, X., Bronson, R. T., Spencer, C. & Davisson, M. T. (1990). Stargazer: a new neurological mutant on chromosome 15 in the mouse with prolonged cortical seizures. *Epilepsy Research, 7*(2), 129-135.

Oh, M. C., Derkach, V. A., Guire, E. S. & Soderling, T. R. (2006). Extrasynaptic membrane trafficking regulated by GluR1 serine 845 phosphorylation primes AMPA receptors for long-term potentiation. *The Journal of Biological Chemistry, 281*(2), 752-758.

Partin, K. M., Bowie, D. & Mayer, M. L. (1995). Structural determinants of allosteric regulation in alternatively spliced AMPA receptors. *Neuron, 14*(4), 833-843.

Partin, K. M., Patneau, D. K. & Mayer, M. L. (1994). Cyclothiazide differentially modulates desensitization of alpha-amino-3-hydroxy-5-methyl-4-isoxazolepropionic acid receptor splice variants. *Molecular Pharmacology, 46*(1), 129-138.

Patneau, D. K. & Mayer, M. L. (1991). Kinetic analysis of interactions between kainate and AMPA: evidence for activation of a single receptor in mouse hippocampal neurons. *Neuron, 6*(5), 785-798.

Pelkey, K. A., Barksdale, E., Craig, M. T., Yuan, X., Sukumaran, M., Vargish, G. A., … McBain, C. J. (2015). Pentraxins coordinate excitatory synapse maturation and circuit integration of parvalbumin interneurons. *Neuron, 85*(6), 1257-1272.

Petralia, R. S. & Wenthold, R. J. (1992). Light and electron immunocytochemical localization of AMPA-selective glutamate receptors in the rat brain. *The Journal of Comparative Neurology, 318*(3), 329-354.

Pickard, L., Noël, J., Henley, J. M., Collingridge, G. L. & Molnar, E. (2000). Developmental changes in synaptic AMPA and NMDA receptor distribution and AMPA receptor subunit composition in living hippocampal neurons. *The Journal of Neuroscience, 20*(21), 7922-7931.

Pierce, V. D. & Niu, L. (2019). Stargazin and γ4 slow the channel opening and closing rates of GluA4 AMPA receptors. *Scientific Reports, 9*(1):9570.

Prescott, C., Weeks, A. M., Staley, K. J. & Partin, K. M. (2006). Kynurenic acid has a dual action on AMPA receptor responses. *Neuroscience Letters, 402*(1-2), 108-112.

Priel, A., Kolleker, A., Ayalon, G., Gillor, M., Osten, P. & Stern-Bach, Y. (2005). Stargazin reduces desensitization and slows deactivation of the AMPA-type glutamate receptors. *The Journal of Neuroscience, 25*(10), 2682-2686.

Raman, I. M. & Trussell, L. O. (1992). The kinetics of the response to glutamate and kainate in neurons of the avian cochlear nucleus. *Neuron, 9*(1), 173-186.

Riva, I., Eibl, C., Volkmer, R., Carbone, A. L. & Plested, A. J. (2017). Control of AMPA receptor activity by the extracellular loops of auxiliary proteins. *Elife, 6*.

Robert, A. & Howe, J. R. (2003). How AMPA receptor desensitization depends on receptor occupancy. *The Journal of Neuroscience, 23*(3), 847-858.

Roche, K. W., O'Brien, R. J., Mammen, A. L., Bernhardt, J. & Huganir, R. L. (1996). Characterization of multiple phosphorylation sites on the AMPA receptor GluR1 subunit. *Neuron, 16*(6), 1179-1188.

Rosenmund, C., Stern-Bach, Y. & Stevens, C. F. (1998). The tetrameric structure of a glutamate receptor channel. *Science, 280*(5369), 1596-1599.

Rouach, N., Byrd, K., Petralia, R. S., Elias, G. M., Adesnik, H., Tomita, S., … Nicoll, R. A. (2005). TARP gamma-8 controls hippocampal AMPA receptor number, distribution and synaptic plasticity. *Nature Neuroscience, 8*(11), 1525-1533.

Rousset, M., Cens, T., Restituito, S., Barrere, C., Black, J. L., McEnery, M. W. & Charnet, P. (2001). Functional roles of gamma2, gamma3 and gamma4, three new Ca2+ channel subunits, in P/Q-type Ca2+ channel expressed in Xenopus oocytes. *The Journal of Physiology, 532*(Pt 3), 583-593.

Rozov, A. & Burnashev, N. (1999). Polyamine-dependent facilitation of postsynaptic AMPA receptors counteracts paired-pulse depression. *Nature, 401*(6753), 594-598.

Saglietti, L., Dequidt, C., Kamieniarz, K., Rousset, M. C., Valnegri, P., Thoumine, O., … Passafaro, M. (2007). Extracellular interactions between GluR2 and N-cadherin in spine regulation. *Neuron, 54*(3), 461-477.

Sainlos, M., Tigaret, C., Poujol, C., Olivier, N. B., Bard, L., Breillat, C., … Imperiali, B. (2011). Biomimetic divalent ligands for the acute disruption of synaptic AMPAR stabilization. *Nature Chemical Biology, 7*(2), 81-91.

Salpietro, V., Dixon, C. L., Guo, H., Bello, O. D., Vandrovcova, J., Efthymiou, S., … Houlden, H. (2019). AMPA receptor GluA2 subunit defects are a cause of neurodevelopmental disorders. *Nature Communications, 10*(1):3094.

Salussolia, C. L., Corrales, A., Talukder, I., Kazi, R., Akgul, G., Bowen, M. &, Wollmuth, L. P. (2011). Interaction of the M4 segment with other transmembrane segments is required for surface expression of mammalian α-amino-3-hydroxy-5-methyl-4-isoxazolepropionic acid (AMPA) receptors. *The Journal of Biological Chemistry, 286*(46), 40205-40218.

Salussolia, C. L., Gan, Q., Kazi, R., Singh, P., Allopenna, J., Furukawa, H. & Wollmuth, L. P. (2013). A eukaryotic specific transmembrane segment is required for tetramerization in AMPA receptors. *The Journal of Neuroscience, 33*(23), 9840-9845.

Schmid, S. M., Körber, C., Herrmann, S., Werner, M. & Hollmann, M. (2007). A domain linking the AMPA receptor agonist binding site to the ion pore controls gating and causes lurcher properties when mutated. *The Journal of Neuroscience, 27*(45), 12230-12241.

Schmitz, L. J. M., Klaassen, R. V., Ruiperez-Alonso, M., Zamri, A. E., Stroeder, J., Rao-Ruiz, P., … Spijker, S. (2017). The AMPA receptor-associated protein Shisa7 regulates hippocampal synaptic function and contextual memory. *Elife, 6*.

Schnell, E., Sizemore, M., Karimzadegan, S., Chen, L., Bredt, D. S. & Nicoll, R. A. (2002). Direct interactions between PSD-95 and stargazin control synaptic AMPA receptor number. *Proceedings of the National Academy of Sciences of the United States of America, 99*(21), 13902-13907.

Schwenk, J., Baehrens, D., Haupt, A., Bildl, W., Boudkkazi, S., Roeper, J., … Schulte, U. (2014). Regional diversity and developmental dynamics of the AMPA-receptor proteome in the mammalian brain. *Neuron, 84*(1), 41-54.

Schwenk, J., Harmel, N., Brechet, A., Zolles, G., Berkefeld, H., Müller, C. S., … Fakler, B. (2012). High-resolution proteomics unravel architecture and molecular diversity of native AMPA receptor complexes. *Neuron, 74*(4), 621-633.

Schwenk, J., Harmel, N., Zolles, G., Bildl, W., Kulik, A., Heimrich, B., … Klöcker, N. (2009). Functional proteomics identify cornichon proteins as auxiliary subunits of AMPA receptors. *Science, 323*(5919), 1313-1319.

Sekiguchi, M., Fleck, M. W., Mayer, M. L., Takeo, J., Chiba, Y., Yamashita, S. & Wada, K. (1997). A novel allosteric potentiator of AMPA receptors: 4--2-(phenylsulfonylamino)ethylthio--2,6-difluoro-phenoxyaceta mide. *The Journal of Neuroscience, 17*(15), 5760-5771.

Semenov, A., Möykkynen, T., Coleman, S. K., Korpi, E. R. & Keinänen, K. (2012). Autoinactivation of the stargazin-AMPA receptor complex: subunit-dependency and independence from physical dissociation. *PLoS One, 7*(11).

Shanks, N. F., Maruo, T., Farina, A. N., Ellisman, M. H. & Nakagawa, T. (2010). Contribution of the global subunit structure and stargazin on the maturation of AMPA receptors. *The Journal of Neuroscience, 30*(7), 2728-2740.

Shanks, N. F., Savas, J. N., Maruo, T., Cais, O., Hirao, A., Oe, S., … Nakagawa, T. (2012). Differences in AMPA and kainate receptor interactomes facilitate identification of AMPA receptor auxiliary subunit GSG1L. *Cell Reports, 1*(6), 590-598.

Sheardown, M. J., Nielsen, E. O., Hansen, A. J., Jacobsen, P. & Honoré, T. (1990). 2,3-Dihydroxy-6-nitro-7-sulfamoyl-benzo(F)quinoxaline: a neuroprotectant for cerebral ischemia. *Science, 247*(4942), 571-574.

Shelley, C., Farrant, M. & Cull-Candy, S. G. (2012). TARP-associated AMPA receptors display an increased maximum channel conductance and multiple kinetically distinct open states. *The Journal of Physiology, 590*(22), 5723-5738.

Shi, Y., Lu, W., Milstein, A. D. & Nicoll, R. A. (2009). The stoichiometry of AMPA receptors and TARPs varies by neuronal cell type. *Neuron, 62*(5), 633-640.

Shi, Y., Suh, Y. H., Milstein, A. D., Isozaki, K., Schmid, S. M., Roche, K. W. & Nicoll, R. A. (2010). Functional comparison of the effects of TARPs and cornichons on AMPA receptor trafficking and gating. *Proceedings of the National Academy of Sciences of the United States of America, 107*(37), 16315-16319.

Sia, G. M., Béïque, J. C., Rumbaugh, G., Cho, R., Worley, P. F. & Huganir, R. L. (2007). Interaction of the N-terminal domain of the AMPA receptor GluR4 subunit with the neuronal pentraxin NP1 mediates GluR4 synaptic recruitment. *Neuron, 55*(1), 87-102.

Silberberg, G., Levit, A., Collier, D., St Clair, D., Munro, J., Kerwin, R. W., … Navon, R. (2008). Stargazin involvement with bipolar disorder and response to lithium treatment. *Pharmacogenetics and Genomics, 18*(5), 403-412.

Smith, T. C. & Howe, J. R. (2000). Concentration-dependent substate behavior of native AMPA receptors. *Nature Neuroscience, 3*(10), 992-997.

Sobolevsky, A. I., Rosconi, M. P. & Gouaux, E. (2009). X-ray structure, symmetry and mechanism of an AMPA-subtype glutamate receptor. *Nature, 462*(7274), 745-756.

Sommer, B., Keinänen, K., Verdoorn, T. A., Wisden, W., Burnashev, N., Herb, A., … Seeburg, P. H. (1990). Flip and flop: a cell-specific functional switch in glutamate-operated channels of the CNS. *Science, 249*(4976), 1580-1585.

Sommer, B., Köhler, M., Sprengel, R. & Seeburg, P. H. (1991). RNA editing in brain controls a determinant of ion flow in glutamate-gated channels. *Cell, 67*(1), 11-19.

Song, I. & Huganir, R. L. (2002). Regulation of AMPA receptors during synaptic plasticity. *Trends in Neurosciences, 25*(11), 578-588.

Soto, D., Coombs, I. D., Gratacòs-Batlle, E., Farrant, M. & Cull-Candy, S. G. (2014). Molecular mechanisms contributing to TARP regulation of channel conductance and polyamine block of calcium-permeable AMPA receptors. *The Journal of Neuroscience, 34*(35), 11673-11683.

Soto, D., Coombs, I. D., Kelly, L., Farrant, M. & Cull-Candy, S. G. (2007). Stargazin attenuates intracellular polyamine block of calcium-permeable AMPA receptors. *Nature Neuroscience, 10*(10), 1260-1267.

Soto, D., Coombs, I. D., Renzi, M., Zonouzi, M., Farrant, M. & Cull-Candy, S. G. (2009). Selective regulation of long-form calcium-permeable AMPA receptors by an atypical TARP, gamma-5. *Nature Neuroscience, 12*(3), 277-285.

Stein, E. L. & Chetkovich, D. M. (2010). Regulation of stargazin synaptic trafficking by C-terminal PDZ ligand phosphorylation in bidirectional synaptic plasticity. *The Journal of Neurochemistry, 113*(1), 42-53.

Sumioka, A., Yan, D. & Tomita, S. (2010). TARP phosphorylation regulates synaptic AMPA receptors through lipid bilayers. *Neuron, 66*(5), 755-767.

Sun, Y., Olson, R., Horning, M., Armstrong, N., Mayer, M. & Gouaux, E. (2002). Mechanism of glutamate receptor desensitization. *Nature, 417*(6886), 245-253.

Suzuki, E., Kessler, M. & Arai, A. C. (2008). The fast kinetics of AMPA GluR3 receptors is selectively modulated by the TARPs gamma 4 and gamma 8. *Molecular and Cellular Neurosciences, 38*(1), 117-123.

Swanson, G. T., Kamboj, S. K. & Cull-Candy, S. G. (1997). Single-channel properties of recombinant AMPA receptors depend on RNA editing, splice variation, and subunit composition. *The Journal of Neuroscience, 17*(1), 58-69.

Talukder, I., Borker, P. & Wollmuth, L. P. (2010). Specific sites within the ligand-binding domain and ion channel linkers modulate NMDA receptor gating. *The Journal of Neuroscience, 30*(35), 11792-11804.

Terrier, J., Lüscher, C. & Pascoli, V. (2016). Cell-Type Specific Insertion of GluA2-Lacking AMPARs with Cocaine Exposure Leading to Sensitization, Cue-Induced Seeking, and Incubation of Craving. *Neuropsychopharmacology, 41*(7), 1779-1789.

Tomita, S., Adesnik, H., Sekiguchi, M., Zhang, W., Wada, K., Howe, J. R., … Bredt, D. S. (2005). Stargazin modulates AMPA receptor gating and trafficking by distinct domains. *Nature, 435*(7045), 1052-1058.

Tomita, S., Byrd, R. K., Rouach, N., Bellone, C., Venegas, A., O'Brien, J. L., … Bredt, D. S. (2007). AMPA receptors and stargazin-like transmembrane AMPA receptor-regulatory proteins mediate hippocampal kainate neurotoxicity. *Proceedings of the National Academy of Sciences of the United States of America, 104*(47), 18784-18788.

Tomita, S., Chen, L., Kawasaki, Y., Petralia, R. S., Wenthold, R. J., Nicoll, R. A. & Bredt, D. S. (2003). Functional studies and distribution define a family of transmembrane AMPA receptor regulatory proteins. *The Journal of Cell Biology, 161*(4), 805-816.

Tomita, S., Fukata, M., Nicoll, R. A. & Bredt, D. S. (2004). Dynamic interaction of stargazin-like TARPs with cycling AMPA receptors at synapses. *Science, 303*(5663), 1508-1511.

Tomita, S., Sekiguchi, M., Wada, K., Nicoll, R. A. & Bredt, D. S. (2006). Stargazin controls the pharmacology of AMPA receptor potentiators. *Proceedings of the National Academy of Sciences of the United States of America, 103*(26), 10064-10067.

Tomita, S., Shenoy, A., Fukata, Y., Nicoll, R. A. & Bredt, D. S. (2007). Stargazin interacts functionally with the AMPA receptor glutamate-binding module. *Neuropharmacology, 52*(1), 87-91.

Tomita, S., Stein, V., Stocker, T. J., Nicoll, R. A. & Bredt, D. S. (2005). Bidirectional synaptic plasticity regulated by phosphorylation of stargazin-like TARPs. *Neuron, 45*(2), 269-277.

Traynelis, S. F., Wollmuth, L. P., McBain, C. J., Menniti, F. S., Vance, K. M., Ogden, K. K., … Dingledine, R. (2010). Glutamate receptor ion channels: structure, regulation, and function. *Pharmacological Reviews, 62*(3), 405-496.

Tsui, J. & Malenka, R. C. (2006). Substrate localization creates specificity in calcium/ calmodulin-dependent protein kinase II signaling at synapses. *The Journal of Biological Chemistry, 281*(19), 13794-13804.

Turetsky, D., Garringer, E. & Patneau, D. K. (2005). Stargazin modulates native AMPA receptor functional properties by two distinct mechanisms. *The Journal of Neuroscience, 25*(32), 7438-7448.

Twomey, E. C., Yelshanskaya, M. V., Grassucci, R. A., Frank, J. & Sobolevsky, A. I. (2017). Channel opening and gating mechanism in AMPA-subtype glutamate receptors. *Nature, 549*(7670), 60-65.

Twomey, E. C., Yelshanskaya, M. V., Grassucci, R. A., Frank, J. & Sobolevsky, A. I. (2017). Structural Bases of Desensitization in AMPA Receptor-Auxiliary Subunit Complexes. *Neuron, 94*(3), 569-580.

Twomey, E. C., Yelshanskaya, M. V., Grassucci, R. A., Frank, J. & Sobolevsky, A. I. (2016). Elucidation of AMPA receptor-stargazin complexes by cryo-electron microscopy. *Science, 353*(6294), 83-86.

Vandenberghe, W., Nicoll, R. A. & Bredt, D. S. (2005). Interaction with the unfolded protein response reveals a role for stargazin in biosynthetic AMPA receptor transport. *The Journal of Neuroscience, 25*(5), 1095-1102.

Vandenberghe, W., Nicoll, R. A. & Bredt, D. S. (2005). Stargazin is an AMPA receptor auxiliary subunit. *Proceedings of the National Academy of Sciences of the United States of America, 102*(2), 485-490.

Von Engelhardt, J., Mack, V., Sprengel, R., Kavenstock, N., Li, K. W., Stern-Bach, Y., … Monyer, H. (2010). CKAMP44: a brain-specific protein attenuating short-term synaptic plasticity in the dentate gyrus. *Science, 327*(5972), 1518-1522.

Wang, Q., Chiu, S. L., Koropouli, E., Hong, I., Mitchell, S., Easwaran, T. P., … Kolodkin, A. L. (2017). Neuropilin-2/PlexinA3 Receptors Associate with GluA1 and Mediate Sema3F-Dependent Homeostatic Scaling in Cortical Neurons. *Neuron, 96*(5), 1084-1098.

Ward, S. E., Beswick, P., Calcinaghi, N., Dawson, L. A., Gartlon, J., Graziani, F., … Harries, M. H. (2017). Pharmacological characterization of N-[(2S)-5-(6-fluoro-3-pyridinyl)-2, 3-dihydro-1H-inden-2-yl]-2-propanesulfonamide: a novel, clinical AMPA receptor positive allosteric modulator. *British Journal of Pharmacology, 174*(5), 370-385.

Watson, J. F., Ho, H. & Greger, I. H. (2017). Synaptic transmission and plasticity require AMPA receptor anchoring via its N-terminal domain. *Elife, 6.*

Wenthold, R. J., Petralia, R. S., Blahos, J. II & Niedzielski, A. S. (1996). Evidence for multiple AMPA receptor complexes in hippocampal CA1/CA2 neurons. *The Journal of Neuroscience, 16*(6), 1982-1989.

Wisden, W. & Seeburg, P. H. (1993). Mammalian ionotropic glutamate receptors. *Current Opinion in Neurobiology, 3*(3), 291-298.

Wollmuth, L. P. & Sobolevsky, A. I. (2004). Structure and gating of the glutamate receptor ion channel. *Trends in Neuroscience, 27*(6), 321-328.

Wright, A. & Vissel, B. (2012). The essential role of AMPA receptor GluR2 subunit RNA editing in the normal and diseased brain. *Frontiers in Molecular Neuroscience, 5*:34.

Xia, J., Zhang, X., Staudinger, J. & Huganir, R. L. (1999). Clustering of AMPA receptors by the synaptic PDZ domain-containing protein PICK1. *Neuron, 22*(1), 179-187.

Yamasaki, M., Fukaya, M., Yamazaki, M., Azechi, H., Natsume, R., Abe, M., … Watanabe, M. (2016). TARP γ-2 and γ-8 Differentially Control AMPAR Density Across Schaffer Collateral/Commissural Synapses in the Hippocampal CA1 Area. *The Journal of Neuroscience, 36*(15), 4296-4312.

Yamazaki, M., Fukaya, M., Hashimoto, K., Yamasaki, M., Tsujita, M., Itakura, M., … Watanabe, M. (2010). TARPs gamma-2 and gamma-7 are essential for AMPA receptor expression in the cerebellum. *The European Journal of Neuroscience, 31*(12), 2204-2220.

Yamazaki, M., Le Pichon, C. E., Jackson, A. C., Cerpas, M., Sakimura, K., Scearce-Levie, K. & Nicoll, R. A. (2015). Relative contribution of TARPs γ-2 and γ-7 to cerebellar excitatory synaptic transmission and motor behavior. *Proceedings of the National Academy of Sciences of the United States of America, 112*(4), E371-E379.

Yamazaki, M., Ohno-Shosaku, T., Fukaya, M., Kano, M., Watanabe, M. & Sakimura, K. (2004). A novel action of stargazin as an enhancer of AMPA receptor activity. *Neuroscience Research, 50*(4), 369-374.

Yang, Y., Wang, X. B., Frerking, M. & Zhou, Q. (2008). Delivery of AMPA receptors to perisynaptic sites precedes the full expression of long-term potentiation. *Proceedings of the National Academy of Sciences of the United States of America, 105*(32), 11388-11393.

Zhang, W., Devi, S. P., Tomita, S. & Howe, J. R. (2014). Auxiliary proteins promote modal gating of AMPA- and kainate-type glutamate receptors. *The European Journal of Neuroscience, 39*(7), 1138-1147.

Zhang, W., Robert, A., Vogensen, S. B. & Howe, J. R. (2006). The relationship between agonist potency and AMPA receptor kinetics. *Biophysical Journal, 91*(4), 1336-1346.

Zhang, W., St-Gelais, F., Grabner, C. P., Trinidad, J. C., Sumioka, A., Morimoto-Tomita, M., … Tomita S. (2009). A transmembrane accessory subunit that modulates kainate-type glutamate receptors. *Neuron, 61*(3), 385-396.

Zhao, Y., Chen, S., Swensen, A. C., Qian, W. J. & Gouaux, E. (2019). Architecture and subunit arrangement of native AMPA receptors elucidated by cryo-EM. *Science, 364*(6438), 355-362.

Zhao, Y., Chen, S., Yoshioka, C., Baconguis, I. & Gouaux, E. (2016). Architecture of fully occupied GluA2 AMPA receptor-TARP complex elucidated by cryo-EM. *Nature, 536*(7614), 108-111.

Zheng, Y., Mellem, J. E., Brockie, P. J., Madsen, D. M. & Maricq, A. V. (2004). SOL-1 is a CUB-domain protein required for GLR-1 glutamate receptor function in C. elegans. *Nature, 427*(6973), 451-457.

Zhou, Z., Liu, A., Xia, S., Leung, C., Qi, J., Meng, Y., … Jia, Z. (2018). The C-terminal tails of endogenous GluA1 and GluA2 differentially contribute to hippocampal synaptic plasticity and learning. *Nature Neuroscience, 21*(1), 50-62.

Zhu, J. J., Esteban, J. A., Hayashi, Y. & Malinow, R. (2000). Postnatal synaptic potentiation: delivery of GluR4-containing AMPA receptors by spontaneous activity. *Nature Neuroscience, 3*(11), 1098-1106.

Zwart, R., Sher, E., Ping, X., Jin, X., Sims, J. R. Jr., Chappell, A. S., … Witkin, J. M. (2014). Perampanel, an antagonist of α-amino-3-hydroxy-5-methyl-4-isoxazolepropionic acid receptors, for the treatment of epilepsy: studies in human epileptic brain and nonepileptic brain and in rodent models. *The Journal of Pharmacology and Experimental Therapeutics, 351*(1), 124-133.

ACKNOWLEDGEMENTS

First and foremost, I would like to thank my Ph.D. supervisor, Prof. Andrew Plested, for being such a great mentor, creating a very positive working atmosphere and giving me opportunities to grow as a scientist and person.

Then I would like to acknowledge Anna Carbone, co-supervisor for the first two years of my Ph.D., for teaching me the bases for working in a lab and representing a strong example of an independent scientist.

Also, I would like to thank all the present and past colleagues in the lab for the delightful time together. Especially, an heartfelt thank to Marcus, for always being so helpful, Anahita, Yuchen, Sonja and Sebastian, for being great Ph.D. mates, Clarissa, for the productive collaboration, Jelena and Hector, for the many times they assisted me, Vale, for still being a good friend, and Niccolò and Saeid, for all the fun and laughter.

Finally, the biggest and warmest thanks to my parents, my brother Lorenzo and Paolo, because I am so lucky to have them.